AD743072

..........contributing to man's
understanding of the environment world

ANALYSIS OF TELESEISMIC DATA FOR THE NUCLEAR EXPLOSION MILROW

D. H. von SEGGERN
D. G. LAMBERT
SEISMIC DATA LABORATORY

13 APRIL 1972

D D C

RECEIVED

JUN 18 1972

C

TELEDYNE GEOTECH

ALEXANDRIA LABORATORIES

APPROVED FOR PUBLIC RELEASE; DISTRIBUTION UNLIMITED

ACCESSION for

EFSTJ   WHITE SECTION ☒
DOG   BUFF SECTION ☐
UNANNOUNCED   ☐
JUSTIFICATION

BY
DISTRIBUTION/AVAILABILITY CODES

DIST.   AVAIL and/or SPECIAL

A

DOCUMENT CONTROL DATA - R&D

(Security classification of title, body of abstract and indexing annotation must be entered when the overall report is classified)

1 ORIGINATING ACTIVITY (Corporate author)	2a REPORT SECURITY CLASSIFICATION
Teledyne Geotech Alexandria, Virginia	Unclassified
	2b GROUP

3 REPORT TITLE

ANALYSIS OF TELESEISMIC DATA FOR THE NUCLEAR EXPLOSION MILROW

4 DESCRIPTIVE NOTES (Type of report and inclusive dates)

Scientific

5 AUTHOR(S) (Last name, first name, initial)

von Seggern, D.H.; Lambert, D.G.

6 REPORT DATE	7a. TOTAL NO OF PAGES	7b. NO. OF REFS
13 April 1972	147	47

8a CONTRACT OR GRANT NO. F33657-72-C-0009	9a ORIGINATOR'S REPORT NUMBER(S) 258
b. PROJECT NO VELA T/2706	
c. ARPA Order No. 1714	9b OTHER REPORT NO(S) (Any other numbers that may be assigned this report)
d.ARPA Program Code No. 2F-10	

10 AVAILABILITY/LIMITATION NOTICES

APPROVED FOR PUBLIC RELEASE; DISTRIBUTION UNLIMITED.

11 SUPPLEMENTARY NOTES	12 SPONSORING MILITARY ACTIVITY Advanced Research Projects Agency Nuclear Monitoring Research Office Washington, D.C.

13 ABSTRACT

MILROW, the second United States underground nuclear explosion on Amchitka Island, was an order of magnitude larger than LONG SHOT, the first test there. Magnitude-yield scaling between the two for both surface waves and body waves followed theoretical predictions well and agreed with Nevada Test Site (NTS) scaling. A computed location of MILROW using LONG SHOT travel-time anomalies was only 1.2 km in error horizontally and 11.8 km vertically, a substantial improvement over a location using no anomalies. The presence of direct shear waves and Love waves for MILROW can be attributed to causes other than tectonic strain release, such as mode conversion, crack formation, and structural features of the surrounding medium. The detection of Love waves from LONG SHOT and the MILROW cavity collapse were important results bearing on the determination of the shear-generating mechanism. All the common identification criteria were applied to MILROW and its collapse: location and depth, M_s vs m_b, spectral ratios, complexity, shear-wave excitation, and radiation patterns. MILROW appeared to be typical of explosions while, in contrast, the collapse was much like an earthquake.

14 KEY WORDS

Travel time
Amplitude
Magnitude
Location
Depth of focus
Energy relationships
M_s vs m_b

ANALYSIS OF TELESEISMIC DATA FOR THE

NUCLEAR EXPLOSION MILROW

SEISMIC DATA LABORATORY REPORT NO. 258

AFTAC Project No.:	VELA T/2706
Project Title:	Seismic Data Laboratory
ARPA Order No.:	1714
ARPA Program Code No.:	2F-10
Name of Contractor:	TELEDYNE GEOTECH
Contract No.:	F33657-72-C-0009
Date of Contract:	01 July 1971
Amount of Contract:	$ 1,314,000
Contract Expiration Date:	30 June 1972
Project Manager:	Royal A. Hartenberger (703) 836-7647

P. O. Box 334, Alexandria, Virginia

ABSTRACT

MILROW, the second United States underground nuclear explosion on Amchitka Island, was an order of magnitude larger than LONG SHOT, the first test there. Magnitude-yield scaling between the two for both surface waves and body waves followed theoretical predictions well, but there are significant intercept changes in the magnitude-yield relations from the Nevada Test Site to Amchitka Island. A computed location of MILROW using LONG SHOT travel-time anomalies was only 1.2 km in error horizontally and 11.8 km vertically, a substantial improvement over a location using no anomalies. The presence of direct shear waves and Love waves for MILROW can be attributed to causes other than tectonic strain release, such as mode conversion, crack formation, and structural features of the surrounding medium. The detection of Love waves from LONG SHOT and the MILROW cavity collapse were important results bearing on the determination of the shear-generating mechanism. All the common identification criteria were applied to MILROW and its collapse: location and depth, M_s vs m_b, spectral ratios, complexity, shear-wave excitation, and radiation patterns. MILROW appeared to be typical of explosions while, in contrast, the collapse was much like an earthquake.

TABLE OF CONTENTS

TABLE OF CONTENTS (CONT'D.)

LIST OF FIGURES

LIST OF FIGURES (Cont'd.)

LIST OF FIGURES (Cont'd.)

LIST OF TABLES

INTRODUCTION

On 29 October 1965 the first underground nuclear explosion on Amchitka Island in the Aleutians, LONG SHOT, was detonated. It engendered a voluminous analysis of distant seismological data and significantly increased our knowledge pertaining to location and identification of underground nuclear tests, as well as our general knowledge of the earth.

On 2 October 1969 a second explosion, MILROW, was detonated on Amchitka Island with a yield about an order of magnitude larger than LONG SHOT. The purpose of this report is to document and analyze the teleseismic data from MILROW, mainly that recorded by the LRSM mobile vans deployed at the time and by the three VELA arrays, UBO, TFO, and LASA. Some additional data taken from the WWSS network of the NOS is presented, but is not to be considered complete or final at this time. Important studies of near-source behavior are being conducted by government agencies and private contractors; their results have not reached publication although some preliminary reports have been presented orally (McKeown et al., 1970; Blackford et al., 1970). Eventually, we hope that the near-source studies can be integrated with the teleseismic data to explain the MILROW source dynamics in detail.

Since most of the data available for this report at the Seismic Data Laboratory and through the WWSS was recorded at sites identical to those for LONG SHOT, since MILROW was detonated only 2.3 km from LONG SHOT, and since the overall quantity of data is reduced, we will avoid presentation of any analysis which would merely be redundant in relation to

the vast amount of literature previously prepared about LONG SHOT. In particular, little new seismological information is to be expected from the P and PcP signals of MILROW because of the excellent and numerous global recordings of these signals from LONG SHOT.

This report will place attention on the presence of shear phases which were not seen on LONG SHOT recordings. The magnitude-yield scaling over the limited range of 80 to 1000 kt will be ascertained and related to theoretical predictions. The occurrence of a considerable collapse of the MILROW cavity two days afterward produced data relevant to the determination of whether MILROW caused any tectonic strain release. A thorough application to MILROW of current discrimination criteria will be made and the results will be compared with those of LONG SHOT.

Basic spatial and temporal location information on MILROW and its collapse are given in Table I. The SDL's own report on LONG SHOT (Lambert et al., 1969) is the basic reference for this report, and it is hoped that the reader will have access to that reference. To eliminate repetition, we will usually omit further reference to Lambert et al.; and data, results, or conclusions pertaining to LONG SHOT discussed in this report, unless attributed to another source or newly produced in this report, are taken from that LONG SHOT report.

-2-

THE SOURCE ENVIRONMENT

Physical setting

A summary of geological and geophysical data concerning
the Aleutian arc and Amchitka Island in particular was given
in the LONG SHOT report and need not be repeated here. One
additional noteworthy reference is the comprehensive report
on the Aleutians by Anderson, 1970. A lithologic log at the
MILROW site (Snyder, 1969) revealed mainly consolidated vol-
canic breccia beds with some layers of andesite, basalt, and
sandstone. For comparison, the lithology of the LONG SHOT site,
2.3 km away, was mostly interbedded tuff and breccia.

Magnitude-vs-yield

LONG SHOT was detonated within an andesite sill while
MILROW was detonated in breccia; however, at these depths
(2000-4000 feet) the overburden pressure and degree of water-
saturation may influence the medium response and degree of
energy radiation more than the exact composition of the rock.
For reference, we use the recent magnitude-vs-yield empirical
documentation by Evernden (1970) on "hard rock and mesa
tuff" events, between which there is no clear separation.
LONG SHOT, reported to be 80 kt (USAEC, 1967), has an m_b (5.85)
which is greater by about three-tenths of a unit than predicted
by events detonated in these media; and MILROW, reported to
be 1 Mt (USAEC, 1969), also has an m_b (6.42) greater by the
same amount than predicted on the basis of these other events.
All of the events for hard rock and mesa tuff in Evernden's
illustrations are from the NTS; thus the effect of a
combination of a different source environment, different
travel paths, and different recording networks on

-3-

the magnitude-vs-yield curve is apparently to increase
body-wave magnitude a few tenths of a unit for a given
yield on Amchitka relative to NTS. Orphal et al. (1970)
reported that the close-in response at 1.0 cps was equal
to that predicted for a 1 Mt event on the basis of NTS
experience. We must state that both the reported yields
for LONG SHOT and MILROW are pre-shot figures, subject
to any errors inherent in predicting the yield of a
nuclear device.

Near-source behavior

Tectonic strain release at the site was not revealed
by teleseismic data for LONG SHOT although close-in seismic
measurements indicated some non-circularity in the energy
radiation at the source. As will be shown in a later section
of this report, teleseismic data from MILROW does indicate
strain release or some other shear-generating mechanism
at the source. Close-in instruments recorded significant
horizontally-polarized shear-wave motion (Orphal et al., 1970).
McKeown et al. (1970) report that some surface fractures
appeared after MILROW and that vertical displacements up to
tens of centimeters were caused by MILROW out to distances
of at least 3 km. With the large number of near-normal
faults on the island (Figure 1), permanent vertical displace-
ments of this magnitude are not unexpected. McKeown et al.,
however, do not report horizontal displacements, which are
excellent indicators of tectonic strain release (Bucknam, 1969).

LOCATION USING TELESEISMIC P ARRIVALS

Arrival times for 18 Long Range Seismic Measurements (LRSM) stations; for the center seismometers at the VELA arrays LASA, UBO and TFO; and for many additional stations globally distributed were available to locate MILROW. The arrival times of P waves recorded at the LRSM stations and VELA arrays were all measured at the SDL. All of the P arrival times which had less than a seven-second residual (Jeffreys-Bullen table) were extracted as listed from Earthquake Data Report No. 649-69 (U.S. Department of Commerce, ESSA, 22 October 1969). Some additional arrival times were determined at the SDL after more records became available through the NOS. In the following discussion, all locations were computed using the 1968 P travel-time tables (H68) as presented in the Bulletin of the Seismological Society of America, Volume 58, No. 4. Only stations between 20° and 100° epicentral distance were used.

MILROW was first located without restraining the depth using the 158 arrival times listed in Table II. The result was a 23.2 km hypocenter shift at an azimuth of 356° from the true location and a computed depth of 66 km. This compares with the LONG SHOT shift of 20.6 km at an azimuth of 6° with a 78 km depth using 329 stations (also between 20° and 100° distance) with the H68 travel-time table. Azimuthal coverage for both events was excellent, except for the southeast quadrant.

The MILROW event was relocated again using the 158 arrival times but with depth restrained to its actual value. The

resultant shift from the actual location was 22.2 km on an azimuth of 344° as depicted in Figure 2. This shift is nearly coincident with the depth-restrained shift of 20.1 km on an azimuth of 346° for LONG SHOT using its 329 stations, also depicted in Figure 2. Nearly the identical location bias has appeared for MILROW as for LONG SHOT. A discussion of this bias and analysis of the LONG SHOT travel-time data can be found in Lambert et al. (1969). Herrin and Sorrells (1969), Davies and McKenzie (1969), and Jacob (1970) have proposed structural models below Amchitka Island to account for this bias.

Next, a network of 73 stations which recorded both LONG SHOT and MILROW and which supplied good azimuthal coverage was used to locate both events with depths restrained to actual values. Travel-time residuals calculated for MILROW at these 73 stations are presented in Figure 3 vs epicenter-station azimuth; this shows the trend of the residuals with azimuth which produces the bias of the LONG SHOT and MILROW locations. With this common network LONG SHOT shifted 22.7 km on an azimuth of 335° and MILROW shifted 21.9 km on an azimuth of 333° as shown in Figure 2. The near identity in shift is not surprising since Figure 4 shows anomalies (travel-time residuals referenced to the UBO residual of -.02 seconds) to be nearly identical for the two events; within reading error, the common network solutions shown in Figure 2 exhibit the same separation as the actual locations.

Finally, MILROW was located applying the LONG SHOT anomalies shown in Figure 4 to the MILROW arrival times, and vice-versa, in the manner described by Chiburis (1968) using his program SHIFT, again with depths restrained to the known values. MILROW

shifted 1.2 km on an azimuth of 21° and LONG SHOT shifted 0.9 km on an azimuth of 190° as depicted in Figure 2. The two vectors are very short and nearly mirror images of one another. Thus, we conclude that the MILROW and LONG SHOT sites can be adequately handled by a single set of travel-time anomalies and that location bias does not change from one site to the other for the network used.

RECORDED PHASES

Amplitudes

All the amplitude data that was available to the Seismic
Data Laboratory is listed in Tables III and IV. Corresponding
travel times are figured for the first visible emergence of
the phases recorded on short-period instruments, or long-period
instruments if the phase is unrecorded on short-period ones.
Table III contains data from the LRSM stations and VELA arrays,
and this data was all visually measured at the Seismic Data
Laboratory. In Table III, "SPR" and "LPR" refer to true radial
components for MILROW; likewise, "SPT" and "LPT" refer to
true transverse components. The horizontal recordings at most
MILROW stations were rotated on the digital computer to
provide these orientat ons. Table IV contains data from sta-
tions reporting to the NOS. Some of this data relating to
body-wave and surface-wave magnitude was reviewed at the
Seismic Data Laboratory, but most of the information was
communicated through the NOS and has not been reviewed by
them nor verified by us. All the amplitude data is plotted in
the amplitude-distance graphs that follow and is employed in
average magnitude determination.

Several phases were recorded from MILROW which were not
seen from LONG SHOT. These comprised direct shear waves, long-
period compressional waves, Love waves, and some late-arriving
core phases. These were all of such amplitude that, with the
yield difference between MILROW and LONG SHOT, we presume
that similar phases for LONG SHOT were not visible on tele-
seismic recordings simply because they were below the noise
level in amplitude. Figures 5 through 8 are plots of recorded

amplitudes vs distance for the most widely-recorded phases from MILROW: P, PcP, LQ (Love), and LR (Rayleigh), respectively. "Amplitude" here means one-half the maximum peak-to-peak amplitude, corrected for system response and divided by the period of the maximum motion. For body-wave phases, maximum motion is measured no farther than three or four cycles after first motion; and for surface-wave phases, maximum motion is measured on group arrivals having a period of about twenty seconds.

No detailed discussion of compressional-wave and Rayleigh-wave amplitudes is desirable since it would be repetitious with the thorough report on LONG SHOT data. We have examined the MILROW data in regard to amplitude variations and have detected no change in the overall pattern of MILROW P, PcP, and LR amplitudes compared to the same LONG SHOT amplitudes. For body waves, the data base is much less than for LONG SHOT; and for Rayleigh waves, even though several new stations recorded these for MILROW, the new data is so sparsely distributed or else so near LONG SHOT stations that it does not add any signif .ant regional information.

Shear energy and possible mechanisms

The recording of horizontally polarized shear-wave motion (SH) cannot be accounted for by modeling the explosion as a spherically symmetric compressive source. However, the presence of prominent LQ waves from NTS explosions have led investigators to propose a mechanism of tectonic strain release (Brune and Pomeroy, 1963; Toksoz et al., 1965). Kim and Kisslinger (1967) have shown with model experiments that SH motion is generated in prestressed media by explosions and that only P motion is generated when the media is not prestressed. Also,

-9-

Kisslinger et al. (1961) have shown that horizontally
polarized shear motion can occur due to crack formation
about an explosive source. We cannot ascertain the exact
generating mechanism with the teleseismic data available,
and our intent in this section is merely to call attention
to the presence of horizontally polarized shear-wave energy
on MILROW recordings. Several stations in Tables III and IV
recorded LQ, and group travel times were such that these
waves must have originated at, or near, the MILROW site.
Direct shear waves were visible on short-period instruments
at KN-UT, SHL, COL, TUC, and GUA; and, although separation
into radial and transverse components was impractical for
the WWNSS stations, rotation at KN-UT positively revealed
a horizontally polarized shear arrival. Long-period, direct
shear waves were found on FB-AK, KN-UT, LC-NM, RK-ON, and
NP-NT recordings; horizontally-polarized shear waves were
positively identified at three of these (FB-AK, KN-UT, and
LC-NM) after horizontal components were rotated into radial
and transverse components. The horizontal shear amplitudes
will be discussed later in relation to their utility for
discrimination. Vertically polarized shear energy was
recorded at some of the above stations, but this can be
explained by incidence of compressional waves on any
elastic boundary near the source rather than by some shear-
generating mechanism at the source.

MAGNITUDE

Teleseismic magnitude estimates of MILROW

Body-wave and surface-wave magnitude estimates of MILROW were made according to routine SDL procedure. Body-wave magnitude for stations from 16° to 100° distance was computed by the formula

$$m_b = \log_{10}(A/T) + B$$

where

A = zero-to-peak ground motion (millimicrons),

T = period (seconds),

B = distance correction factor of Gutenberg and Richter (1956).

To obtain A, the maximum peak-to-peak amplitude of the P phase within the first three or four cycles on the record is halved and corrected for system magnification at the period T of the maximum amplitude.

Figure 9 shows m_b vs distance for the 51 stations in Tables III and IV which have P amplitudes. The average m_b, obtained by averaging the 51 individual magnitudes without weights, is 6.42; and the standard deviation about this average is 0.40.

Rayleigh-wave magnitudes for stations out to 100° distance were computed by the formula:

$$M_s = \log_{10}(A/T) + 1.66 \log_{10}\Delta - 0.18$$

-11-

where

> A = peak-to-peak ground motion (millimicrons),
>
> T = period (seconds),
>
> Δ = epicentral distance (degrees).

The value A is obtained by measuring the maximum peak-to-peak
amplitude on the record at a period T of about twenty seconds
and correcting for system magnification at T seconds. Figure
10 shows M_s vs distance for the 47 stations having LR ampli-
tudes in Tables III and IV. The average M_s, obtained as for
m_b, is 4.84; and the standard deviation is 0.28.

The fact that the M_s estimate has less variance than the
m_b estimate was also true for LONG SHOT. As for amplitudes, it
would be repetitious with the analysis of LONG SHOT magnitudes
to discuss MILROW magnitudes vs distance or region since we
examined the data and saw that it essentially duplicated
the LONG SHOT data.

Relative amplitude of MILROW and LONG SHOT

For purposes of determining a yield difference and of
perhaps detecting a change in the shape of the source spectra,
it is important to determine accurately the magnitude difference,
both m_b and M_s, between MILROW and LONG SHOT. To do this for
m_b, we measured the amplitude of the first compressional move-
ment from zero-to-peak for the two explosions at common stations
because this first quarter-cycle of motion should be uncontami-
nated with other arrivals (the surface reflection at the source
being the primary problem) and therefore clearly indicative
of relative source magnitude. Use of common stations eliminates

propagation effects. Only film was employed in this analysis; and for various reasons, mostly excessive amplitudes for MILROW or low film amplitudes for LONG SHOT, only nine stations provided reliable amplitudes for both events. The nine stations and the corresponding amplitude ratios are listed in Table V. The average of these ratios is 0.154, which represents an m_b difference of 0.81. These nine amplitude ratios form a sample large enough to determine the m_b difference, especially in consideration of the small standard deviation (0.019) of the ratios. We have neglected period in these measurements because there is no strong evidence for claiming that the MILROW periods for the first quarter-cycle are different than those of LONG SHOT at these nine common stations, and the inclusion of a period measurement to produce A/T would only introduce error into an already satisfactory measure of relative amplitudes. Also, on the assumption of equal periods, relative ground motion amplitudes were determined by dividing film amplitudes by the magnification at 1.0 cps always, regardless of actual observed period.

We can compare this precisely determined m_b difference of 0.81 between MILROW and LONG SHOT with the unadjusted m_b difference of 0.57 using all available data which resulted in an m_b of 5.85 for LONG SHOT (274 stations) and of 6.42 for MILROW as stated in the previous section (51 stations). Thus, routine m_b estimation from short-period recordings has produced a 0.24 error in the relative m_b difference between MILROW and LONG SHOT if we accept 0.81 as the correct m_b difference. Part of this error is due to the fact that different sets of stations were used to estimate

the magnitudes of the two explosions; and part is due to surface, and other, reflections which enhance or diminish the amplitudes of peaks after the first and distort the observed periods of maximum motion.

To determine relative M_s for MILROW and LONG SHOT, we employed the match-filter concept at all the common LRSM stations (except LC-NM which had a timing rate error on tape for the LONG SHOT recording period). LONG SHOT locations WH-YK, CR-NB, and PG-BC were changed to WH2YK, CR2NB, and PG2BC for MILROW; but the distance of the move was so small in comparison with Rayleigh wave lengths that we can consider these three pairs as common stations for the two events. Alexander and Rabenstine (1967) have shown how the size of one event can be found relative to that of a reference event used to match filter it by comparing the amplitude of the crosscorrelation peak for the two events with the amplitude of the autocorrelation peak for the reference event. We assume that the spectra are identical in shape so that the relative size of the two events remains constant with frequency for the band-limited signal on the long-period LRSM recordings. Signal-to-noise ratios for MILROW are about 10 while for LONG SHOT they are typically 1 to 2. Table VI lists the stations used in the match filtering and the amplitude of the LONG SHOT LR signals relative to those of MILROW obtained by match filtering. The average of the nine LR ratios in Table VI is 0.091, which implies an M_s difference of 1.04 between MILROW and LONG SHOT. For comparison, we have a M_s difference of 0.78 if we accept the routine magnitude estimate of 4.84 for MILROW as stated in the previous section (47 stations) and of 4.06 for LONG SHOT (55 stations). An examination of the visually-measured LR amplitudes as given in Table III of this

-14-

report for MILROW and in Table II of the LONG SHOT report reveals that the ratio of these amplitudes is about twice as high, on the average, as the ratios from the match-filter output given in Table VI. It is most likely that noise on these nine LONG SHOT recordings accounts for this doubling of the true LR amplitude; and, if we can extend this assumption to all other recordings of LONG SHOT, we can appreciate how the real magnitude difference of 1.04 is reduced to 0.78 using visual analysis of LONG SHOT since the logarithm of 2 is 0.30. We conclude that LONG SHOT should really be about M_s = 3.80 because we accept the visually-determined M_s estimate of MILROW to be 4.84 as obtained from all avaliable data and we accept the M_s difference of 1.04 as obtained by match filtering.

We have fixed the m_b difference between MILROW and LONG SHOT at 0.81 and the M_s difference at 1.04; thus there is a twofold increase in LR amplitudes for MILROW over what would be expected on the basis of the m_b difference, and the source spectrum as a whole has changed shape with a slight boost in long-period energy for MILROW compared to LONG SHOT. Source spectral shapes vs yield shown by von Seggern and Lambert (1969) predict such a result in the yields under consideration (100 to 1000 kt); we reproduce their granite curves in Figure 11. These curves indicate that M_s (at T≈20 secs) will always be directly proportional to the logarithm of the yield while m_b (at T≈1 sec) will level off at higher yields after increasing proportional to the logarithm of the yield up to about 100 kt. This M_s-vs-yield behavior is true for all geologic medium, but the exact relation of m_b to yield will vary with medium. If we assume that the predicted yields of LONG SHOT (80 kt) and MILROW (1000 kt) are good estimates of the actual yields, our

M_s difference (1.04) agrees very well with the difference (1.10) of the logarithms of the yields. Also, we see that the 0.81 m_b difference between LONG SHOT and MILROW agrees very well with the difference of the logarithms of the spectral amplitude at a period of one second for 1000 and 80 kt shots in granite, approximately 0.80 in Figure 11. Thus magnitude-yield scaling at Amchitka on the basis of these two shots follows closely the predictions for both short and long periods given by von Seggern and Lambert who used the source-spectrum scaling theory of Haskell (1967). It should be mentioned that Haskell used empirical measurements from very small (<5 kt) explosions to formulate theoretical predictions.

Haskell neglected depth of detonation in his theory, but Mueller and Murphy (1971) have derived the following long-period approximation which includes depth:

$$\frac{A_1}{A_2} = \left(\frac{d_2}{d_1}\right)^{.33} \left(\frac{Y_1}{Y_2}\right)^{.87}$$

where A is the amplitude, d is the depth, and Y is the yield of an underground explosion. This applies only to events detonated in the same medium, and this condition is not strictly satisfied by LONG SHOT and MILROW. Using the given values of depth and yield, the amplitude ratio A_1/A_2 for LONG SHOT to MILROW is .134 which implies a M_s difference of 0.87. This is somewhat smaller than the 1.04 difference determined by match filtering above. Thus Amchitka M_s-vs-yield data

-16-

agree better with Haskell's predictions; however, since Mueller and Murphy convincingly establish depth dependency in their formulation, the closer agreement of Haskell's theory with the data may be due to a fortuitous set of parameters for the two shot sites on Amchitka. We are not fully satisfied that a theoretical M_s-vs-yield relation has been established.

For the case of m_b, Mueller and Murphy provide a depth-dependent scaling theory which, although it is impossible to assign exact values to all the pparameters, indicates an m_b difference between LONG SHOT and MILROW which is less than the 0.80 predicted by Haskell's simple theory. Again the parameters at the two sites may be fortuitously valued, such that Haskell's predictions agree better with observations; and we do not accept as established any m_b-vs-yield theoretical scaling relation.

APPLICATION OF DIAGNOSTIC CRITERIA TO MILROW AND ITS
COLLAPSE WITH REFERENCE TO LONG SHOT AND EARTHQUAKES

The purpose of this section is to compare the MILROW
explosion and its collapse to the LONG SHOT explosion, and
to earthquakes, using diagnostic criteria developed primarily
from NTS explosions and from earthquakes in the Western United
States. These diagnostics placed LONG SHOT in the explosion
population although severe travel-time bias caused such great
errors in epicenter position and depth that location by itself
would not have identified it as an explosion. MILROW suffered
the same location bias (Location Using Teleseismic P Arrivals
Section). However, the surface-reflected pP phase for both
MILROW and LONG SHOT indicate shallow source depths in close
agreement with the known depths of detonation. These depths
suggest explosion sources. All the diagnostics used for LONG
SHOT place MILROW in the explosion population. The same
diagnostics tend to place the MILROW collapse in the earthquake
population. If one knew that LONG SHOT was an explosion, then
MILROW is positively identified as such because of its epi-
center and depth position determined using LONG SHOT anomalies
and because of its close similarity to LONG SHOT in its entire
seismic signature. We will now discuss in detail the applica-
tion of the various diagnostic criteria to MILROW and its
collapse. Basic seismic data on the collapse are given in
Table VII.

Location and depth of focus

Since location and depth of focus, determined independently

-18-

of the seismic signature, are such unique and powerful discriminants, we consider these first.

Using raw arrival times, MILROW, just as LONG SHOT, was located at sea and well into the upper mantle (Locations Using Teleseismic P Arrivals Section); this result alone would cause one to suspect it was an earthquake. If travel-time anomalies determined from LONG SHOT are employed, the MILROW location is only 1.2 km from ground zero. However, even with the LONG SHOT anomalies, a depth-free run of SHIFT with the 73 stations used in the Locations Using Teleseismic P Arrivals Section resulted in a -10.6 km depth (minus meaning above the surface) compared to a 66 km depth using raw arrival times. Thus, with precisely-known time anomalies, the depth of MILROW is not estimated as accurately as the areal location, although the -10.6 km depth certainly implies an event close to the surface. Large depth and origin time instability in location is acknowledged for raw arrival times; for the case of MILROW some improvement in this error has resulted from the application of LONG SHOT travel-time anomalies. Chiburis and Ahner (1970) have documented the depth estimate improvement found at NTS using relative travel-time anomalies on many events, and this improvement at Amchitka is about the same.

For the collapse, only six P-wave arrival times, these being dubious, were available for location. Even using LONG SHOT anomalies, the collapse located 77 km away from ground zero, at a depth of 86 km.

Cohen (1970) has shown how detonation depth of a nuclear explosion can be determined from the spectra of the P arrival and P coda. This method yielded a depth estimate of LONG SHOT

only 30 per cent greater than the actual depth of 702 meters.
The method involves averaging P-wave spectra from as many
stations as possible to suppress noise, and then using the
average spectrum to obtain the delay time associated with the
surface-reflected pP by measuring the periodic undulation in
the spectrum due to pP-P interference. The output presented
here consists of the average power spectrum from many stations
(individual spectra are normalized to 1.0 before summing) and
the dot-product of the pseudo-autocorrelation and cepstrum
functions. Results for MILROW, MILROW collapse, and LONG SHOT
are shown in Figure 12. The final spectra were formed by
averaging 17 LRSM and VELA station spectra for MILROW, six
spectra for MILROW collapse, and 27 spectra for LONG SHOT.
Further, the average spectra from 17 sub-array center instru-
ments at LASA for MILROW, MILROW collapse, and LONG SHOT are
shown in Figure 13. The most prominent negative peak that
appears in the dot-product trace at time τ provides an
objective measure of the periodic spectral minima due to
the interference of pP with P. This delay time τ is related
to depth by

$$d \approx \frac{\tau \overline{V}}{2}$$

where $\overline{V}$ is the average compressional-wave velocity of the shot
overburden. For the LONG SHOT site, $\overline{V}$ was determined to be
3.48 km/sec from an uphole time of 0.202 sec reported by Day
and Murrell (1967). For the MILROW site, an uphole time of
0.320 sec (W.R. Perret, Sandia Corp., personal communication)
for the explosion gives an average overburden velocity of
3.73 km/sec, which agrees well with the bore-hole velocity survey

(Snyder, 1969). From Figure 12, τ = 0.65, 0.65, and 0.50 for MILROW, MILROW collapse, and LONG SHOT respectively. Thus the depth for MILROW and MILROW collapse can be estimated as 1.210 km which is nearly equal to the actual depth of 1.216 km. For LONG SHOT the depth estimate with τ = 0.50 is 0.870 km, 24% greater than the actual depth of 0.702 km. This latter result disagrees slightly with the result given in the LONG SHOT report because of certain refinements in the cepstral analysis and the fact that previously τ = 0.55 secs was used for the LONG SHOT delay time. The delay time τ can be estimated to no greater than 0.05 sec since the digitizing rate for the time series is 20 samples per second, and in fact the choice between 0.50 and 0.55 is somewhat arbitrary. In Figure 13, which shows the analysis for LASA sub-array centers, τ's of 0.60, 0.60, and 0.50 second are indicated for MILROW, MILROW collapse, LONG SHOT respectively. The values of τ using LASA only for the three events as seen in this figure are identical or nearly identical to those using all LRSM and VELA station (including LAO) spectra averaged together as shown in Figure 12.

Since the cepstral analysis leading to the dot-product trace is merely a means of detecting the undulation in the spectra caused by pP interference, it is not necessary to utilize it if the troughs, especially the first one, are readily apparent in the spectra. Cohen emphasizes that where τ is of the order of 0.5 or less, the first spectral trough will be at 2.0 cps or greater with further periodic troughs hidden by noise; and the dot product estimate of τ may be unreliable. In the case of MILROW and LONG SHOT the first spectral troughs are readily apparent in Figure 12 at about 1.2 cps and 1.8 cps respectively. Then, since τ = 1/f, delay times of .83 and .56 seconds result for MILROW and LONG SHOT

respectively. These give depths of 1.550 km for MILROW and 0.970 km for LONG SHOT, which are actually poorer estimates than obtained from the dot-product trace. We have no good explanation of why the pP analysis has given depths which exceed the true depths here. For the collapse, the summed spectrum in Figure 12 shows no apparent trough and no energy beyond 1.4 cps; this means the depth estimate from the cepstral analysis is suspect.

One further aspect of the depth discriminant is the lack on MILROW recordings of observed depth phases distinctly arriving several seconds after P motion. Identification of such a phase would indicate a crustal or upper mantle earthquake. However, many shallow earthquakes do not produce observable pP phases, and absence of pP alone cannot be used to classify an event as an explosion.

All location and depth information taken together is inconclusive in identifying MILROW as an explosion. Without the benefit of LONG SHOT calibration, the MILROW depth estimate of 66 km implies an earthquake even though spectral analysis supports about a 1.5 km source depth. Spectral analysis in itself cannot be decisive since occasional earthquakes at all depths may have mechanisms that would produce phases with small time delays relative to P right at the source. But the -10.6 km depth from relative travel-time location and the success of spectral analysis in finding pP corresponding to a near-surface event together lend credence to the idea that this new event on Amchitka Island was an explosion if one had no independent information on MILROW.

M_s vs m_b

Using the MILROW magnitude estimates made with all the
available stations (Magnitude Section) of M_s = 4.84 and
m_b = 6.42 and the MILROW collapse average magnitudes from
Table VII of M_s = 4.06 and m_b = 4.20, these M_s vs m_b points
are compared in Figure 14 with those from LONG SHOT and
shallow Aleutian Island earthquakes. Also included in
Figure 14 is a M_s vs m_b relation (Lambert, 1971) for 39 NTS
events which illustrates the absolute necessity of regionalizing
the M_s vs m_b discriminant. The important fact is that, regard-
less of their relation to NTS shots, Amchitka shots separate
clearly from shallow earthquakes in the surrounding region.
This result would not be changed if the m_b of MILROW were
changed to agree with the relative m_b differences from LONG
SHOT as obtained in the Magnitude Section; in fact, such
correction would enhance MILROW's separation from the earth-
quakes in Figure 14. As stated in the Magnitude section we
regard M_s of MILROW to be well-determined because of the
high signal-to-noise ratios. In the same section, it was
shown that the M_s of LONG SHOT should be revised downward;
this would further separate LONG SHOT from earthquakes.

The MILROW collapse with an M_s equal to that of LONG SHOT
and an m_b over an order of magnitude lower is in the far
extreme of the earthquake population of Figure 14. An expla-
nation of the M_s-m_b character of collapses is the prolonged
mechanism of these events which is explained in detail by
Houser (1969). He suggests a time duration of "several seconds
to several tens of seconds", depending on the medium, for the
process of collapse. Smith (1963) and Toksoz et al. (1964)
both conclude from far-field seismic evidence that the rise-
time and duration of the collapse displacement-time function

-23-

is greater than that of explosions. This mechanism would tend to produce small body waves since short-period energy is generated incoherently over several seconds, but long-period energy is essentially in phase and additive even if the duration is several seconds.

Shear waves

Short-period SH/P ratios (horizontally-polarized shear A/T to compressional A/T) determined for MILROW from four stations give an average ratio of 0.16 (Table VIII). Shillong, India, recorded an SH; but the P amplitude was too large to be read. For LONG SHOT, the one observation of a short-period SH phase was at Shillong; and this gave a SH/P ratio of .076. Thus no direct comparison between MILROW and LONG SHOT is possible for short-period SH excitation.

Long-period SH and SV were observed at five stations for MILROW, but only three of these stations recorded long-period P motion. For these three, long-period SV/P ratios range in value from 1.30 to 5.17; and the single available long-period SH/P ratio, at FB-AK, is 2.79 (Table VIII). No long-period shear phases were observed on LONG SHOT recordings, and so no comparison can be made for long-period SH excitation.

For MILROW, twelve stations from Table III had observable LQ waves, and the LQ/LR average ratio from these (Table IX) is 0.56. (Note that no LQ/LR ratio could be formed at FB-AK because LR was clipped.) For LONG SHOT and the MILROW collapse, Love waves were detected and measured by the match-filter technique. This will be discussed more fully in the Tectonic Strain Release Section in conjunction with the question of tectonic strain release. Basically, the results gave LQ/LR

-24-

ratios for LONG SHOT and the collapse which were about equal to and about one-third of, respectively, the ratio for MILROW.

For comparison with MILROW long-period and short-period SH/P and LQ/LR ratios, Tables VIII and IX give similar ratios taken from stations recording BENHAM and BOXCAR, two large-yield NTS underground explosions; these values show no significant difference between the Amchitka and NTS areas in regard to the amount of horizontally-polarized shear energy generated relative to compressional energy. Movement along known faults has been triggered by both these NTS explosions (McKeown and Dickey, 1969) implying strain release as the mechanism for shear excitation. McKeown et al. (1970) report smaller observed movements along surface faults and fractures for MILROW than for NTS events, but large (tens of centimeters) elevation changes indicative of normal faulting at depth. So tectonic strain release may have played a role in shear-wave generation for MILROW also.

It remains to compare MILROW SH/P and LQ/LR ratios with earthquakes. We have for MILROW a short-period SH/P ratio of 0.16, an average from four stations; a long-period SH/P ratio of 2.79, from a single station; and a LQ/LR ratio of 0.56, from eleven stations. Unpublished data at the SDL taken from LRSM van and VELA observatory earthquake bulletins, comprising data on thousands of earthquakes, shows that recordings at these stations have on the average a short-period SH/P of 2.5, a long-period SH/P of 2.0, and a LQ/LR of 0.7. Thus MILROW's short-period SH/P ratio is over an order of magnitude smaller than typical earthquakes while the long-period SH/P and LQ/LR ratios are not significantly different from

corresponding earthquake average ratios. Still, the long-period P and S phases from MILROW are about an order of magnitude smaller than similar phases for earthquakes of equivalent m_b, as are the LR waves.

To regionalize the shear discriminant, we measured shear and compressional phases on recordings of the VELA observatory UBO from over a hundred earthquakes having epicenters in the Aleutian Islands. We found that the average short-period SH/P ratio was 1.21 for earthquakes, about one-half the world-wide average given above. Compare this again with the average short-period SH/P from four stations of 0.16 for MILROW. We mention that no single earthquake of those analyzed had a short-period SH/P ratio $\lesssim$ 0.16. Thus short-period SH/P offers a good diagnostic for identifying explosions in the Aleutian region. With the same data base of Aleutian Island earthquakes, an average long-period SH/P ratio of 1.86 emerged, about the same as the world-wide average given above; the MILROW long-period SH/P ratio of 2.79 (one station) is larger and does not provide any diagnostic aid.

Complexity

The ratio of energy in the P-wave coda to that in the first few seconds after the intitial P impulse was suggested by Carpenter (1965) as an aid to discrimination. The SDL has routinely calculated this ratio, termed "complexity", for many events over the past several years; and a detailed explanation of this calculation is found in the LONG SHOT report. MILROW complexities (F_c) for seventeen stations are plotted as a function of distance in Figure 15. Complexities

for LONG SHOT and the MILROW collapse at stations common with any of these seventeen are also plotted in Figure 15. All these complexity values are listed in Table X.

Comparison of ten common station complexities for MILROW and LONG SHOT shows similar complexity values. The ten-station average complexity for MILROW is 3.34 and for LONG SHOT is 3.16. These averages include complexity values from stations at slightly different locations: WH2YK, PG2BC, and CR2NB for MILROW vs WH-YK, PG-BC, and CR-NB for LONG SHOT. We cannot account for the large difference in complexities at BE-FL between MILROW and LONG SHOT.

Comparison of six common-station complexities between MILROW and MILROW collapse shows that the collapse is much more complex than the explosion. The common-station average complexity for MILROW is 2.55 and for the collapse is 6.25.

Thus, as expected, the complexities for MILROW are approximately equivalent to those of LONG SHOT. Further, the collapse is about 2.5 times more complex than either MILROW and LONG SHOT; this is explained by our previously stated (in the Application of Diagnostic Criteria Section) concept of the collapse mechanism which must be of greater time duration to account for much greater energy arriving in the P coda than for the explosion. The LONG SHOT average complexity (2.51) is about one-half that of an Andreanoff Island earthquake (4.53) recorded at common stations as determined by Lambert et al. MILROW, with an average complexity nearly equal to LONG SHOT, could be distinguished from this earthquake also on this basis; but the MILROW collapse average of 6.25 would place it above this earthquake in complexity.

P-wave spectra

Comparison of the P-wave spectra for MILROW, MILROW
collapse, and LONG SHOT at common stations should exhibit
primarily differences in source functions and depth since
these three events share the same or nearly the same epi-
center and thus have identical path and site effects on their
signals. One factor in the scaling and identification problem
is the relative content of longer-period to shorter-period
energy as a function of magnitude. However, interference by
pP causing spectral minima, as discussed in the Application
of Diagnostic Criteria Section, can complicate the P-wave
spectra.

To obtain spectra for this report, Fourier amplitude
coefficients are computed for a signal and a noise sample of
equal length; then the noise and signal coefficients are
squared and the noise spectrum subtracted. The resultant
spectrum is reduced to an amplitude spectrum corrected for
system response and static magnification. The spectrum is
then plotted for a frequency band of 0.2 to 6.0 cps in terms
of acceleration density ($m\mu/sec^2/cps$). Signal sample lengths
range from 2.5 to 5.3 secs (real time) after the first
detectable motion of P. Spectra for MILROW and LONG SHOT
for nine common stations are shown in Figure 16. Nine
additional spectra for MILROW are shown in Appendix I.
Six spectra for the MILROW collapse are shown in Figure 17.
These figures also show the corresponding signal transformed.

Comparison of the waveforms and spectra among events at
common stations show significant differen even though
path and recording site are nearly identi . These results
clearly indicate substantial differences in the source-time

-28-

function, depth of detonation, or geological structure at the event sites.

Spectral amplitude ratios for MILROW and MILROW collapse are determined, as for LONG SHOT, thus:

$$S_1 = \sum_{f_1}^{f_2} A(f_i) / \sum_{f_3}^{f_4} A(f_i)$$

$A(f_i)$ = value of the amplitude spectrum at each 0.1 cps,

f_1 = 0.5 cps,

f_2 = 1.0 cps,

f_3 = 1.1 cps,

f_4 = 2.0 cps.

These ratios are listed in Table XI and show more energy for MILROW in the longer-period portion of the spectra relative to LONG SHOT. Further, the collapse ratios show about the same amount of longer-period energy as MILROW. However, the signal-to-noise ratios for the collapse P-waves are low, and the spectral estimates are not as accurate as those for MILROW and LONG SHOT. Comparing ratios indicates that they are higher by a factor of two to three for MILROW except at PG-BC and KN-UT. Here PG-BC for LONG SHOT is high due to an anomalously low signal-to-noise ratio. We cannot explain the relationship of ratios at KN-UT other than to suggest that the P amplitude for MILROW may have exceeded the linear portion of the dynamic range of the instrument since the P-wave magnitude is nearly an order of magnitude greater

than the mean for MILROW (Table III). It is clear that MILROW does show more longer-period energy in the P-waves relative to LONG SHOT on the basis of the S_1 ratio alone.

Figure 18 compares the average spectra at 18 stations for MILROW and 27 stations for LONG SHOT. To obtain the average, the basic amplitude spectra were squared and normalized so that the shape of the spectrum at each station would be given equal weight. These normalized spectra were summed, multiplied by frequency squared, and divided by the number of stations to obtain the average energy spectrum for each event. In Figure 18 we point out the presumed periodic spectral troughs associated with pP interference; since data above 4 cps may merely be earth noise or spectral leakage, troughs at these higher frequencies may be spurious. At the low frequency end, because the short-period spectral estimates are determined from signal samples of about 3.0 to 5.0 secs, the spectra are generally not reliable below 0.33 cps. Theoretical source energy spectra for granite and tuff at 100 and 1000 kt using scaling parameters and equations from von Seggern and Lambert (1969) are shown in Figure 19. We include spectra for MILROW and LONG SHOT formed by connecting peaks in the energy spectra in Figure 18 with smooth lines; these spectra are positioned on the abscissa of the graph relative to each other and to the theoretical spectra only for comparison of spectral shapes. The peak frequency for MILROW is lower than that for LONG SHOT. Frequency-dependent attenuation would be expected to shift the real peaks to lower frequencies than the theoretical ones, and in the case of LONG SHOT the nulling at 1.85 cps due to the interference of pP could also give an apparent shift to a lower frequency. Below 1 cps the slopes of the observed spectra roughly

correspond to the predicted; however, for the higher frequency portion (1 to 4 cps) they do not, and attenuation increasing with frequency should account for this. Beyond 3 cps much of the energy may simply be leakage from the spectra at lower frequencies because of the rectangular time window used. In any case the peak frequencies do show the predicted shift as a function of magnitude or yield; this shift has been previously documented for lower yields by Berg and Papageorge (1964).

Regarding the identification problem, short-period spectral amplitude ratios for many Asian earthquakes and explosions have been determined at LASA by Lacoss (1970) using ten-second samples. These ratios are computed as follows:

$$S_2 = \int_{1.45}^{1.95} A(f)df / \int_{0.35}^{0.85} A(f)df$$

The MILROW ratio computed on this basis is 0.90 with a magnitude of 6.72 at LAO, and the MILROW collapse ratio is 0.16 with a LASA-beam magnitude of 4.22. We show both these ratios plotted with those of Lacoss in Figure 20. MILROW clearly falls into the explosion population as did LONG SHOT, and the collapse falls well into the earthquake population.

Therefore, MILROW P-wave spectra behave as expected for explosions. The collapse ratio at LASA shows the collapse to be typical of earthquakes; but as Table XI shows the six collapse spectral ratios are highly variable, and the low signal-to-noise values for this event makes spectral ratios, and thus discrimination based on them, dubious.

-31-

Rayleigh-wave spectra

von Seggern and Lambert (1969) have indicated that for explosions the shape of the theoretical source spectrum in the frequency band of 0.067 cps (T = 15 sec) to 0.020 cps (T = 50 sec) should not change with magnitude. Therefore MILROW and LONG SHOT, having virtually the same epicenter, should have identical Rayleigh-wave spectra at common stations. With regard to collapse mechanisms, Houser (1969) suggested a time duration of several seconds to tens of seconds which is dependent upon the medium. There is evidence from the short-period P-wave spectra at LASA and LRSM stations (Figures 12 and 13) that more longer-period energy is present for the collapse relative to MILROW. Further, the M_s-vs-m_b relationship also implies that the source function is extended over a greater span of time than for explosions. Thus, we expect more longer-period energy in Rayleigh-wave spectra for the MILROW collapse relative to MILROW and LONG SHOT.

Rayleigh-wave amplitude spectra are estimated in the same manner as described in the preceding section on P-wave spectra for velocity windows of about 3.7 to 2.5 km/sec. Spectral estimates for twelve stations common to MILROW and LONG SHOT are shown in Figure 21, again in terms of accleration density. Seven additional spectra for MILROW are shown in Appendix II. The shapes of the spectra are very similar for five of the twelve common stations (PG-BC, KN-UT, RK-ON, TFO, HN-ME) for MILROW and LONG SHOT in the frequency band 0.020 to 0.067 cps; however, as stated previously, the signal-to-noise ratios for LONG SHOT ranged from one to two and thus the LONG SHOT spectra are greatly affected by the

-32-

noise. The average normalized energy spectra for the twelve common stations in Figure 22 show that MILROW and LONG SHOT are similar within the frequency band of about 0.02 to 0.075 cps. (Average normalized energy spectra are determined as described in the preceding section.) At higher frequencies, 0.075 to 0.10 cps, the noise dominates the spectra for LONG SHOT and comparison with MILROW is impossible.

Thirteen Rayleigh-wave spectral estimates for the MILROW collapse are shown in Figure 23. Here most of the spectra correspond to MILROW with respect to the positions of spectral maxima and minima, but most also show much more longer-period energy. The average normalized energy spectra for MILROW and the collapse, Figure 24, clearly illustrates this fact.

Energy ratios between adjacent bands of frequency for Rayleigh waves have been used by Lambert and von Seggern (1969) as an aid in the identification problem. For events recorded at distances greater than 1000 km and M_s greater than 3.0, their preferred ratio, $\bar{R}_1$, is determined as follows:

$$\bar{R}_1 = \frac{1}{n} \sum_{m=1}^{n} \left(\int_{f_1}^{f_2} E_m(f)\,df \Big/ \int_{f_2}^{f_3} E_m(f)\,df \right)$$

where $\bar{R}_1$ equals the average energy ratio for n stations recording one event and E_m is the energy spectrum at station m. The limits of integration are:

$$f_1 = 0.0208 \ (T_1 = 48 \text{ seconds}),$$

$$f_2 = 0.0455 \ (T_2 = 22 \text{ seconds}),$$

$$f_3 = 0.0667 \ (T_3 = 15 \text{ seconds}).$$

Calculated ratios for MILROW, LONG SHOT, and the MILROW collapse are plotted as a function of magnitude in Figure 25. Explosion ratios are independent of magnitude only if the signal-to-noise ratio is high enough to allow a valid analysis. The Rayleigh-wave magnitude for this figure is determined from the spectral estimates by having the computer pick the maximum A/T in the ground velocity spectrum between periods of 17 and 23 seconds and use this value in the standard M_s formula given in the Magnitude Section. Therefore these magnitudes will usually differ somewhat from those determined from film analysis.

In Figure 25 $\bar{R}_1$ determined from 19 stations for MILROW is clearly in the explosion population which forms a horizontal band at $\bar{R}_1 \approx 0.1$. In addition, the value is nearly equal to that of LONG SHOT. $\bar{R}_1$ determined from 13 stations for the MILROW collapse is greater than $\bar{R}_1$ for MILROW and, in fact, greater than $\bar{R}_1$ for any Aleutian earthquake analyzed. Thus $\bar{R}_1$ shows that the observed MILROW Rayleigh-wave spectrum in the 15 to 50 seconds' band is similar to other explosions while the collapse spectrum is definitely not.

Although the Rayleigh-waves at individual stations common to both MILROW and LONG SHOT do not show exactly identical spectra, mostly due to the low signal-to-noise ratios for LONG SHOT, the average spectral ratios do show that the energy in

adjacent bands of frequency (0.028 to 0.0455 and 0.0455 to
0.0667) are about equal. With regards to the collapse and
MILROW, the similarity in positions of maxima and minima at
individual stations plus similarity of spectral shapes at
shorter periods indicates similar radiation patterns between
events. The presence of more longer-period energy in the
collapse signals suggests a longer time function or larger
spatial dimensions for the source. We can certainly eliminate
the second possibility from mere physical intuition of the
collapse mechanism and from its smaller magnitude as reflected
by M_s or m_b.

Radiation patterns

Amplitude and phase radiation patterns of seismic energy
from the source have been utilized very little in discrimina-
tion. One major difficulty is that, in determining radiation
patterns for short-period or long-period waves, the influence
of path and recording site on amplitudes must be minimized. We
do not feel that we have sufficiently accurate information on
these factors to undertake the proper amplitude equalization
of body and surface waves from MILROW. Figure 26 displays all
the available m_b values from Tables III and IV vs epicenter-
station azimuth in a polar plot; Figure 27 does likewise for
M_s. The distance-correction factors used in determining m_b
and M_s according to the standard formulas given in the Magnitude
Section are the only amplitude equalization applied. It is
apparent that, in addition to the erratic scatter of the data,
the azimuthal coverage is unsatisfactory in both cases; and
no radiation pattern can be inferred with confidence. The
systematically low values of M_s in the azimuth range of 60°-90°
(western, central, and southern United States stations), also

-35-

observed for LONG SHOT, are just as probably the result of
path and site effects as of a radiation pattern at the source.

In the LONG SHOT report P and LR radiation patterns of
LONG SHOT were fitted to theoretical patterns based on
double-couple force systems, and it was concluded that a
circular radiation pattern is as valid a fit as any non-
circular pattern associated with double-couple mechanisms.
Since we have examined the MILROW data in relation to LONG SHOT
with polar plots of amplitude ratios for body and surface waves
at all stations common to both events and have seen no good
indication of a different energy radiation pattern for MILROW,
we will extend this conclusion to MILROW without performing
the programmed radiation-pattern fitting. We show in Figure 28
the polar plot of LR and LQ ratios determined by match filtering
the LONG SHOT recordings with the MILROW signals as described in
the Magnitude Section and Application of Diagnostic Criteria to
MILROW and its Collapse with Reference to LONG SHOT and Earth-
quakes Section, respectively, and P-wave first-quarter-cycle
ratios determined by visual measurement as described in the
Magnitude Section. Since only one quadrant of this type of
data is available, any conclusions are entirely speculative;
however, we see no strong indication of radiation pattern
differences between LONG SHOT and MILROW here.

Other investigators (Brune and Pomeroy, 1963; Toksoz
et al., 1965) have used explosion-collapse ratios at NTS
to delineate better the explosion radiation patterns with
the assumption that the collapse released no tectonic strain
and so had a circular radiation pattern. We do not attempt this
for MILROW because again the available values would be confined
to less than one quadrant and also because we have already found

-36-

by match filtering LQ waves that the MILROW collapse did generate horizontally-polarized shear waves and was therefor not an event with a circular pattern.

One further aspect of radiation patterns is first motion, which can only reliably be used to identify earthquakes and not explosions. The absence of rarefactional first motions for a suspicious event may only mean that the recording coverage was incomplete rather than that it was an explosive source; on the other hand, the presence of clear rarefactional first motions for an event positively identifies it as an earthquake. Evernden (1969) has pointed out that the lack of rarefactional first motions outside USSR and China is characteristic of Kamchatka/Kuril earthquakes because of the orientation of the fault planes and the slip vectors. No rarefactional first motions were observed for MILROW; however, for the reason just given, this is only a feeble diagnostic aid, and its improvement as a diagnostic aid for this source region requires the study of many earthquakes in the area surrounding Amchitka. P waves from the MILROW collapse, recorded at only six stations (Table VII), were too low in signal-to-noise ratio to determine direction of first motion.

Radiation pattern analysis, including first motion, will be a marginal aid to discrimination in the Aleutian source region until precise information on path effects can be assembled, more earthquake mechanism solutions for this region become available, and, perhaps most important, better azimuthal recording coverage with LRSM-quality stations is supplied.

Synopsis of diagnostics

We have applied the principal diagnostic criteria to the

-37-

MILROW event and to its collapse, and we will summarize this
investigation in a tabular format where each diagnostic pro-
vides a decision on whether the event was an explosion. Most
diagnostics did not provide unambiguous answers and this will
be indicated by question marks. Application of diagnostics on
a regional basis is more meaningful than on a global basis, and
we have attempted to regionalize discrimination for M_s-vs-m_b
and for shear excitation by presenting the results for many
Aleutian earthquakes. All the other diagnostic aids suffer
from lack of Aleutian earthquake analysis in respect to these
diagnostics; however, such analysis would require a great
expenditure of time. For LONG SHOT, one shallow earthquake
of equivalent m_b in the Andreanoff Islands was studied in
detail and compared with LONG SHOT; we will weigh the answer
to some of the classification questions by comparison of MILROW
and its collapse to LONG SHOT and by the differences between
LONG SHOT and this one earthquake.

Table XII, then, is the synopsis of the diagnostic criteria.
It shows that with the exception of location and depth, MILROW
is identified as an explosion by all the criteria although only
two are considered as unambiguous. With the assistance of LONG
SHOT travel-time calibration, the location-depth criteria would
also tend to classify it as an explosion. Also, with the
knowlege that LONG SHOT was an explosion, one would more
positively identify MILROW as an explosion via the other
diagnostics because of the similarity of these two events over
the entire seismic signature at all common stations. For the
collapse, mostly earthquake characteristics are indicated by
the diagnostics. The most powerful discriminant, M_s-vs-m_b, very
definitely places it outside the explosion population. It has
a complexity 2.5 times that of MILROW and greater than the

-38-

selected Andreanoff Islands earthquake previously mentioned.
Short-period and long-period spectral ratios, of lesser value
in discrimination, place it in the earthquake population.
Radiation pattern information for the collapse is uniformative
or, at best, vague. In other words, the MILROW collapse would
definitely not have been designated an explosion but may have
been designated as an earthquake from analysis of teleseismic
data alone. Only the inability to locate it accurately in
relation to MILROW because of small P-wave amplitudes at tele-
seismic distances prevents its designation as a collapse,
barring independent information on it, since as a whole its
seismic signal characteristics were as expected from a cavity-
collapse mechanism.

TECTONIC STRAIN RELEASE ON AMCHITKA ISLAND

It has been shown that seismicity in the Aleutians as seen by a local network is nearly void of shallow (<40 km) earthquakes along the island arc (Murdock, 1969). At Amchitka Island in particular, a very localized network of land and ocean-bottom seismometers revealed only infrequent and low-magnitude shallow shocks and only very proximate and weak seismicity around the MILROW site after the detonation (Engdahl and Tarr, 1970; Adams et al., 1970). The MILROW aftershocks were all confined to m_b below 3.4 (personal communication from E.R. Engdahl, NOS). Morris (1970) states that faults on Amchitka Island have been inactive for at least a quarter of a million years. Thus there appears to be little tectonic strain accumulation and release in the crust around the MILROW site. In contrast, strain accumulation in the crust of the NTS region is an accepted fact; release of this strain by shallow earthquakes is well documented (Molnar et al., 1969; Slemmons et al., 1965). Also attesting to a higher strain field at NTS are the aftershocks of many NTS explosions, notably BOXCAR, which had at least seven after-shocks with $m_b > 4.0$ (Boucher et al., 1969). Therefore, we believe that another type of shear-generating mechanism such as crack formation as discussed by Kisslinger et al. (1961) could have a significant, if not the dominant, role in pro-duction of horizontally-polarized shear waves observed on MILROW recordings. Again, we must state that without thorough near-source seismic measurements and geologic observations we cannot precisely define the mechanism of shear generation.

One piece of evidence which clearly demonstrates that MILROW Love waves cannot be due entirely to mode conversion

-40-

is that for the collapse the amplitude ratio of Love to Rayleigh waves was smaller than that of MILROW. The reasoning is that if conversion were to account for the Love waves, the relative conversion to Love waves should be equal for both the shot and the collapse. This argument has been used previously in the cases of HAYMAKER and MISSISSIPPI by Toksoz et al. (1965). The evidence is as follows. Both LONG SHOT and the MILROW collapse have an M_s = 4.06 from visual analysis. Thus the Rayleigh-wave magnitude difference of 1.04 between LONG SHOT and MILROW obtained from match filtering (Magnitude Section) also applies to MILROW and its collapse. Since Love waves were not visible on LONG SHOT and MILROW collapse recordings, match filtering was the only method to determine LQ/LR ratios. It was judged that only four MILROW LRSM stations had an LQ wavetrain of sufficient signal-to-noise ratio over a sufficient duration to use as a match filter: PG2BC, RK-ON, KN-UT, and SJ-TX. KN-UT was eliminated from the analysis because of a tape recording problem during the collapse surface-wave arrivals. Both LONG SHOT and MILROW collapse recordings at the remaining three stations were band-passed from .025 to .065 cps over the expected LQ arrival window. Horizontal traces for all recordings were rotated into a purely transverse component. The outputs of the match-filter program for these three stations are shown for LONG SHOT in Figure 29 and for the MILROW collapse in Figure 30. Love-wave amplitudes of the two events relative to those of MILROW were obtained from the match-filter outputs and are listed in Table XIII. From the figures it is evident that the LONG SHOT match-filter peaks near the predicted time on the last traces are more prominent than those from the collapse. (Predicted times for the match-filter peaks in

-41-

this and subsequent figures are based on the origin times given in Table I.) Note that the MILROW collapse peaks appear to be negative and about one-quarter to one-eighth cycle later than if the source functions for Love waves were 180° out-of-phase. A 180° phase reversal is well-documented for Rayleigh waves from explosion-collapse pairs (Brune and Pomeroy, 1963; Smith, 1963; Toksoz et al., 1964); but no explosion-collapse phase relation has been previously reported for Love waves, and in fact the authors are unaware of any previously reported detection of Love waves from a nuclear cavity collapse. To affirm this phase reversal for long periods between MILROW and its collapse, the collapse Rayleigh waves at the same three stations were match filtered with the MILROW Rayleigh-wave recordings. As shown in Figure 31, the peaks are definitely negative and again, as for the Love waves, approximately one-quarter cycle later than expected. Similar match filtering of LONG SHOT Rayleigh waves in Figure 32 shows the expected positive crosscorrelation peaks at approximatley the expected time. From Table XIII the average Love-wave amplitude ratio between LONG SHOT and MILROW is .109 implying a Love-wave magnitude difference of 0.96. This is nearly equal to the Rayleigh-wave magnitude difference of 1.04 between LONG SHOT and MILROW and is an interesting and important result. Whatever the shear-generating mechanism of MILROW was, LONG SHOT had a proportional amount, almost exactly scaled to the yield difference between the two. Again from Table XIII, the average Love-wave amplitude ratio between the MILROW collapse and MILROW itself is .035 implying a Love-wave magnitude difference of 1.46 which is .42 greater than the Rayleigh-wave magnitude difference between the two. And we regard the value .035 to be in error on the high side because a significant portion of the amplitude of the match-filter peaks in the correlation traces for the collapse must

-42-

be noise contributions (more than for the LONG SHOT peaks at least). Thus the MILROW collapse had an LQ/LR ratio of at least three times lower than LONG SHOT and MILROW itself, and we cannot accept mode conversion to explain completely Love waves from Amchitka events for this reason. The answer to why the MILROW collapse should have any Love waves at all may be: 1) some degree of mode conversion along the path; 2) non-circularity in the source space-time function; 3) inhomogeneity in the immediate source area; 4) peculiar geometry of bedding planes, joints, and faults around the MILROW shot point; 5) asymmetric release of MILROW-induced strain in the surrounding medium. The last reason is suggested because Engdahl and Tarr (1970) report that the MILROW collapse brought an abrupt cessation of MILROW aftershock activity as though the main collapse was the final event in the reduction of MILROW-induced strain in the surrouding medium to a value sufficiently small that no further sudden strain adjustments would occur. If the residual strain field from MILROW were asymmetric at the time of collapse, Love waves could be generated. However, we do not have sufficient evidence to prefer this explanation for collapse Love waves over any of the others listed above. Likewise, for MILROW itself (and LONG SHOT too) we cannot make definite conclusions about the shear-generating mechanisms. For the shots we can only state that mode conversion cannot account for all the Love wave amplitude and that tectonic strain release may not have been operative at all since the lack of shallow earthquakes under Amchitka Island, of recent natural fault movement, and of significant post-shot seismic activity indicates there may be no appreciable ambient tectonic stresses in the upper crust there.

-43-

RELATIVE DELAY TIMES FOR MILROW COLLAPSE
AND LONG SHOT SURFACE WAVES

The differences between actual and expected times for the match-filter output peaks in Figures 29 to 32 for LONG SHOT and the MILROW collapse deserve further attention.

In Figure 30 and 31 the negative collapse peaks are conspicuously later than expected if we assume that the source mechanism causes a polarity reversal relative to MILROW but that its source time function is nearly equivalent. On the other hand, the polarity reversal and the large time delay are both explained if we assume that the Rayleigh waves are generated by the impact of the collapsed cavity material on the floor of the cavity because a downward point force generates Rayleigh waves 180° out of phase with explosion-generated waves (Harkrider, 1964) and because the generation of high-energy Rayleigh waves could be delayed by the free-fall time through the cavity of material connected with the generation of weak initial P-waves which had emergent arrivals at teleseismic distances. The average delay of the negative peaks in Figures 30 and 31 is 5.0 ± 1.4 sec (95% confidence intervals), and the cavity diameter predicted by the formula of Closmann (1969) would be large enough to allow a delay of this much. This same phenomenon of Rayleigh-wave delay and polarity reversal has been found for the BENHAM cavity collapse (von Seggern, 1971).

The LONG SHOT match-filter peaks show advances from the predicted times in Figures 29 and 32, but only by a second or two. The predicted times do take into account the small differences in epicentral distance to the three stations PG-BC,

-44-

RK-ON, and SJ-TX from the two detonation points. The average time advance for the LONG SHOT surface waves in Figures 29 and 32 is 1.6 $\pm$ 1.0 (95% confidence intervals). Since we do not doubt the reported origin times, we believe some difference in the source functions related to yield, to interference of the pP phase, or to contrasts in the mediums immediately surrounding the two test sites is responsible for this result. The dependence of the phase spectrum of the source on yield can be derived from Haskell's (1967) representation of the source potential. The derivation is straightforward, but long, and we give only the final expression for the phase of the Fourier transform of the displacement-time function at the source:

$$\theta(\omega) = \arctan \frac{\omega k[(24B+1)(5\omega^4-10\omega^2 k^2+k^4)-(\omega^4-10\omega^2 k^2+5k^4)]}{\omega^2(24B+1)(\omega^4-1.0\omega^2 k^2+5k^4)+k^2(5\omega^4-10\omega^2 k^2+k^4)}$$

The parameter k scales as (yield)$^{-1/3}$ and the dimensionless parameter B is independent of yield; both are dependent on medium. We are interested in evaluating the phase lag at a period of 20 secs for yields of 80 and 1000 kt in hard rock. We used Haskell's values of k and B for granite and scaled k from his values for 5 kt. The phase lag of LONG SHOT was calculated to be .0454 radians while that of MILROW was .0959 radians at a period of 20 secs; this gives approximately a 0.2 second advance of the LONG SHOT waves relative to those of MILROW. This is then insufficient to explain the observed early arrival of LONG SHOT surface waves relative to those of MILROW. Thus, Haskell's scaling theory may not be right for

-45-

the phase spectrum or else medium contrasts and differences
in source depth may be causing the observed phenomenon.

SUMMARY AND CONCLUSIONS

The proximity of MILROW and LONG SHOT, their similar
detonation mediums, and their large yield difference enabled
us to obtain a limited magnitude-yield relation for the
Amchitka test area. Surface-wave magnitude scaled directly
proportional to the logarithm of the announced yields, a
result predicted by the work of Haskell (1967). The m_b
difference, not a simple function of yield, also agreed with
the predictions of Haskell. Because Haskell did not include
depth as a variable in his formuation, we regard as somewhat
fortuitous the excellent agreement between M_s and m_b observa-
tions and predictions based on his theory. The Amchitka scaling
appears to be parallel to NTS high-yield scaling for events in
tuff, but slightly higher m_b and much lower M_s for a given yield
on Amchitka are due to entirely different travel paths and
different geological environments in the Amchitka and Nevada
test sites. The fact that dominant periods for NTS Rayleigh
waves in North America are from 10 to 16 sec while those for
MILROW were from 17 to 25 sec greatly accentuates M_s for NTS
events relative to MILROW as shown by Evernden and Filson (1971).

Depth-unrestrained locations of MILROW with raw arrival
times revealed the same large (≈ 20 km) northward location bias
and the same depth error (≈ 70 km) that attended LONG SHOT.
Relative travel-time anomalies were determined for 73 LONG SHOT
stations which also recorded MILROW; application of these
anomalies reduced the location error of MILROW to 1.2 km along
the surface and to -11.8 km in depth (the location having been
made above the earth's surface). So, although relative travel-
time anomalies provide horizontal location accuracy, they still
fail to provide a precise depth estimate. This, however, is not
surprising because of the inherent depth and origin time
instability in the location algorithm.

-47-

Relative magnitudes for MILROW and LONG SHOT were found by measuring the amplitude of the first quarter-cycle at selected common stations in the case of P waves and by measuring the match-filter crosscorrelation peak of LONG SHOT and MILROW and the autocorrelation peak of MILROW in the case of Rayleigh waves. In this way the m_b of MILROW was found to be 0.81 higher than that of LONG SHOT, a figure which is 0.24 greater than the m_b difference found by averaging for each event all the available m_b values determined in the routine manner. Likewise, the precision M_s difference from match-filter processing was 1.04, a figure 0.31 greater than the M_s difference found from routine visual analysis.

Both short-period and long-period instruments recorded direct shear phases from MILROW; horizontally-polarized shear motion was positively identified in some cases. Also, MILROW Love waves were detected at many stations. The detection of previously unseen Love waves from LONG SHOT followed when MILROW recordings were used as match filters. It was surprising, however, to detect Love waves from the MILROW collapse when the same match-filters were applied because detection of Love waves from collapses has never been reported. Release of MILROW-induced strain is a plausible explanation for the collapse Love waves. Also crack formation; mode conversion; source asymmetrics; local geologic inhomogeneities; and the geometry of bedding planes, faults, and joints may account for these recorded Love waves from the collapse. For MILROW itself, due to the absence of shallow earthquakes in the Aleutian region and the limited aftershock activity, we conclude that the above various processes suggested as possibly operative for the collapse caused the shear motions

observed and not tectonic strain release commonly associated with NTS shots.

In the identification problem, MILROW behaved as expected from the authors' previous knowledge of explosion signals and in particular from our study of LONG SHOT characteristics. We would identify MILROW as an explosion, especially if comparisons with LONG SHOT are made. On the other hand, the MILROW collapse definitely does not classify as an explosion. An adequate summary of the individual diagnostics has already been given in Table XII.

The major conclusions of this analysis are as follows:

1) The Amchitka source region has been adequately calibrated with respect to P travel times.

2) Source-spectra vs yield scaling has followed Haskell's predictions closely. In determining this scaling, precise relative magnitude differences should be obtained by measuring initial P-wave excursions at common stations and from Rayleigh-wave match-filter outputs.

3) While tectonic strain release has been the preferred explanation for Love waves from NTS explosions, it probably does not have a large role in Amchitka explosions. Thus the shear-generating mechanism depends on the test area, and probably no general model is appropriate.

4) Diagnostic criteria, especially M_s vs m_b, developed primarily from NTS shots and Western United States earthquakes and from Asian events have worked well in the Amchitka region; however, if hypothetically we were required to identify further explosions in the Aleutians, a more comprehensive study of earthquakes in this region would be helpful.

REFERENCES

Adams, R.M., Linville, A. Frank and Joyner, Gerald L., 1970, Final Report - 1969 Aleutian Islands Experiment - Project MILROW: Texas Instruments, Inc., Services Group.

Alexander, S.S. and Rabenstine, D.B., 1967, Detection of surface waves from small events at teleseismic distances: Seismic Data Laboratory Report No. 175, Teledyne Geotech, Alexandria, Virginia.

Anderson, R.E., 1970, Tectonic setting of Amchitka Island, Alaska: United States Geological Survey Report No. USGS-474-75 (Amchitka-19).

Berg, Joseph W., Jr. and Papageorge, George, 1964, Elastic displacement of primary waves from explosive sources: Bull. Seismol. Soc. Am., v. 54, p. 947-959.

Blackford, M.E., Major, M.W. and Butler, D.L., 1970, Strain steps from the nuclear explosion MILROW: Abstract, American Geophysical Union Fall Meeting 1969, Trans., Am. Geophys. U., v. 51, p. 203.

Boucher, Gary, Ryall, Alan and Jones, Austin E., 1969, Earthquakes associated with underground nuclear explosions: J. Geophys. Res., v. 74, p. 3808-3820.

Brune, J.N. and Pomeroy, P.W., 1963, Surface wave radiation patterns for underground nuclear explosions and small-magnitude earthquakes: J. Geophys. Res., v. 68, p. 5005-5028.

Bucknam, R.C., 1969, Geologic effects of the BENHAM underground nuclear explosion: Bull. Seismol. Soc. Am., v. 59, p. 2209-2220.

REFERENCES (Cont'd.)

Carpenter, E.W., 1965, Explosion seismology: Science,
    v. 147, p. 363-373.

Chiburis, E.F., 1968, Precision location of underground nuclear
    explosions using teleseismic networks and predetermined
    travel-time anomalies: Seismic Data Laboratory Report
    No. 214, Teledyne Geotech, Alexandria, Virginia.

Chiburis, E.F. and Ahner, R.O., 1970, A seismic location
    study of station anomalies, network effects, and regional
    bias at the Nevada Test Site: Seismic Data Laboratory
    Report No. 253, Teledyne Geotech, Alexandria, Virginia.

Closmann, P.J., 1969, On the prediction of cavity radius pro-
    duced by an underground nuclear explosion: J. Geophys.
    Res., v. 74, p. 3935-3939.

Cohen, T.J., 1969, Determination of source depth by spectral,
    pseudo-autocovariance, and cepstral analysis: Seismic
    Data Laboratory Report No. 229, Teledyne Geotech,
    Alexandria, Virginia.

Day, J.D. and Murrell, D.W., 1967, Vela Uniform Project
    LONG SHOT: Ground and water shock measurement, United
    States Army Engineer Waterways Experiment Station,
    Vicksburg, Mississippi.

Davies, D. and McKenzie, D.P., 1969, Seismic travel-time
    residuals and plates: Geophys. J.R. Astr. Soc., v. 18,
    p. 51-63.

Engdahl, E.R. and Tarr, A.C., 1970, Aleutian seismicity -
    MILROW seismic effects: United States Department of Commerce,
    Environmental Science Services Adminstration, Report No.
    CGS-746-102.

REFERENCES (Cont'd.)

Evernden, J.F. and Filson, John, 1971, Regional dependence
    of surface-wave versus body-wave magnitudes, J. Geophys.
    Res., v. 76, p. 3303-3308.
Evernden, J.F., 1969, Identification of earthquakes and explo-
    sions by use of teleseismic data: J. Geophys. Res., v. 74,
    p. 3828-3856.

Evernden, J.F., 1970, Magnitude versus yield of explosions:
    J. Geophys. Res., v. 75, p. 1028-1032.

Gutenberg, B. and Richter, C.F., 1956, Magnitude and energy
    of earthquakes: Ann. Geofis., v. 9, p. 1-15.

Harkrider, D.G., 1964, Surface waves in multilayered elastic
    media. I. Rayleigh and Love waves from buried sources
    in a multilayered elastic half-space: Bull. Seismol. Soc.
    Amer., v. 54, p. 627-679.

Haskell, N.A., 1967, Analytic approximation for the elastic
    radiation from a contained underground explosion: J. Geophys.
    Res., v. 72, p. 2583-2587.

Herrin, Eugene and Sorrells, Gordon, 1969, Travel time models:
    Abstract, American Geophysical Union Annual Meeting 1969,
    Trans., Amer. Geophys.U., v. 50, p. 243.

Houser, F.N., 1969, Subsidence related to underground nuclear
    explosions, Nevada Test Site: Bull. Seismol. Soc. Amer.,
    v. 59, p. 2231-2251.

Jacob, K. H., 1970, P-residuals and global tectonic structures
    investigated by three-dimensional seismic ray tracing with
    emphasis on LONG SHOT data: Abstract, American Geophysical
    Union Annual Meeting 1970, Trans., Amer. Geophys.U., v. 51,
    p. 359.

REFERENCES (Cont'd.)

Kim, W.H. and Kisslinger, C., 1967, Model investigations of
    explosions in prestressed media: Geophys., v. 32, p. 633-
    651.

Kisslinger, C., Mateker, E.J., Jr. and McEvilly, T.V., 1961,
    SH motion from explosions in soil: J. Geophys. Res.,
    v. 66, p. 3487-3496.

Lacoss, R.T., 1969, A large-population LASA discrimination
    experiment: Lincoln Laboratory, Technical Note 1969-24.

Lambert, D.G., 1971, Relationship of body and surface wave
    magnitudes for small explosions and earthquakes: Seismic
    Data Laboratory Report No. 245, Teledyne Geotech, Alexandria,
    Virginia.

Lambert, D.G., von Seggern, D.H., Alexander, S.S. and Galat,
    G.A., 1969, The LONG SHOT experiment, Vol. I: Basic
    observations and measurements, Vol. II: Comprehensive
    analysis: Seismic Data Laboratory Report No. 234,
    Teledyne Geotech, Alexandria, Virginia.

Liebermann, Robert C., King, Chi-Yu, Brune, James N. and
    Pomeroy, Paul W., 1966, Excitation of surface waves by
    the underground nuclear explosion LONG SHOT: J. Geophys.
    Res., v. 71, p. 4333-4339.

McKeown, F.A. and Dickey, D.D., 1969, Fault displacement and
    motion related to nuclear explosions: Bull. Seismol. Soc.
    Amer., v. 59, p. 2253-2270.

McKeown, F.A., Dickey, D.D. and Bucknam, R.C., 1970, Pre-
    liminary analysis of geologic and geodetic data from
    the JORUM and MILROW nuclear events: Abstract, American
    Geophysical Union Fall Meeting 1969, Trans.,Amer. Geophys.
    U., v. 51, p. 203.

REFERENCES (Cont'd.)

Molnar, Peter, Jacob, Klaus and Sykes, Lynn R., 1969, Micro-
earthquake activity in Eastern Nevada and Death Valley,
California, before and after the nuclear explosion
BENHAM: Bull. Seismol. Soc. Amer., v. 59, p. 2177-2184.

Morris, R.H., 1970, A preliminary study of relic marine
terraces of the Western Aleutian Islands, Alaska:
United States Geological Survey Report No. USGS-474-54
(Amchitka 18).

Mueller, Richard A. and Murphy, John R., 1971, Seismic charac-
teristics of underground nuclear detonations: Part I,
Seismic scaling law of underground detonations, (in press).

Murdock, James N., 1969, Short-term seismic activity in the
central Aleutian Region: Bull. Seismol. Soc. Amer., v. 59,
p. 789-798.

Orphal, D.L., Spiker, C.T., West, L.R., and Wronski, M.D.,
1970, Analysis of seismic data - MILROW event:
Environmental Research Corporation, Report No.
NVO-1163-209.

Slemmons, D.B., Jones, A.E. and Gimlet, J.I., 1965, Catalogue
of Nevada earthquakes, 1852-1960: Bull. Seismol. Soc.
Amer., v. 55, p. 519-565.

Smith, Stewart W., 1963, Generation of seismic waves by under-
ground explosions and the collapse of cavities: J. Geophys.
Res., v. 68, p. 1477-1483.

REFERENCES (Cont'd.)

Snyder, Richard P., 1969, Preliminary lithologic log of
    drill hole UAe-2, Amchitka Island, Alaska: United
    States Geological Survey, Report No. USGS-474-52
    and USGS-474-53.

Tcksoz, M.N., Ben-Menahem, A. and Harkrider, D.G., 1964,
    Determination of source parameters by amplitude
    equalization of seismic surface waves. 1. Underground
    nuclear explosions: J. Geophys. Res., v. 69, p. 4355-4366.

Toksoz, M. Nafi, Harkrider, David G. and Ben-Menahem, Ari,
    1965, Determination of source parameters by amplitude
    equalization of seismic surface waves. 2. Release of
    tectonic strain by underground nuclear explosions and
    mechanisms of earthquakes: J. Geophys. Res., v. 70,
    p. 907-922.

United States Atomic Energy Commission, Nevada Operations
    Office, 1967, Consolidated data on selected effects from
    underground nuclear detonations, Flintlock Series,
    Vol. I: Emplacement Information.

United States Atomic Energy Commission, 1969, AEC Press Release,
    No. M-225, 24 September.

von Seggern, D.H. and Lambert, D.G., 1969, Dependence of
    theoretical and observed Rayleigh-wave spectra on
    distance, magnitude, and source type: Seismic Data
    Laboratory Report No. 240, Teledyne Geotech, Alexandria,
    Virginia.

von Seggern, David, 1971, Relative location of seismic
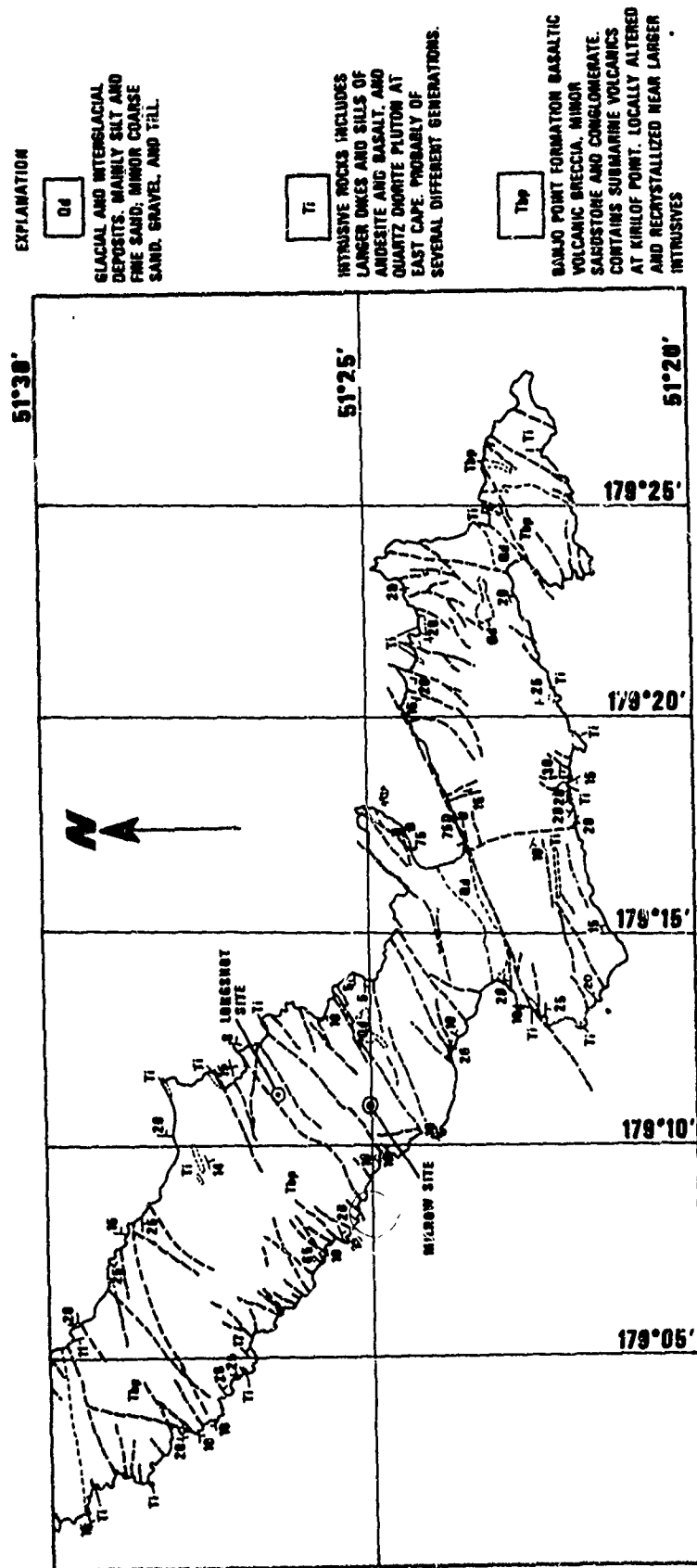   events using surface waves, Geophys. J.R. Astr. Soc.,
    in press.

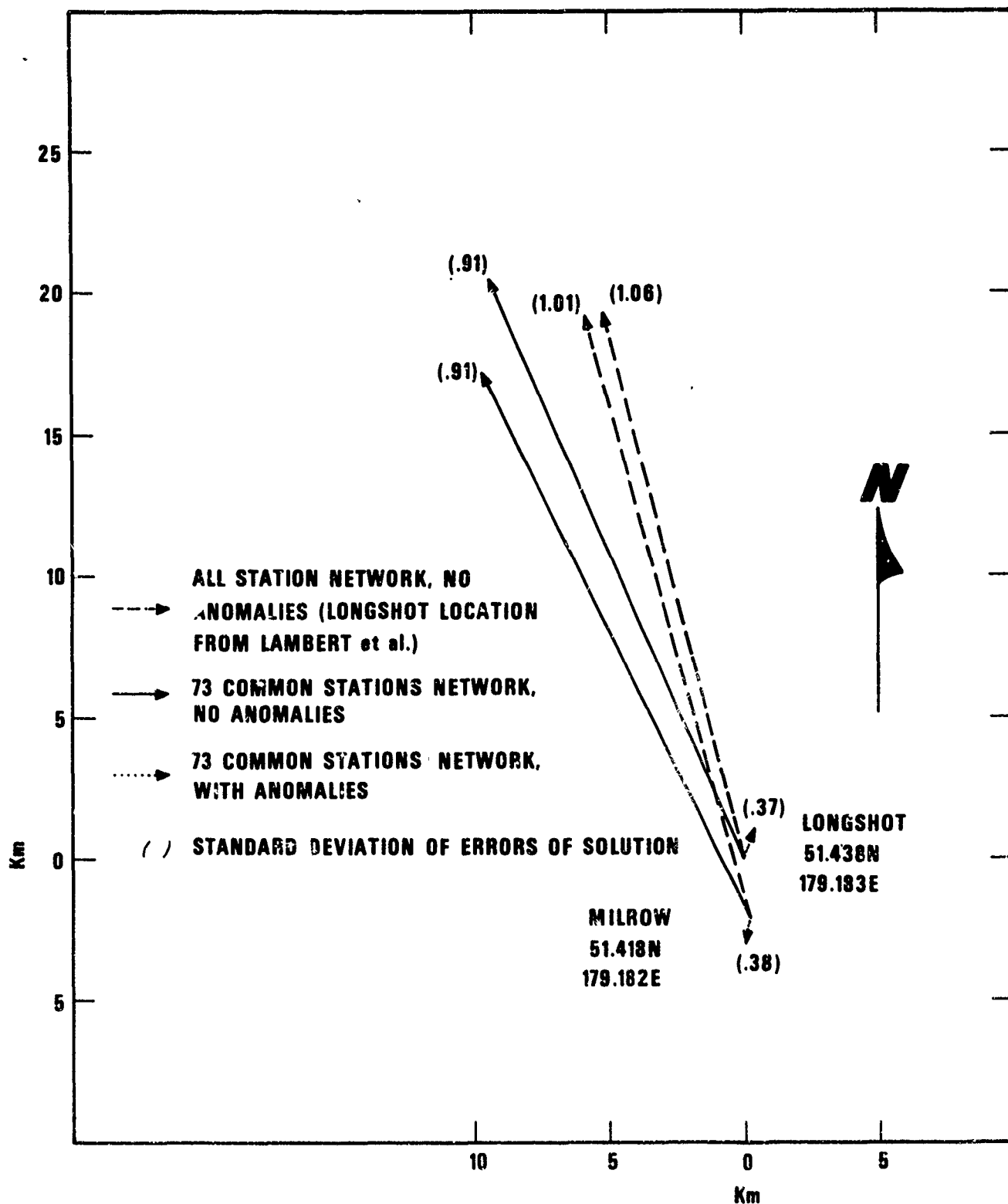Figure 1. Geology of southeastern part of Amchitka Island.

Figure 2. Location results for LONG SHOT and MILROW using Herrin-68
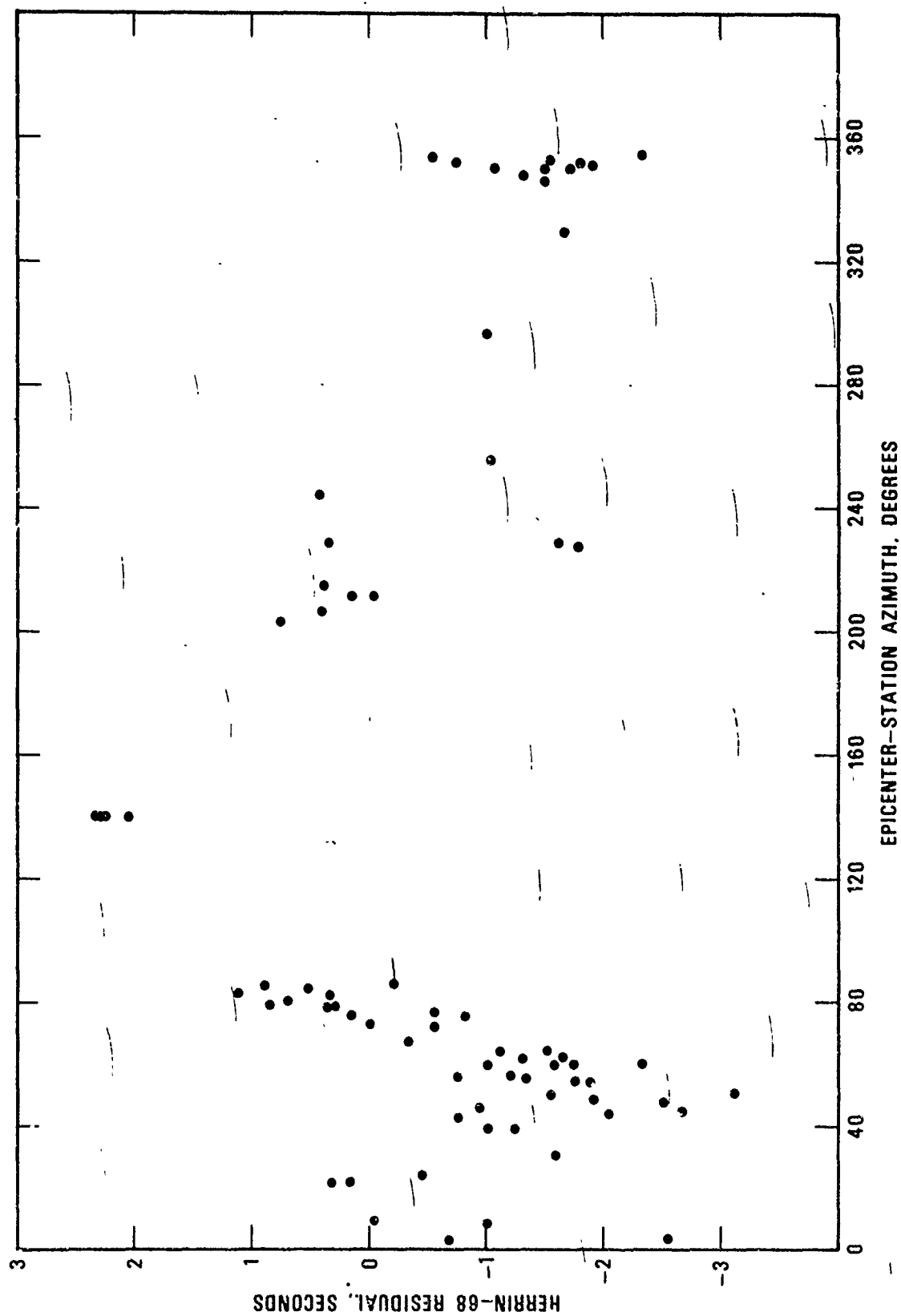travel-time tables and depths restrained to actual detonation depths.

57

Figure 3. Travel-time residuals (observed minus predicted) vs azimuth for MILROW determined from Herrin-68 table at 73 stations common to LONG SHOT.
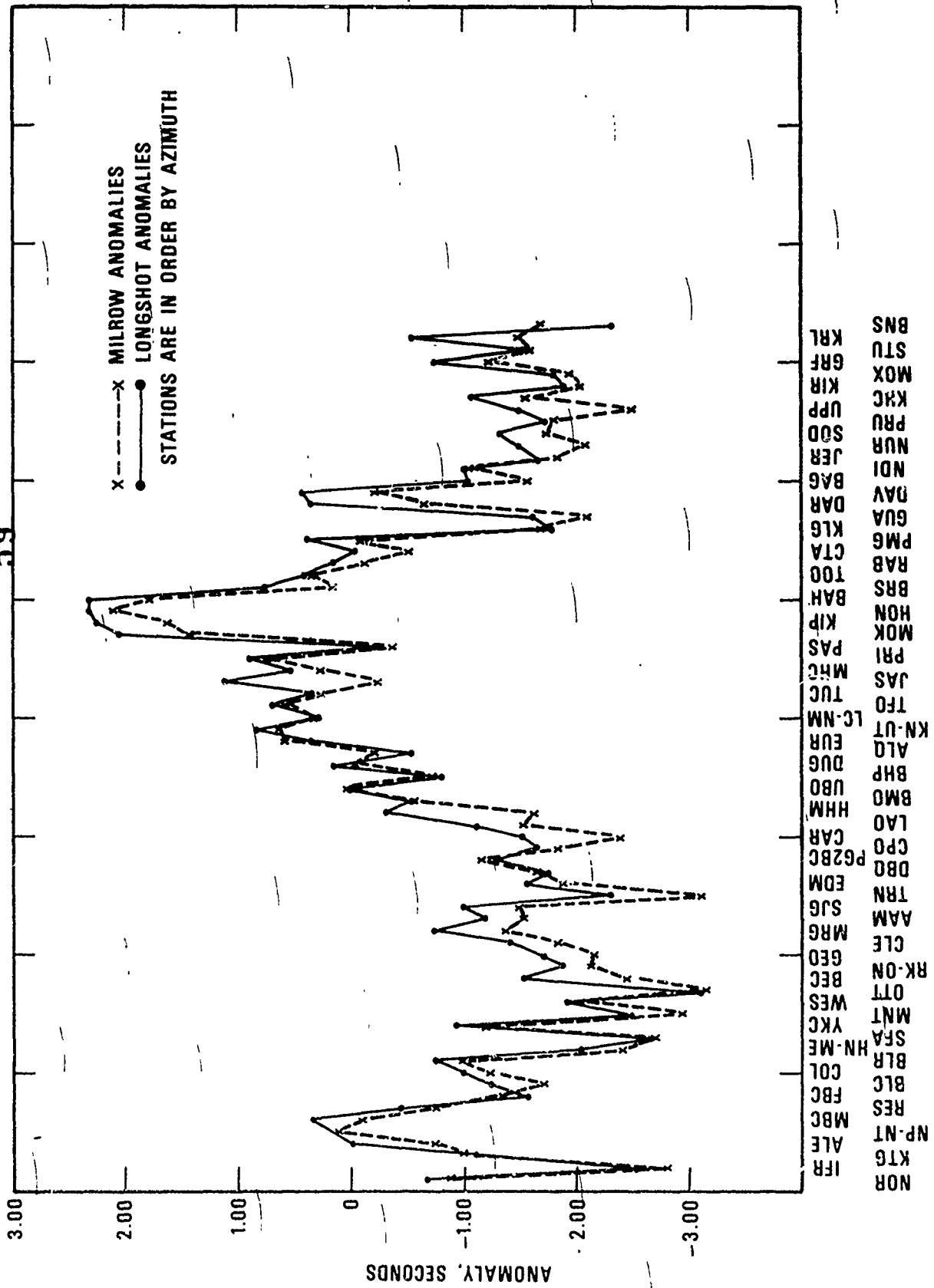
58

Figure 4. Relative travel-time anomalies (referenced to UBO) for MILROW and LONG SHOT from 73-station common network.
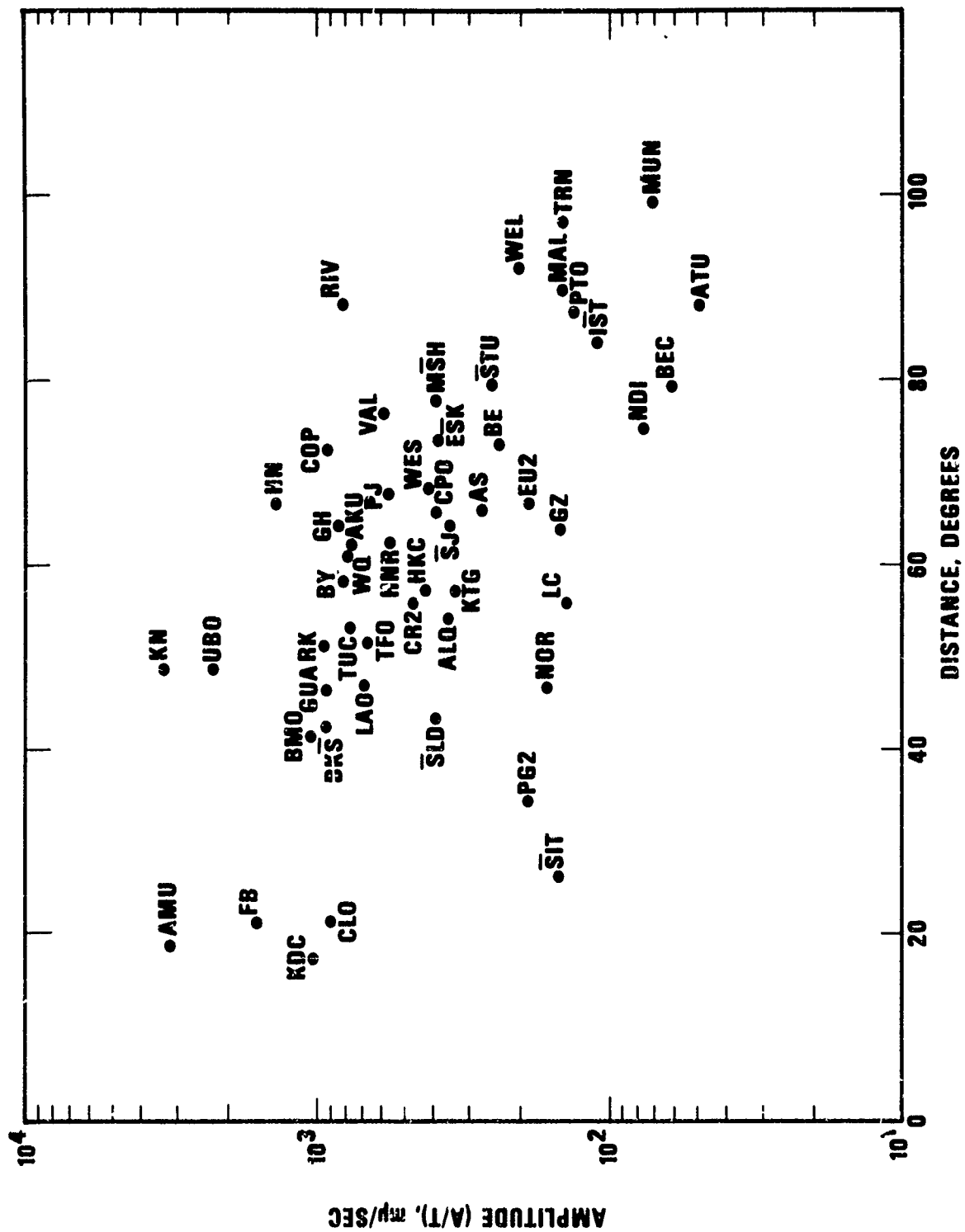
59

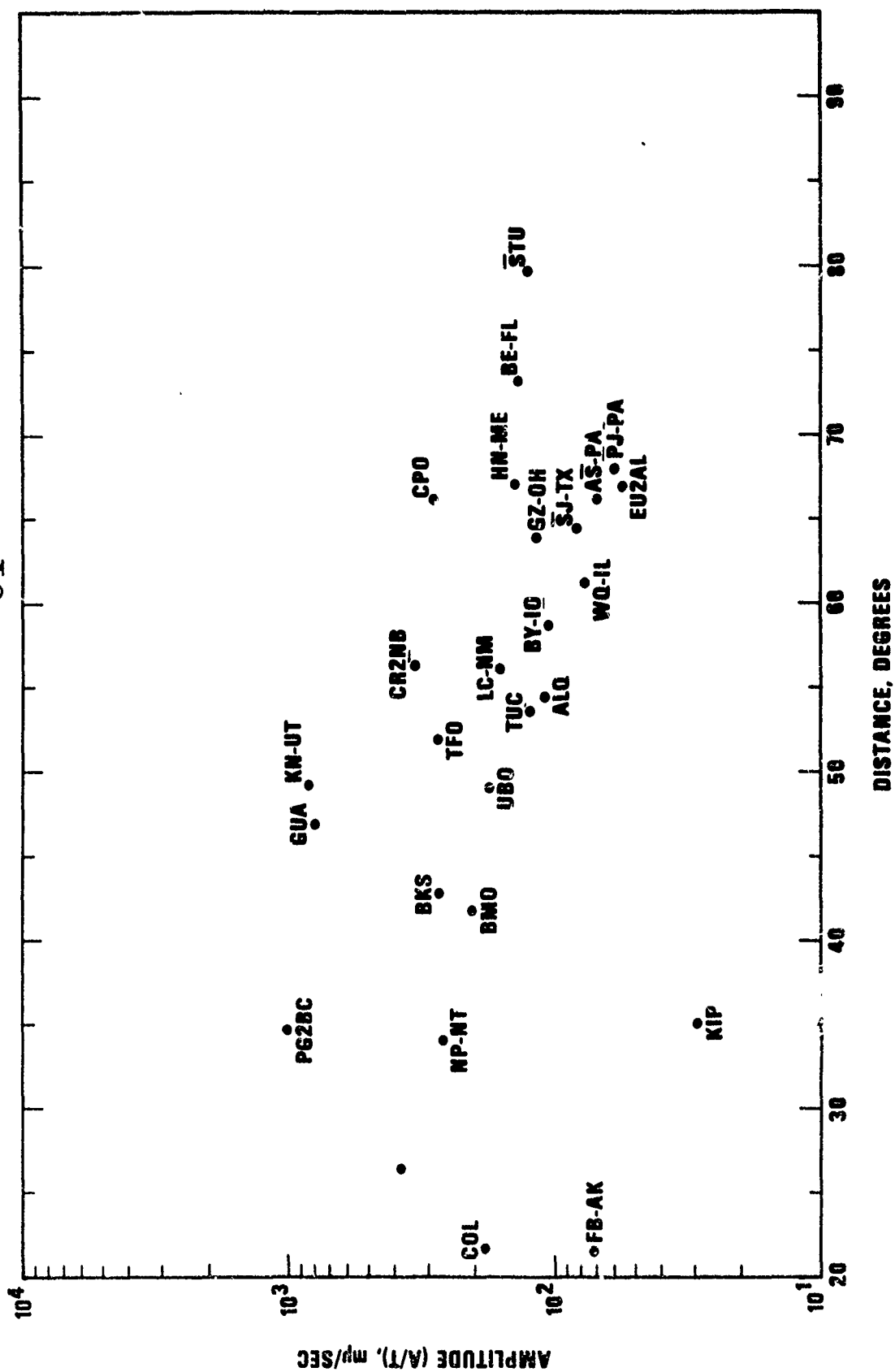Figure 5. Amplitude vs distance for MILROW P waves.

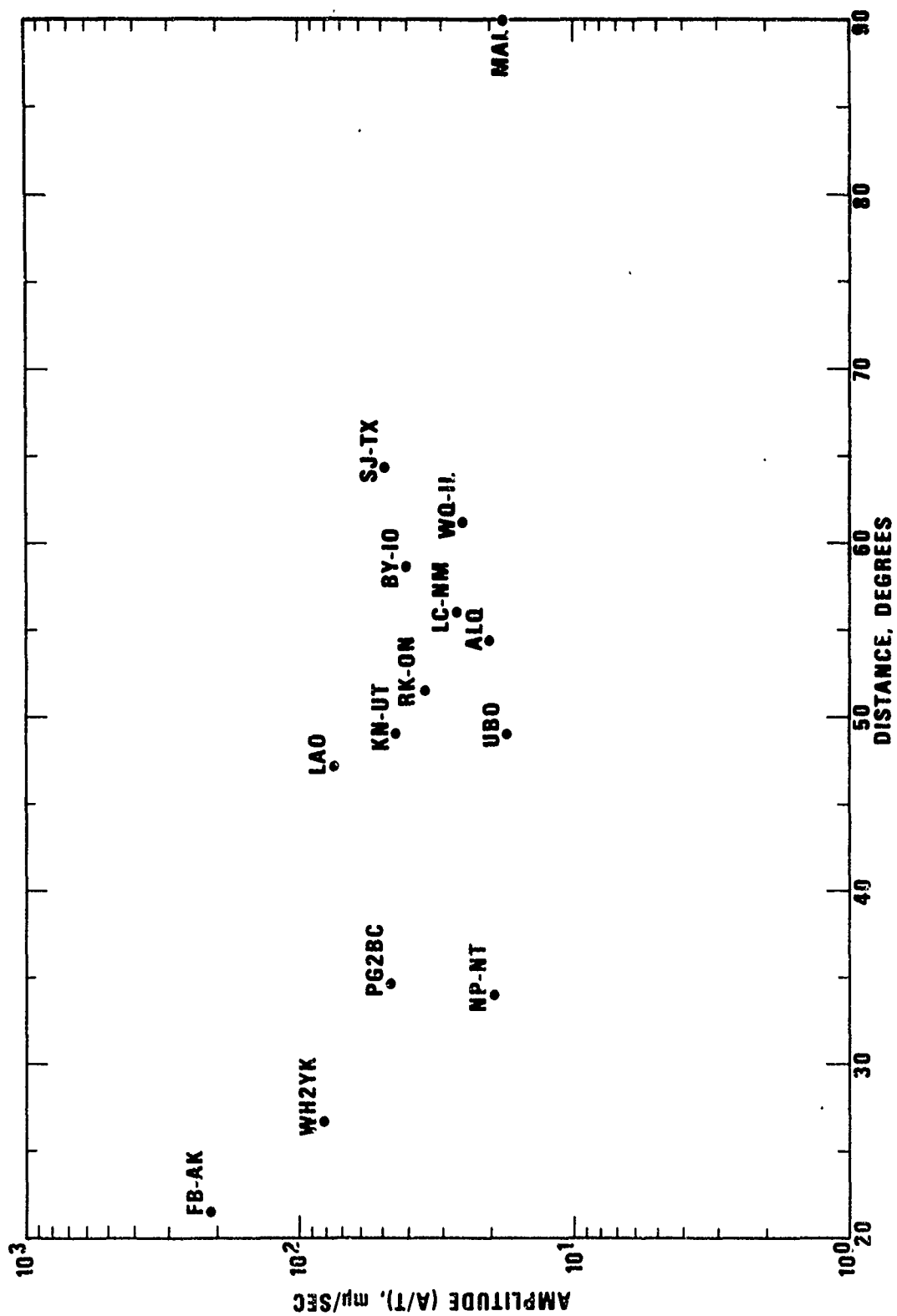60

Figure 6. Amplitude vs distance for MILROW PcP waves.

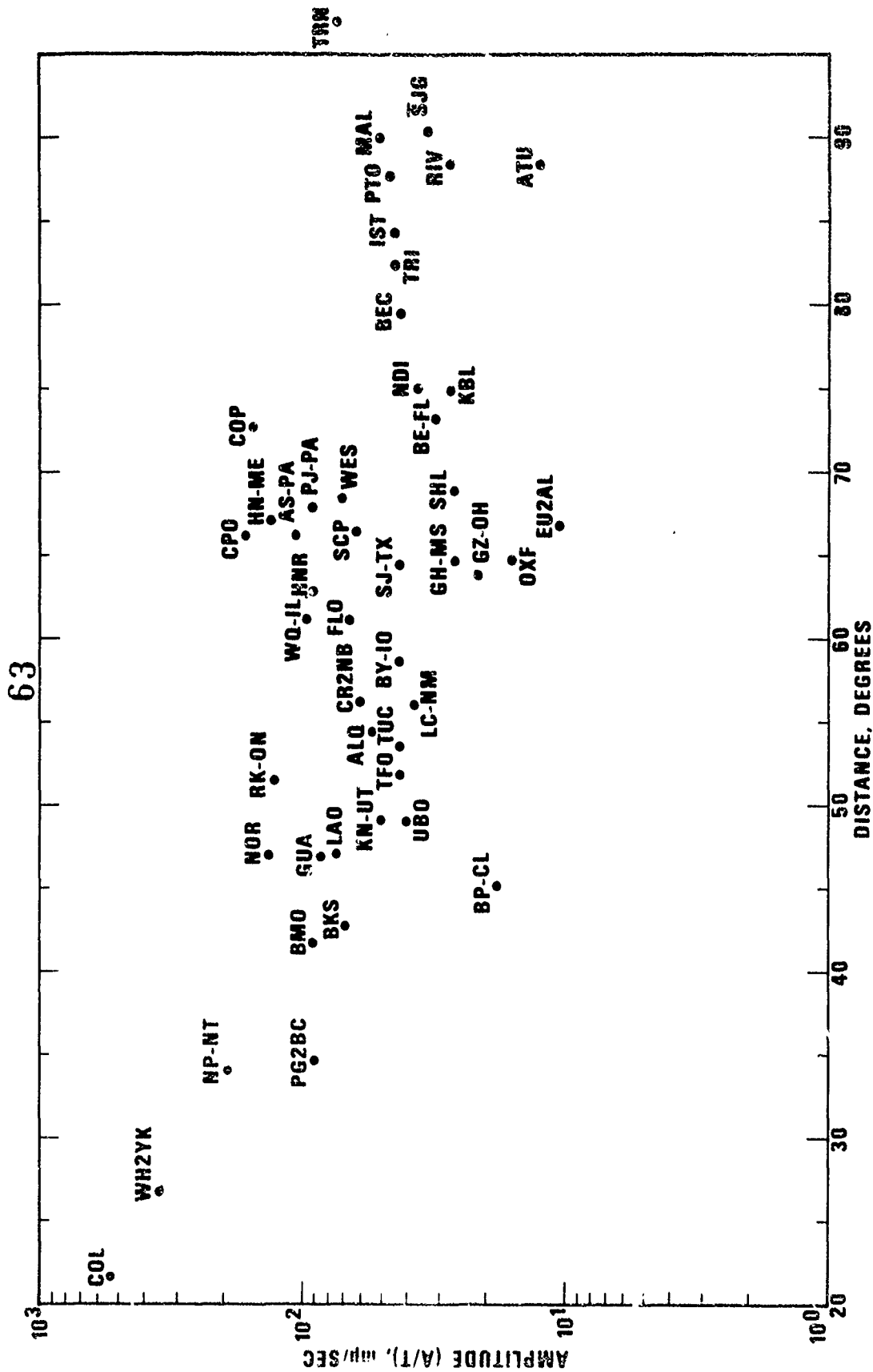Figure 7. Amplitude vs distance for MILROW Love waves.

62

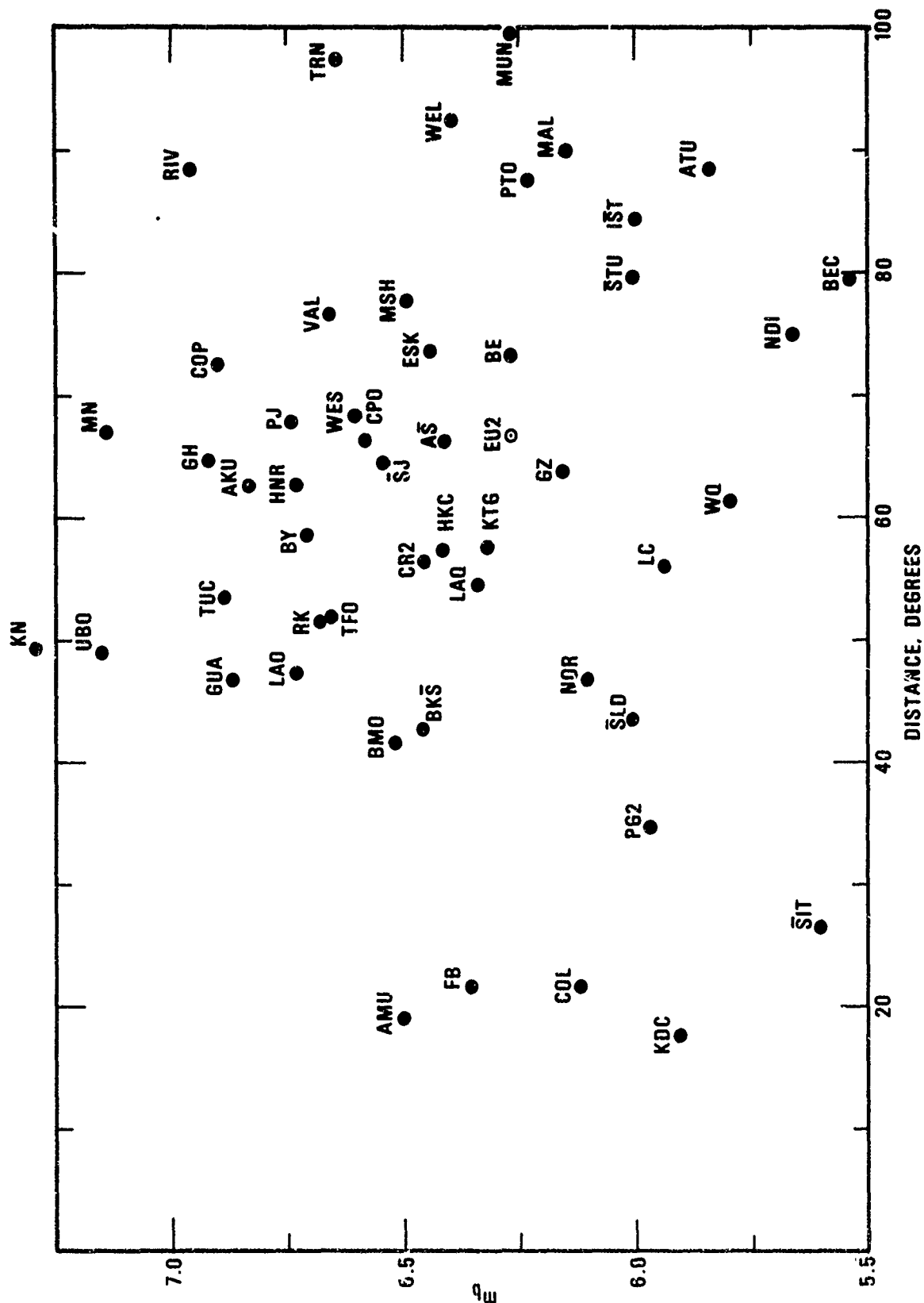Figure 8. Amplitude vs distance for MILROW Rayleigh waves.

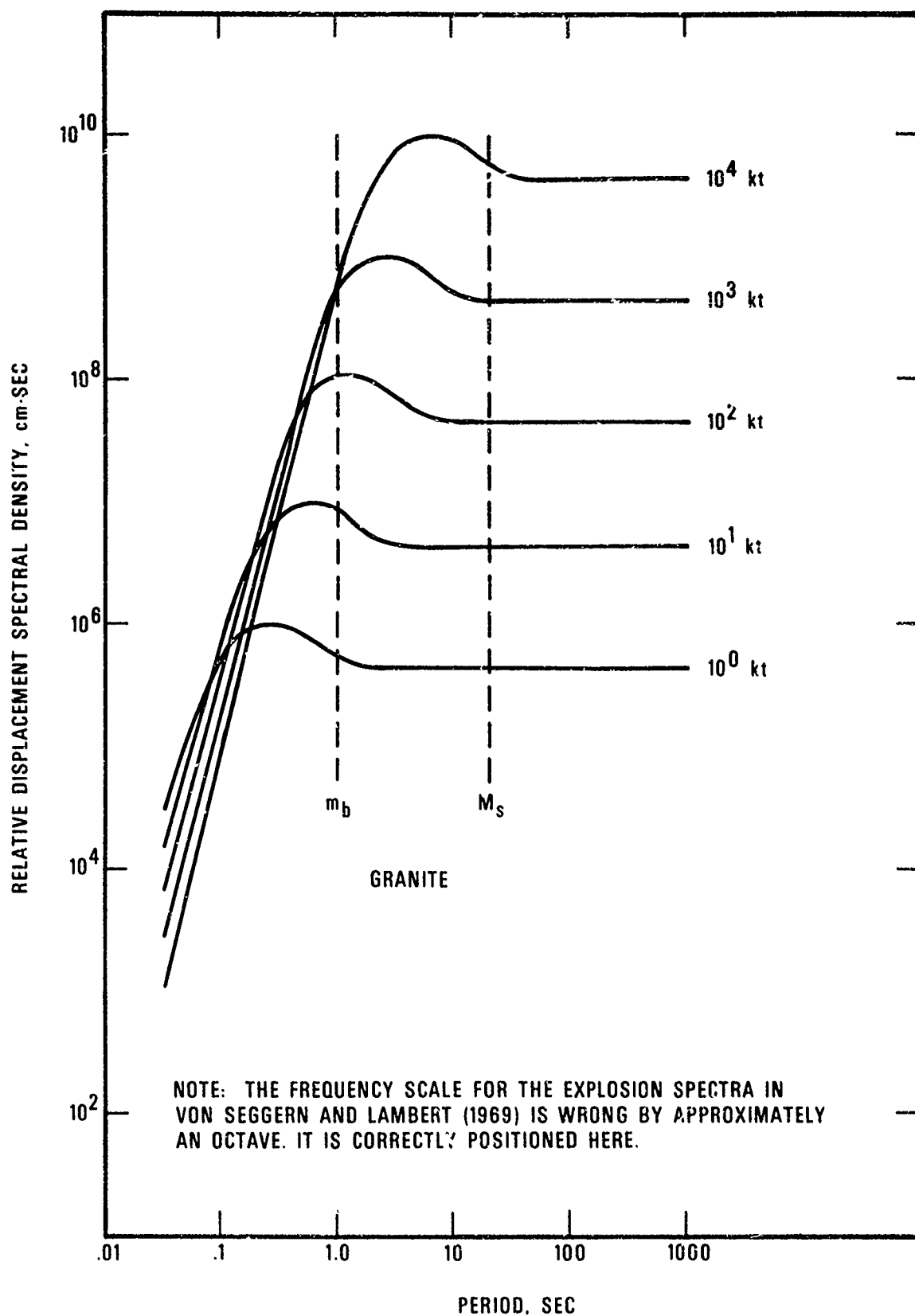Figure 9. Body-wave magnitude (m_b) vs distance for MILROW.

64

Figure 10. Surface-wave magnitude (M_s) vs distance for MILROW.

Figure 11. Source spectral shapes vs yield for explosions in granite.

SUMMED
SOLUTION

PROCESSED
SPECTRUM

DOT-PRODUCT

MILROW

POWER

FREQUENCY (HERTZ)

TIME (SECONDS)

MILROW
COLLAPSE

POWER

FREQUENCY (HERTZ)

DISPLACEMENT^2

TIME (SECONDS)
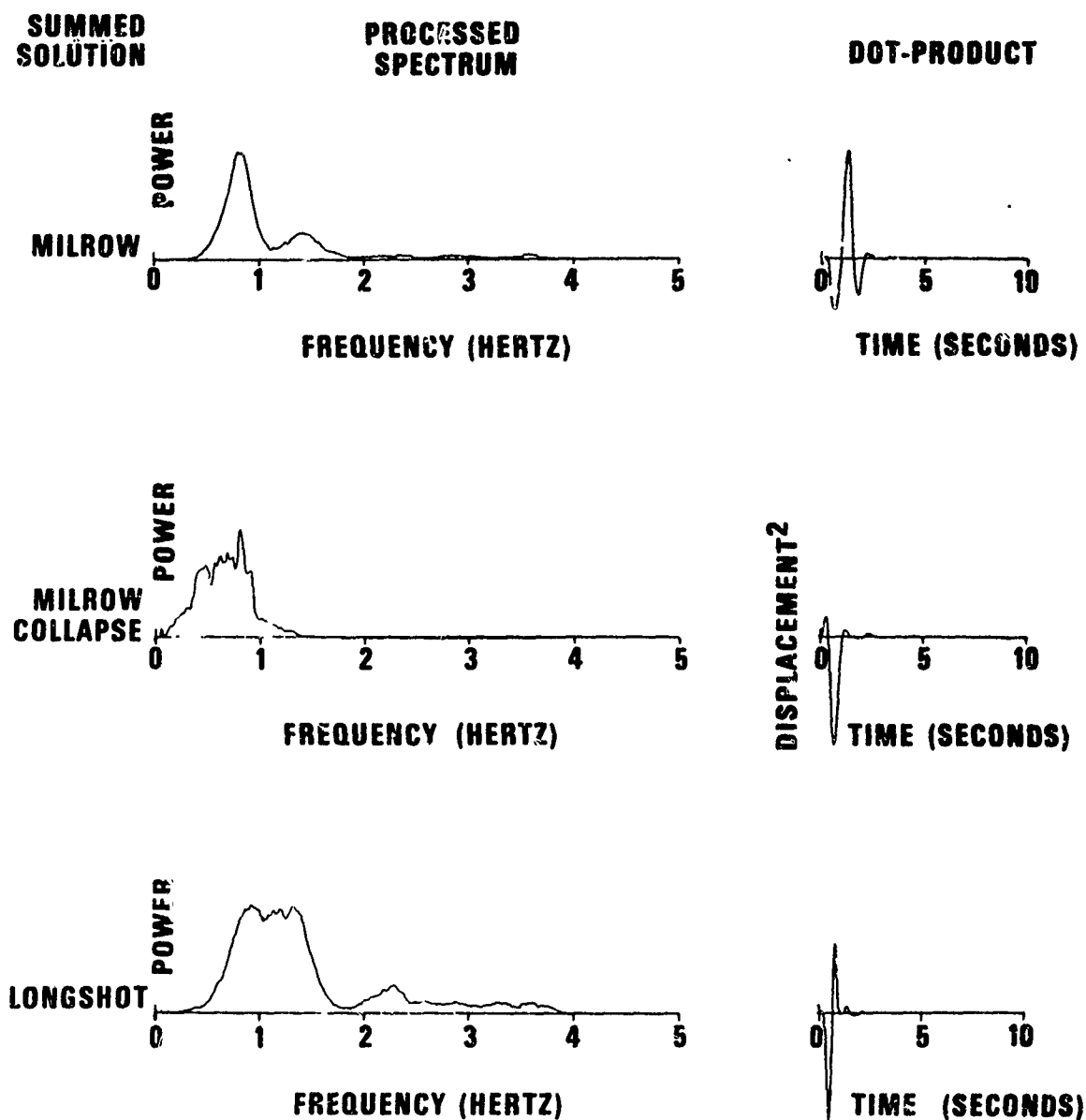
LONGSHOT

POWER

FREQUENCY (HERTZ)

TIME (SECONDS)

Figure 12. Depth-phase (pP) analysis using averaged normalized
for MILROW (17 stations), MILROW collapse (6 stations), and
LONG SHOT (27 stations).
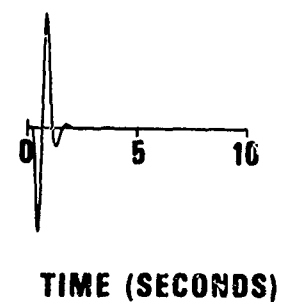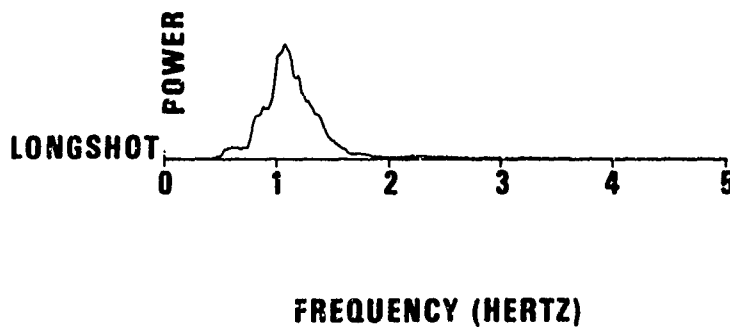
67

SUMMED
SOLUTION

PROCESSED
SPECTRUM

DOT-PRODUCT
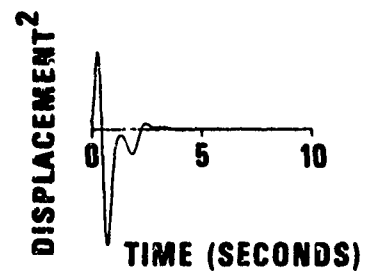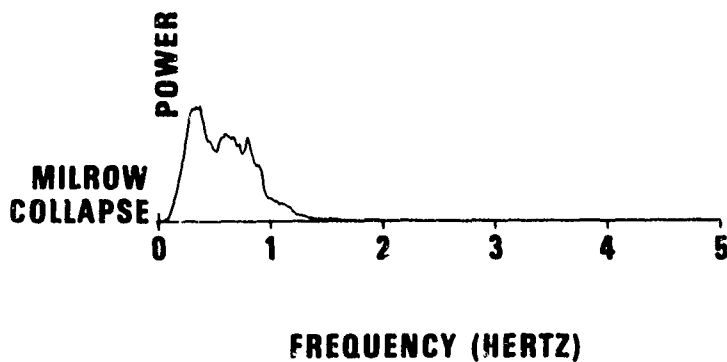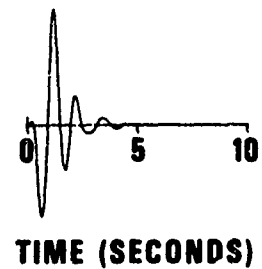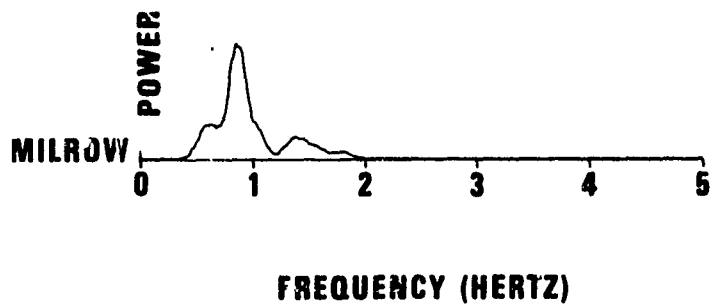
Figure 13. Depth-phase (pP) analysis using LASA subarrays'
average spectra for MILROW, MILROW collapse, and LONG SHOT.

68
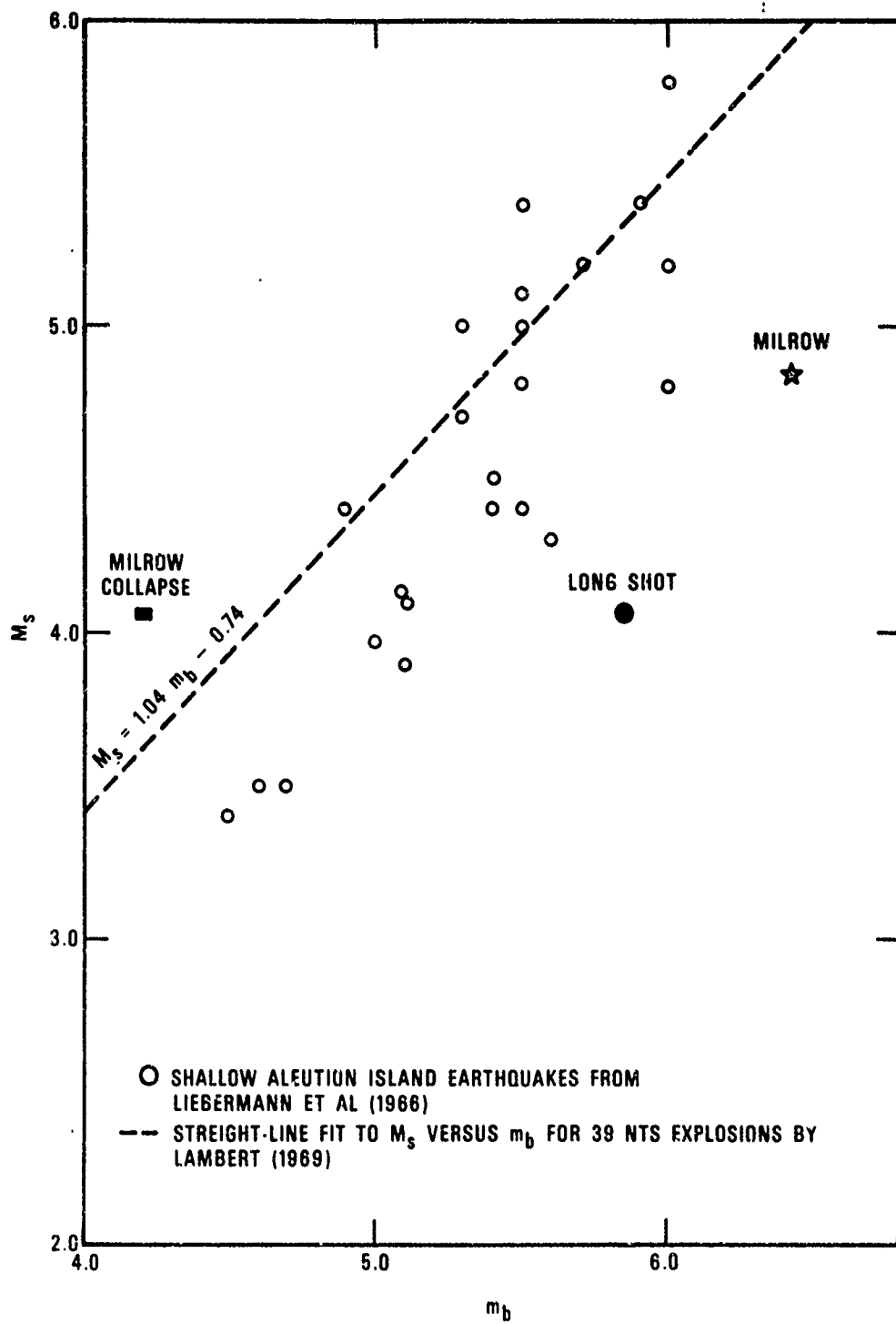
Figure 14. M_s vs m_b for several earthquakes and explosions.

The figure shows a plot of M_s (vertical axis, ranging from 2.0 to 6.0) versus m_b (horizontal axis, ranging from 4.0 to 6.0). Labeled points include MILROW, MILROW COLLAPSE, and LONG SHOT. A dashed line is labeled $M_s = 1.04\ m_b - 0.74$.

Legend:
- ○ SHALLOW ALEUTION ISLAND EARTHQUAKES FROM LIEBERMANN ET AL (1966)
- --- STREIGHT-LINE FIT TO M_s VERSUS m_b FOR 39 NTS EXPLOSIONS BY LAMBERT (1969)
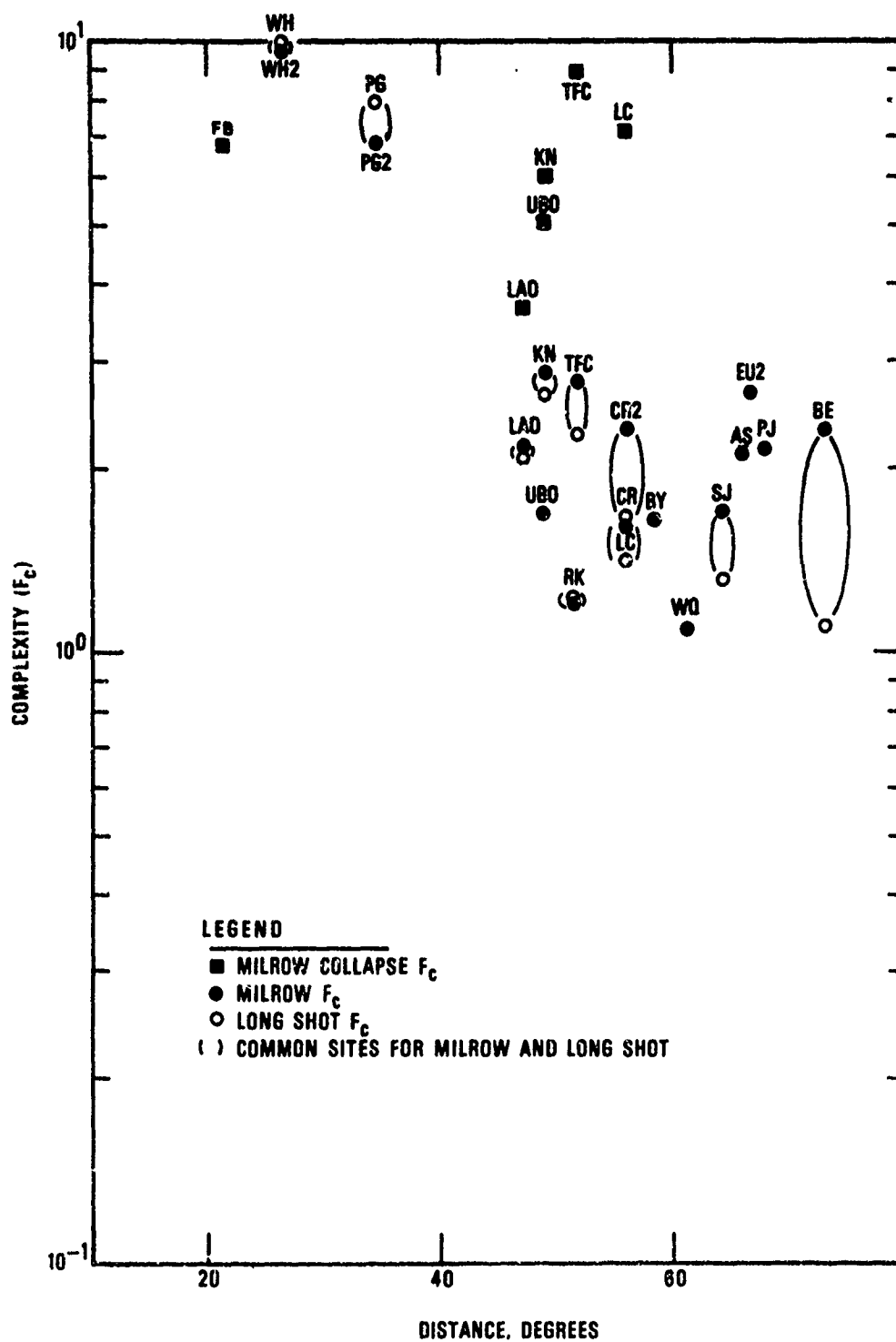
Figure 15. Complexity values for MILROW, LONG SHOT, and the
MILROW collapse vs distance.

70
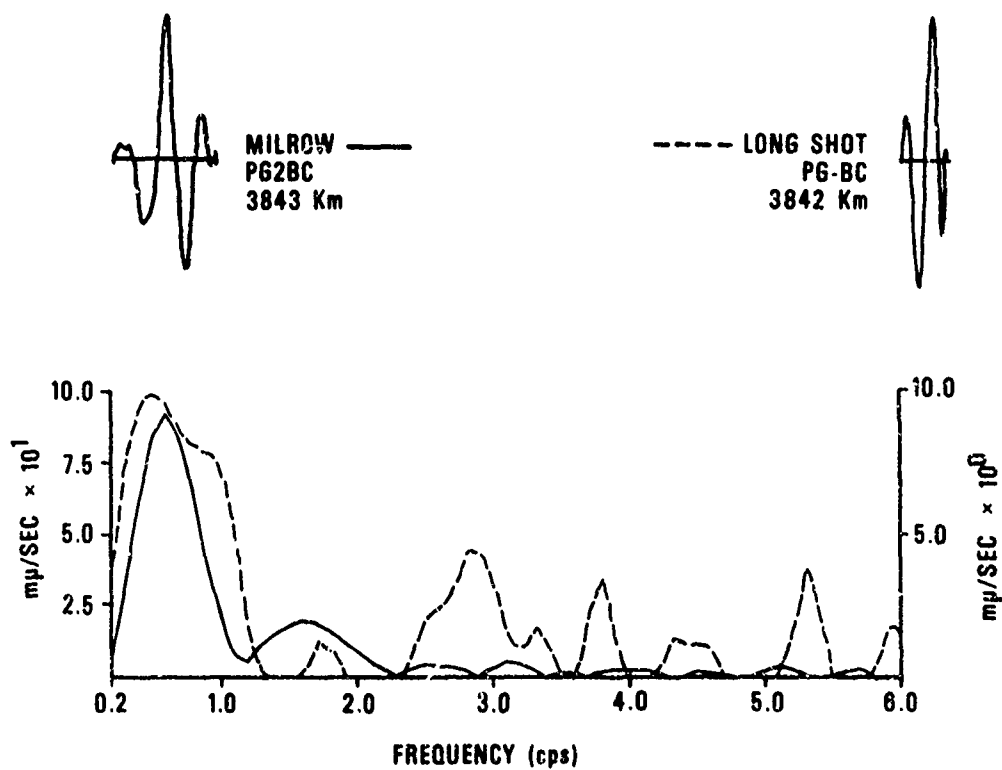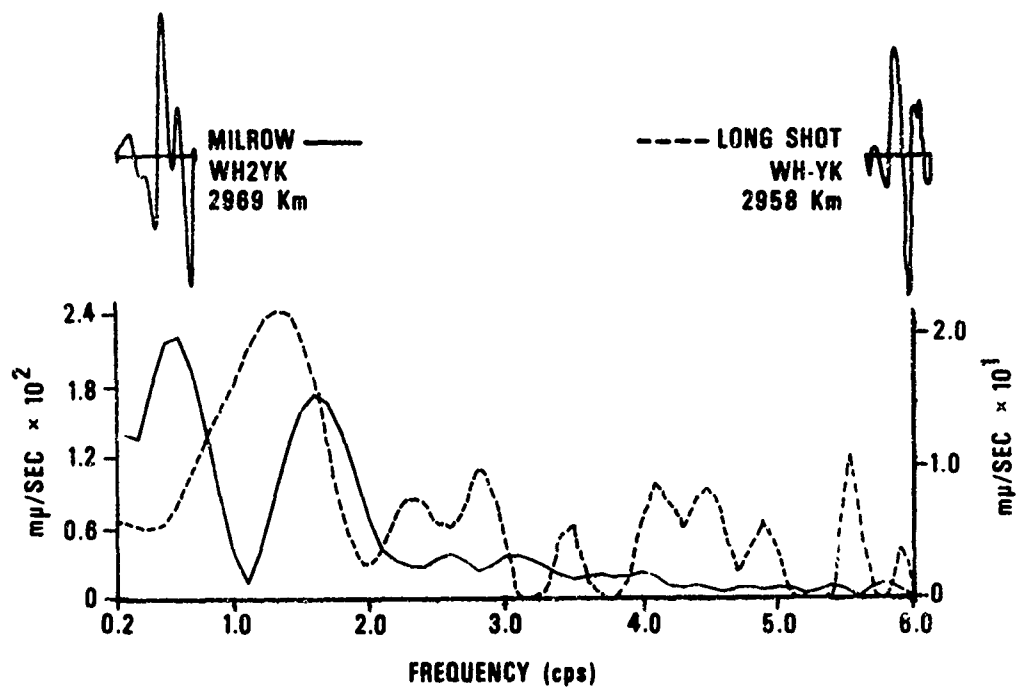
Figure 16. P-wave spectra for stations common to MILROW and LONG SHOT.

71

Figure 16. (Cont'd.)
P-wave spect.a for stations common to MILROW and LONG SHOT.

Figure 16. (Cont'd.)
P-wave spectra for stations common to MILROW and LONG SHOT.

Figure 16. (Cont'd.)
P-wave spectra for stations common to MILROW and LONG SHOT.

74
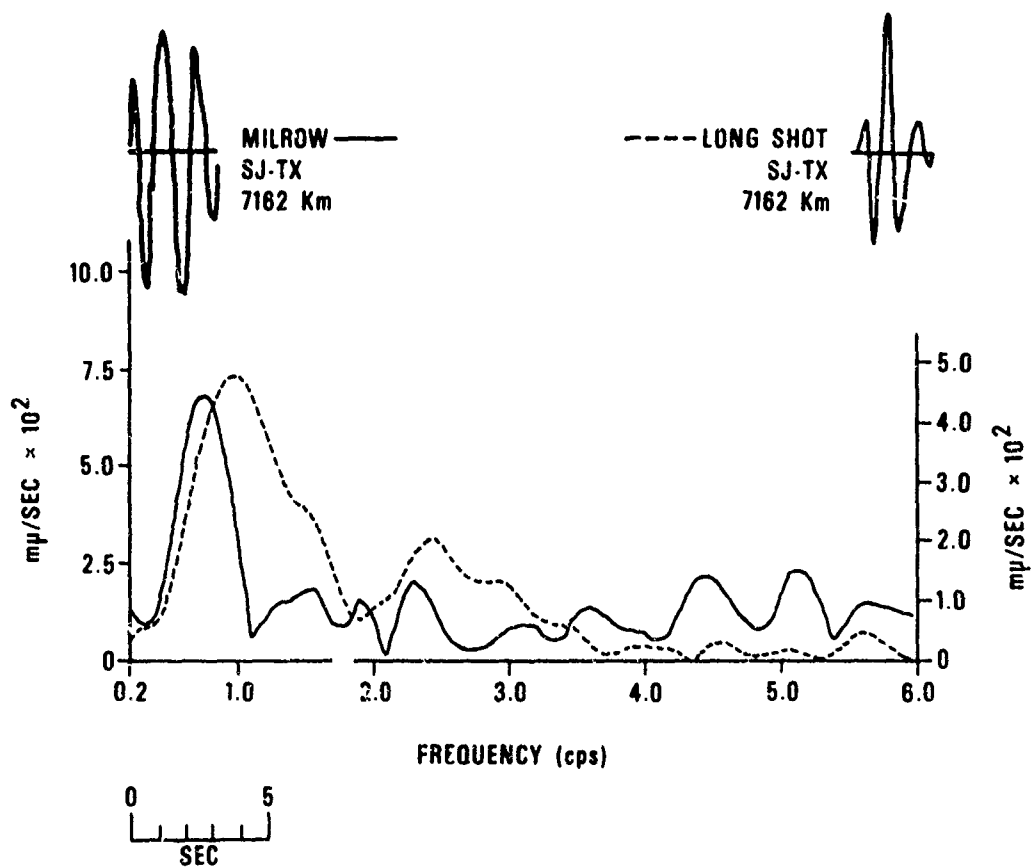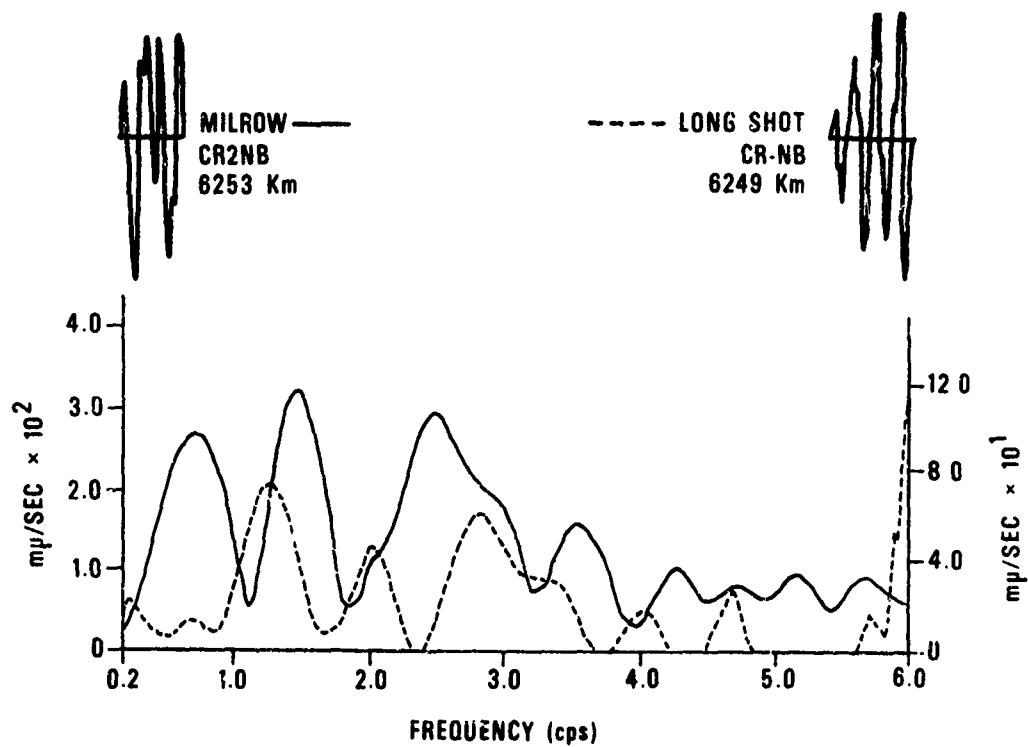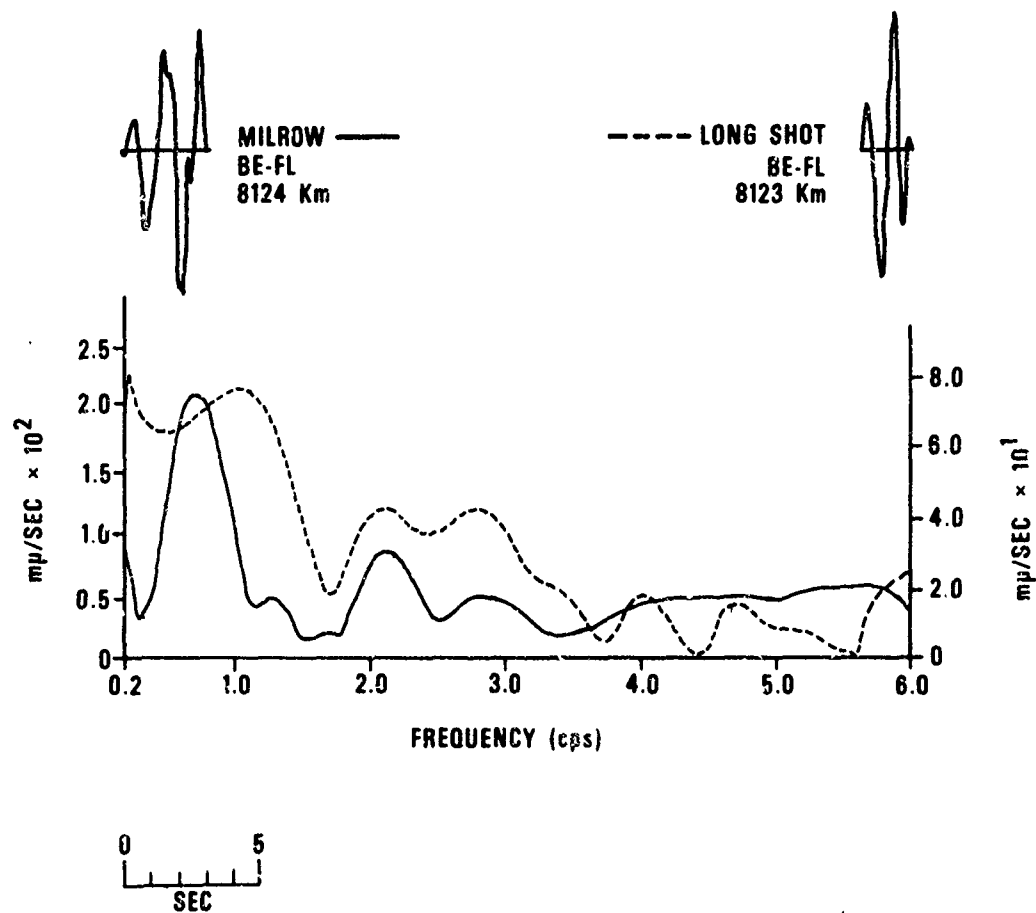
Figure 16. (Cont'd.)
P-wave spectra for stations common to MILROW and LONG SHOT.
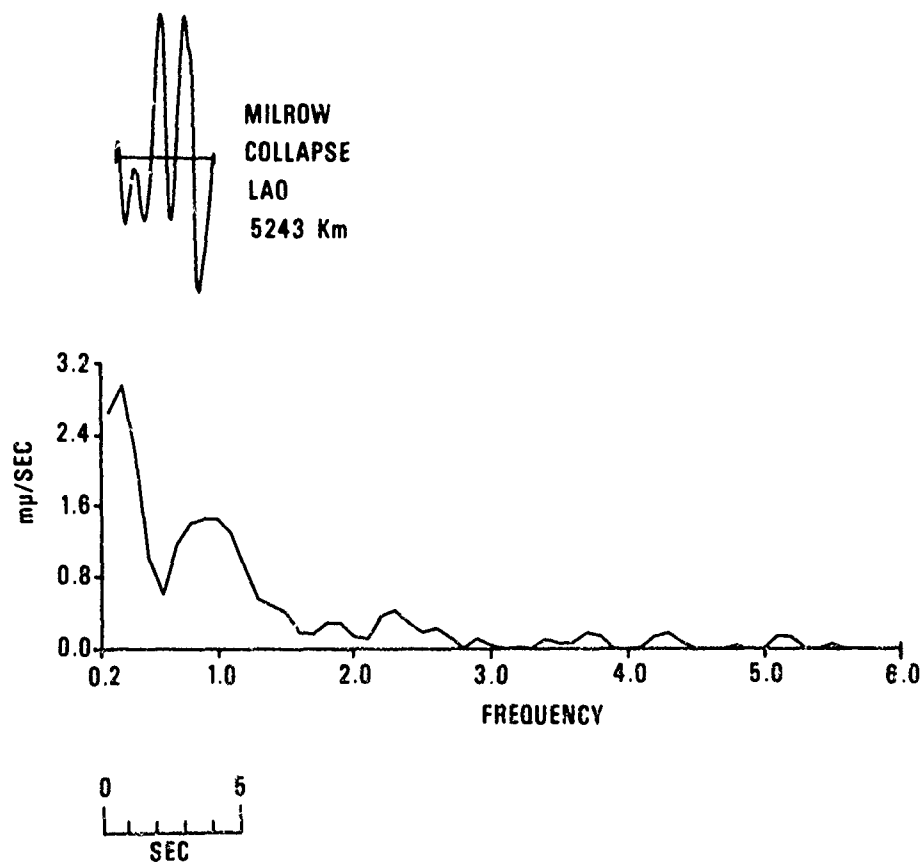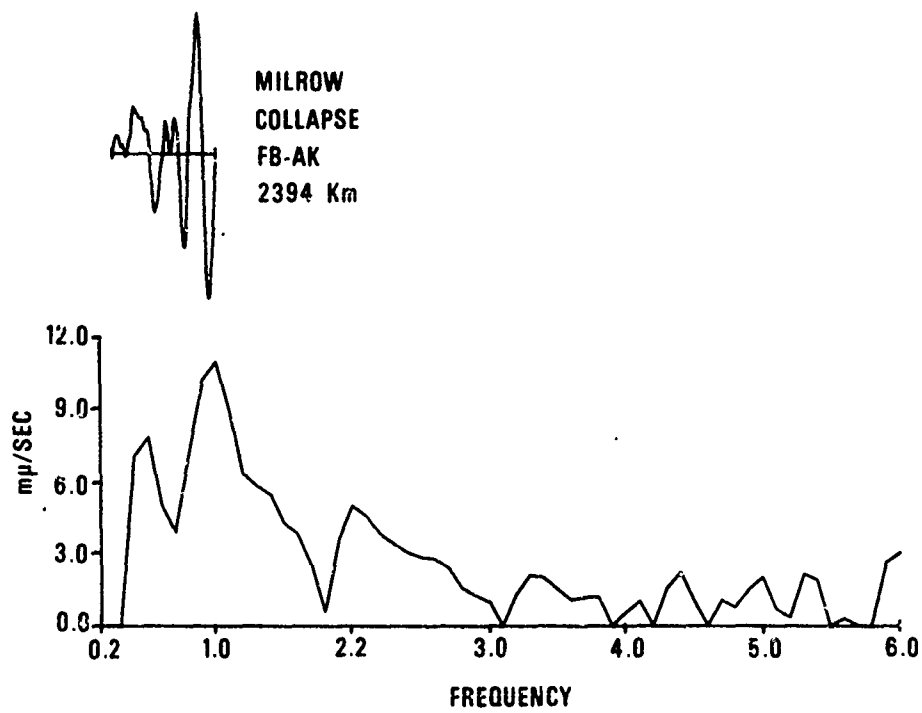
Figure 17. P-wave spectra for the MILROW collapse.

76

MILROW
COLLAPSE
UBO
5445 Km

16.0

12.0

8.0

mμ/SEC

4.0

0.0

0.2   1.0   2.0   3.0   4.0   5.0   6.0

FREQUENCY
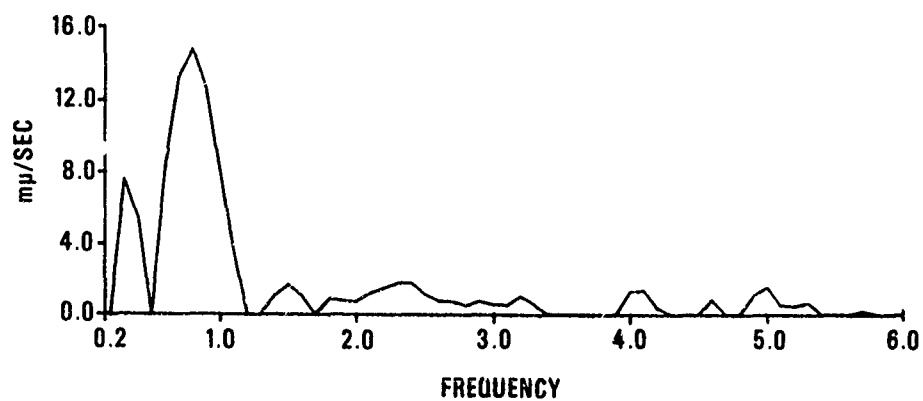
MILROW
COLLAPSE
KN-UT
5455 Km
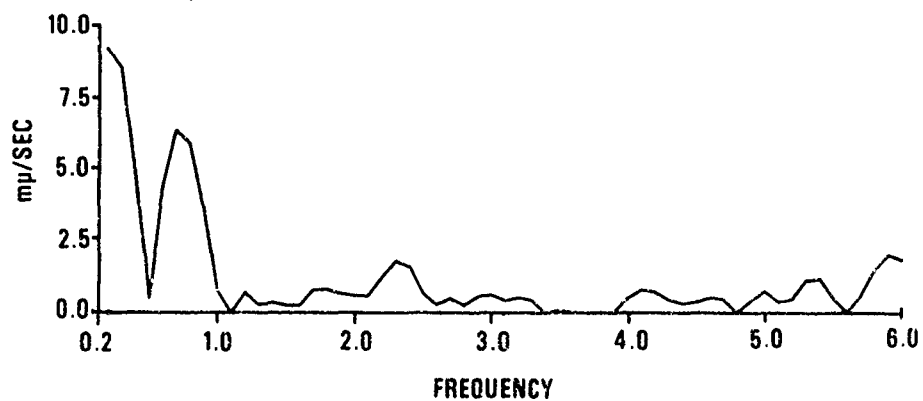
10.0

7.5

5.0

mμ/SEC

2.5

0.0

0.2   1.0   2.0   3.0   4.0   5.0   6.0

FREQUENCY

0   5
SEC

Figure 17. (Cont'd.)
P-wave spectra for the MILROW collapse.

77

MILROW
COLLAPSE
TFO
5760 Km

MILROW
COLLAPSE
LC-NM
6222 Km

Figure 17. (Cont'd.)
P-wave spectra for the MILROW collapse.

78
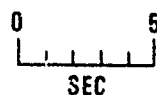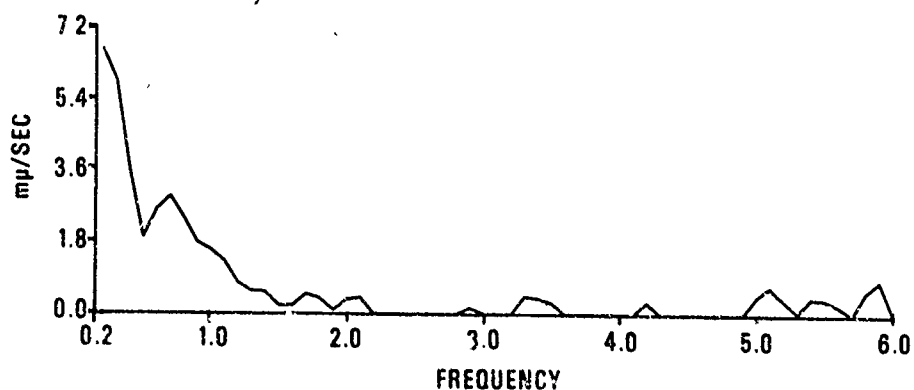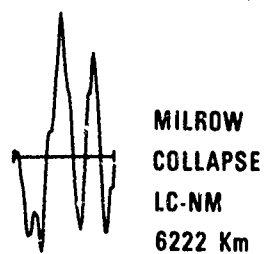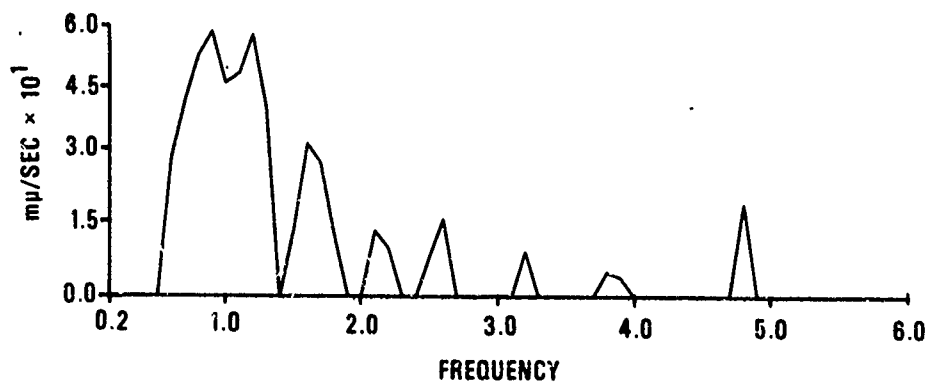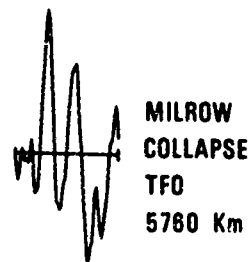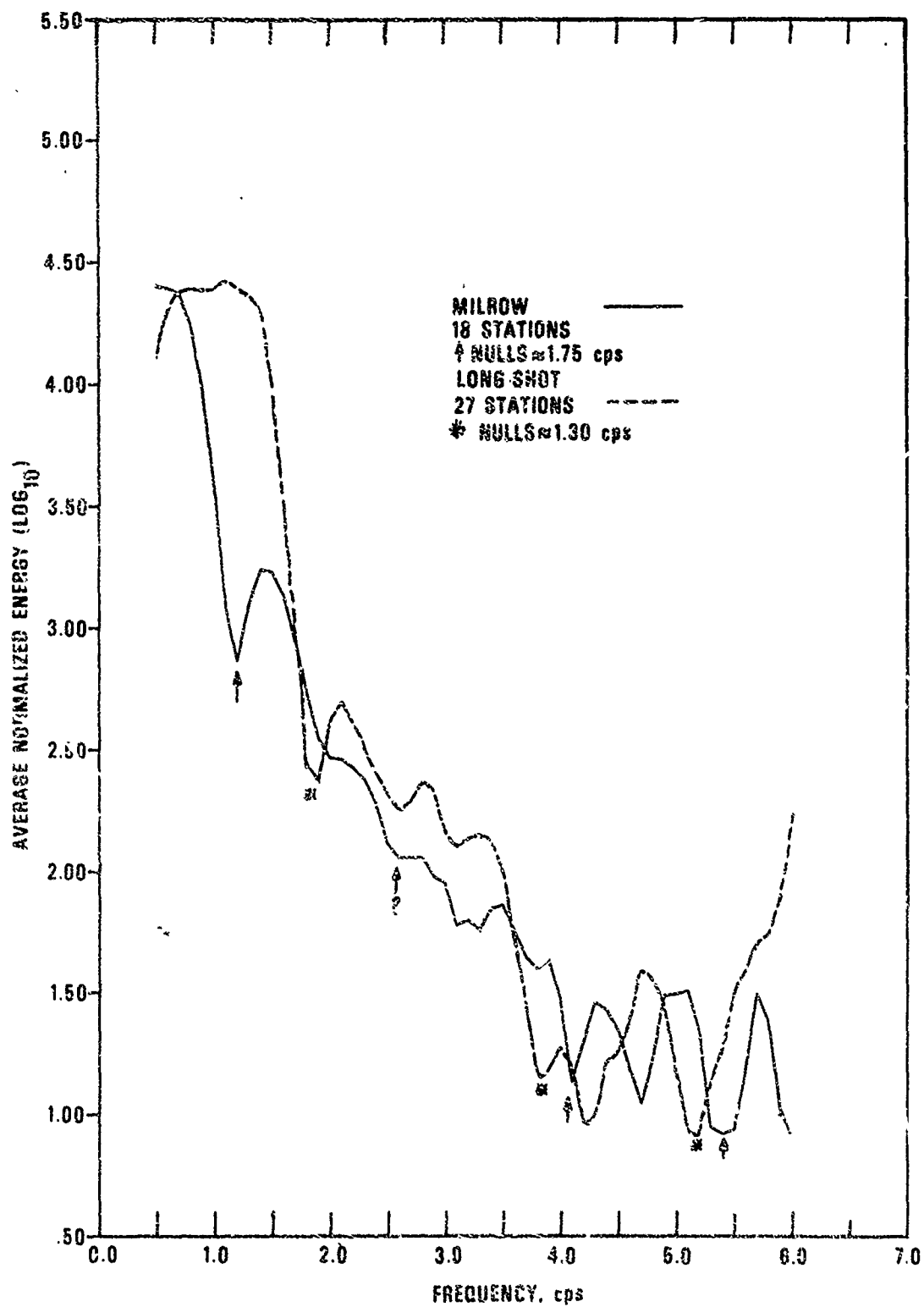
Figure 18. The average P-wave normalized energy spectra for MILROW (18 stations) and LONG SHOT (27 stations).
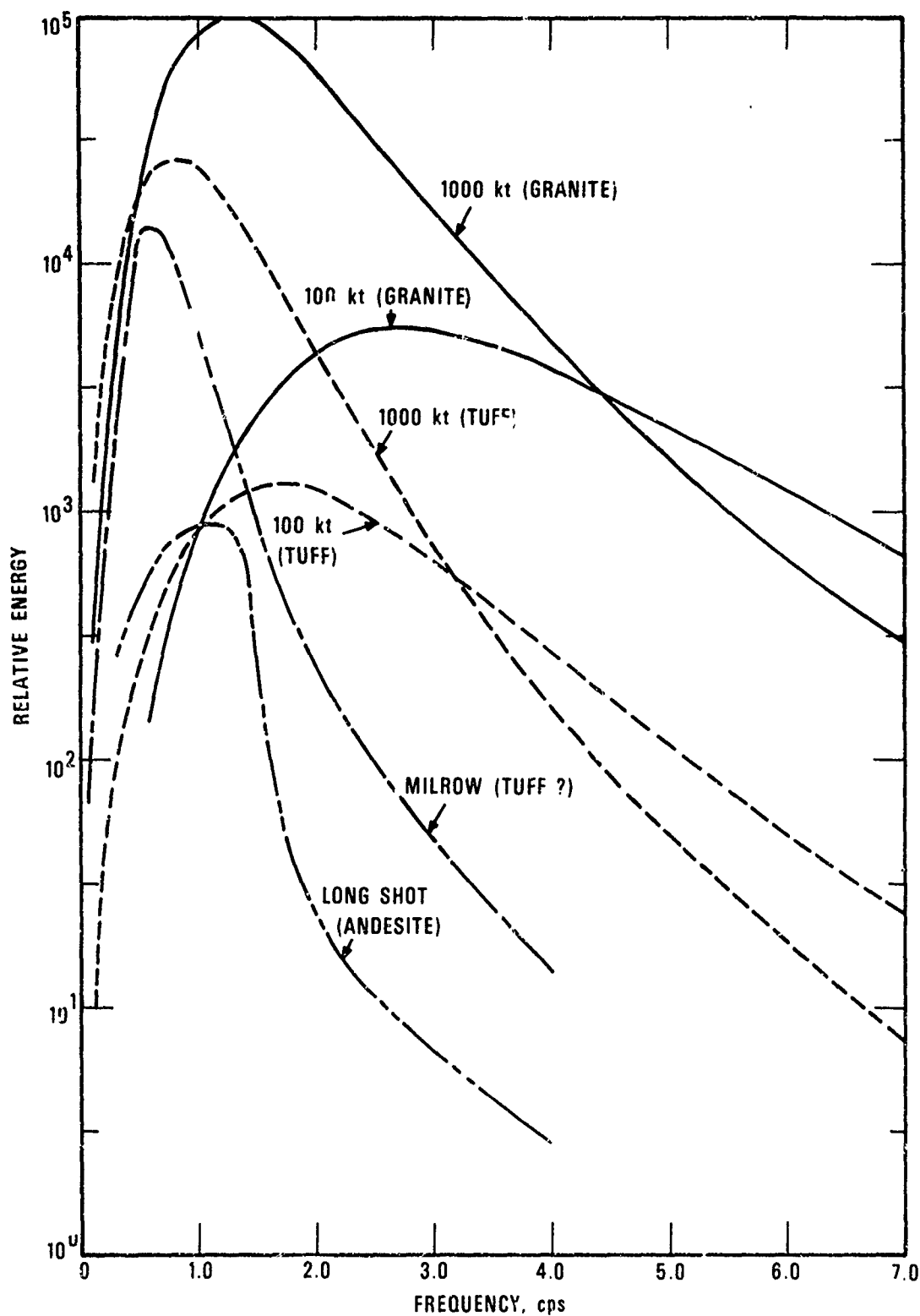
Figure 19. MILROW and LONG SHOT smoothed average P-wave spectra compared to theoretical source spectra.
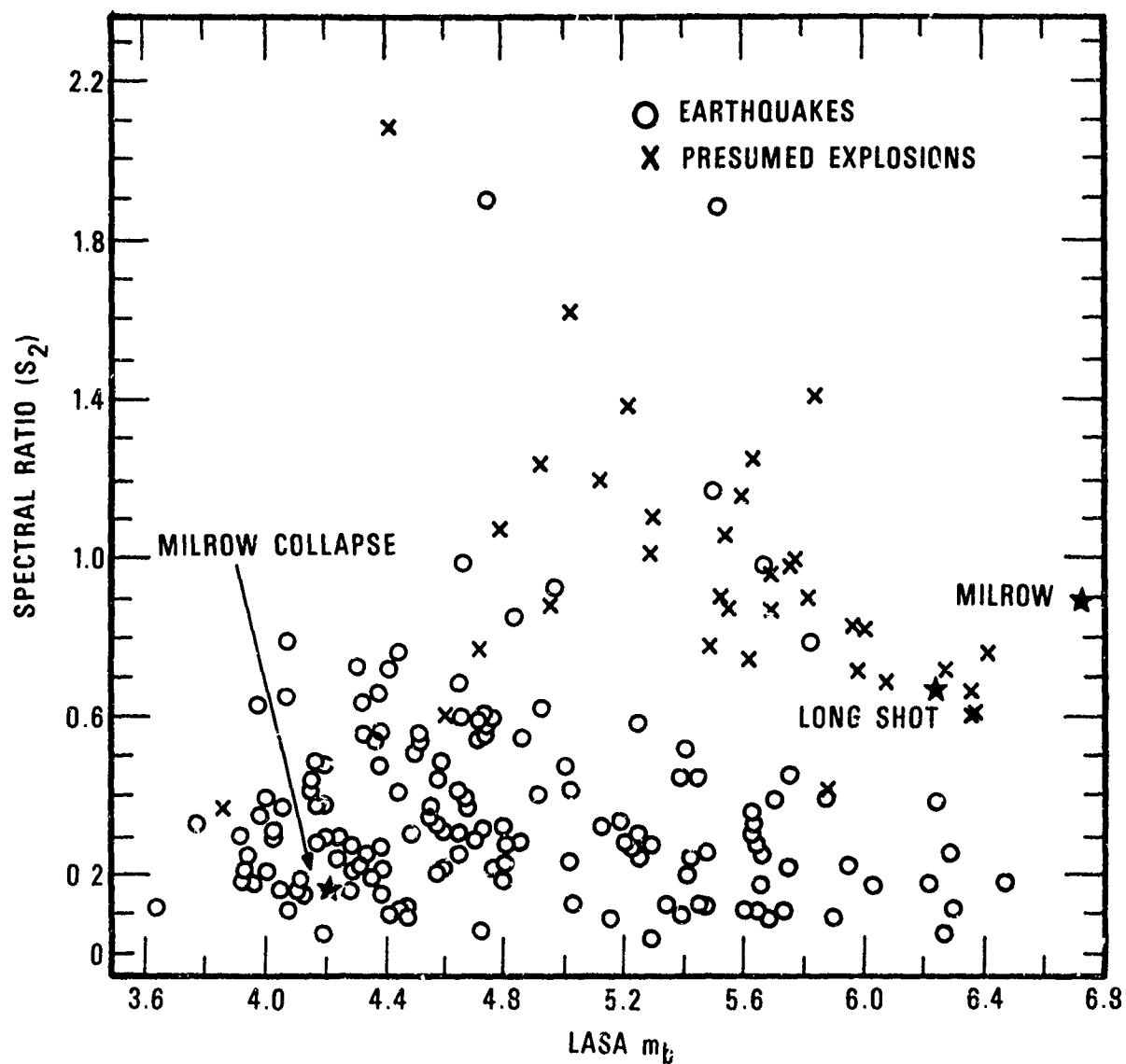
Figure 20. LASA spectral ratios of MILROW and its collapse
compared to data of Lacoss (1970) on Asian earthquakes and
presumed explosions.
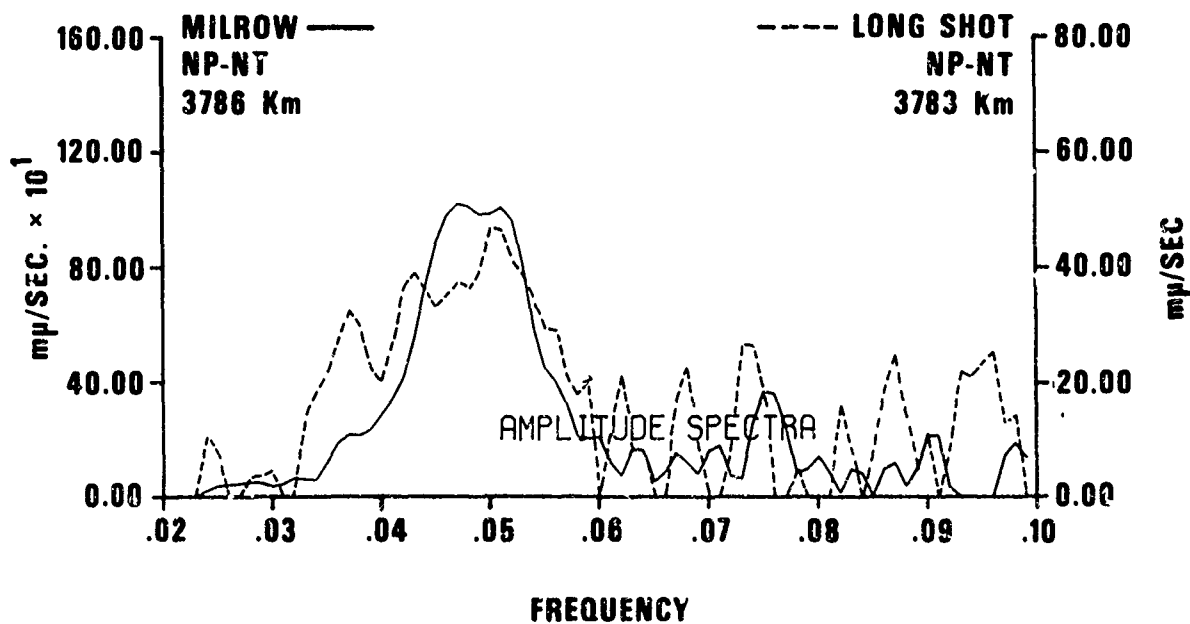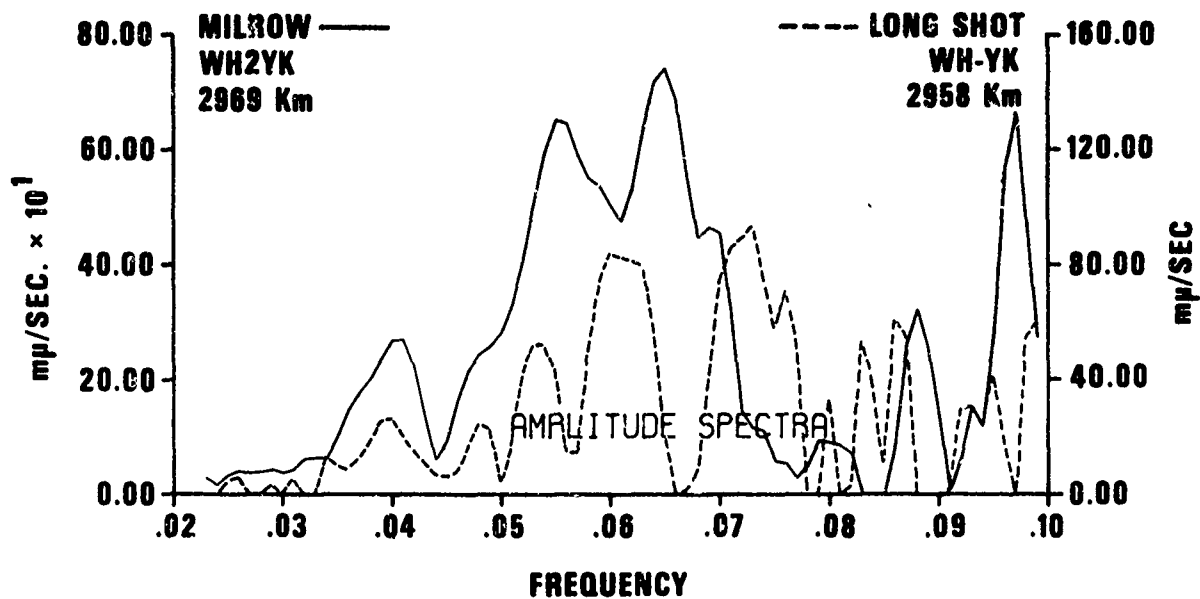
Figure 21. Rayleigh-wave spectra for stations common to MILROW and LONG SHOT.
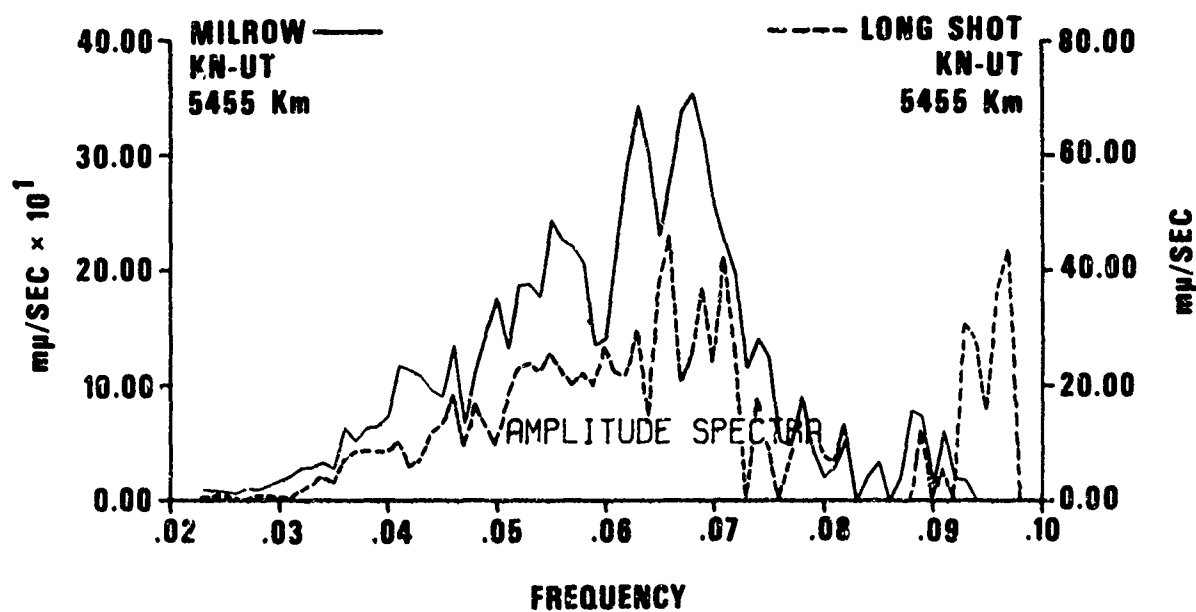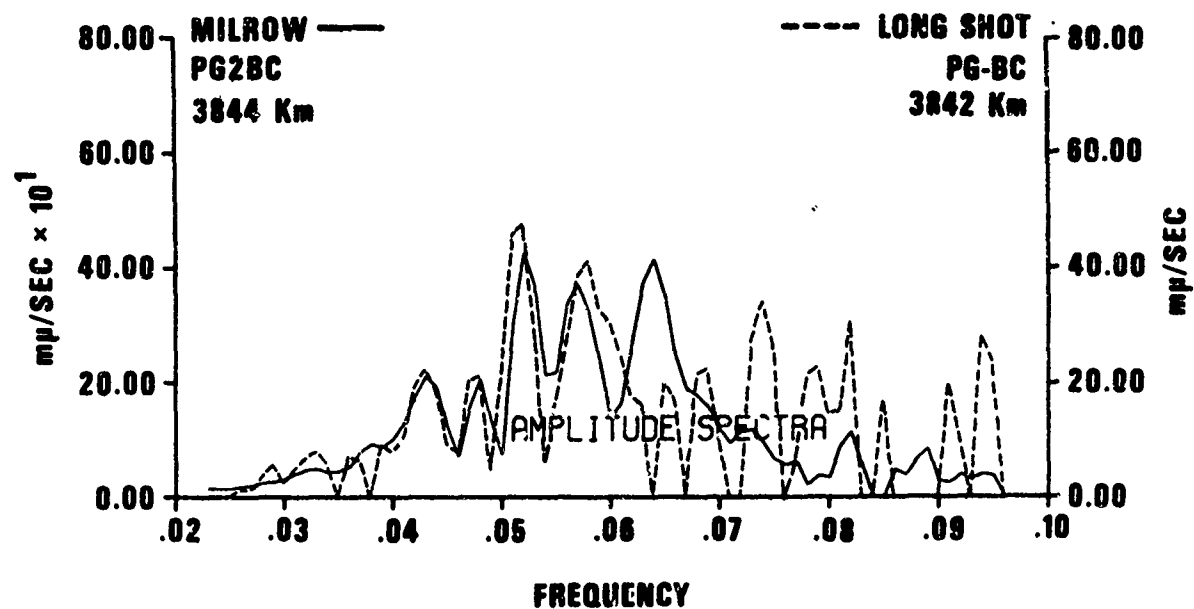
Figure 21. (Cont'd.)
Rayleigh-wave spectra for stations common to MILROW and
LONG SHOT.
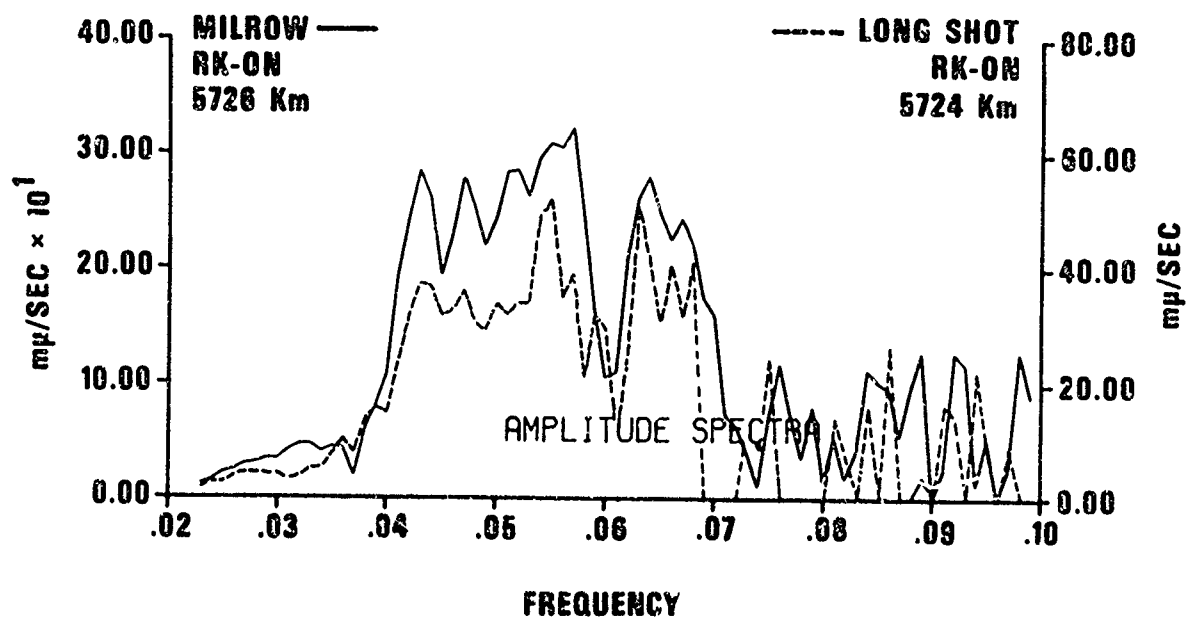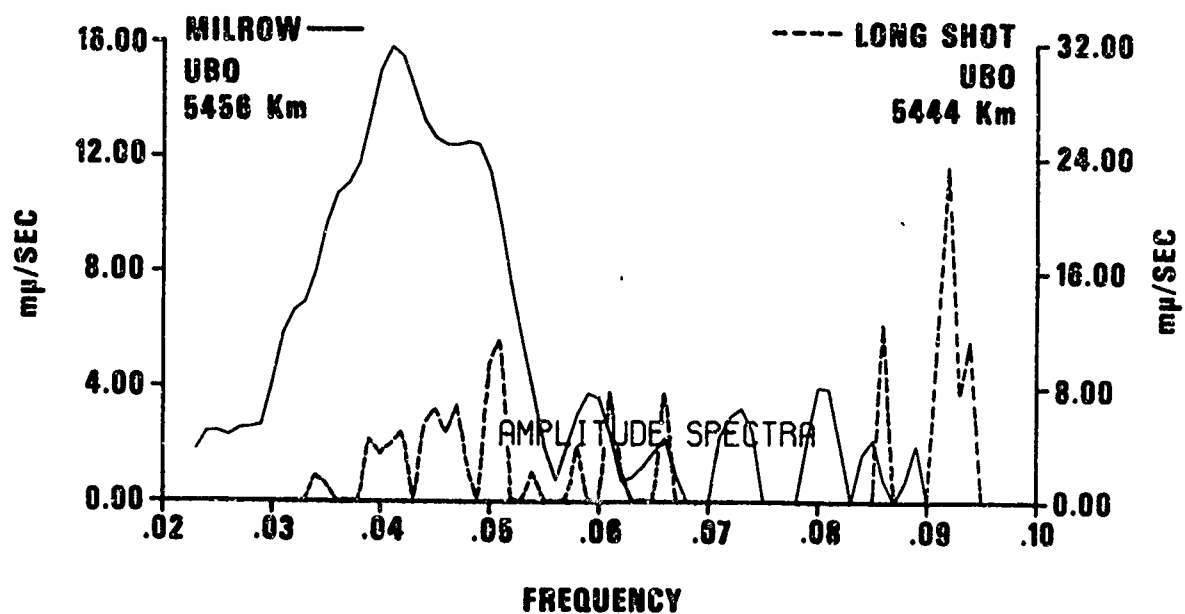
Figure 21. (Cont'd.)
Rayleigh-wave spectra for stations common to MILROW and
LONG SHOT.
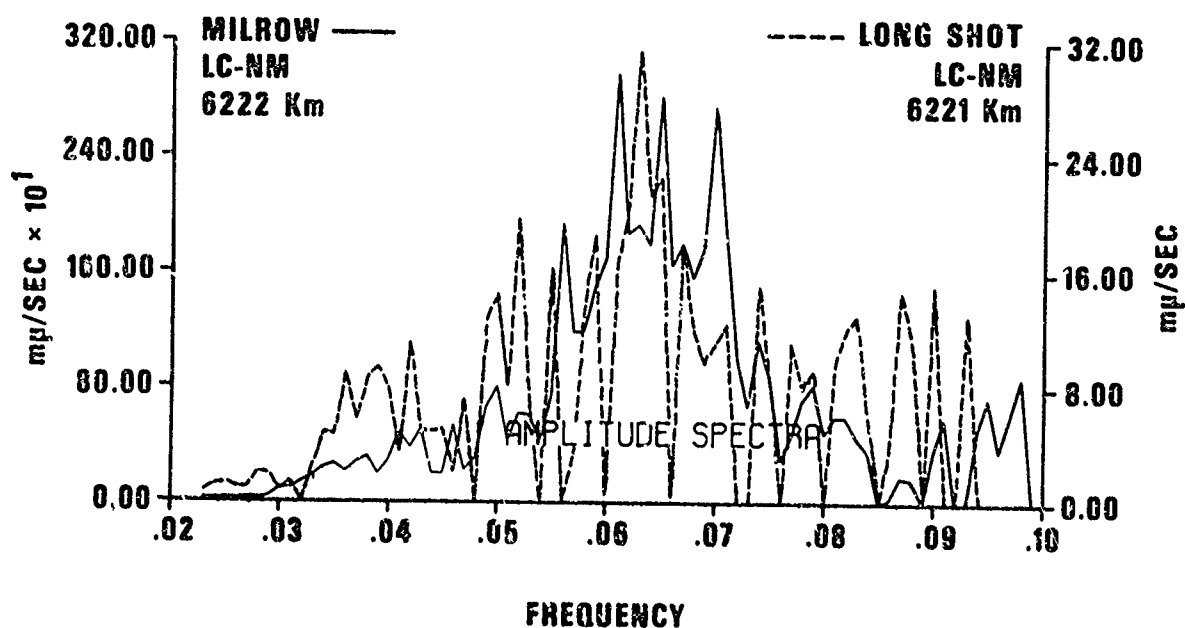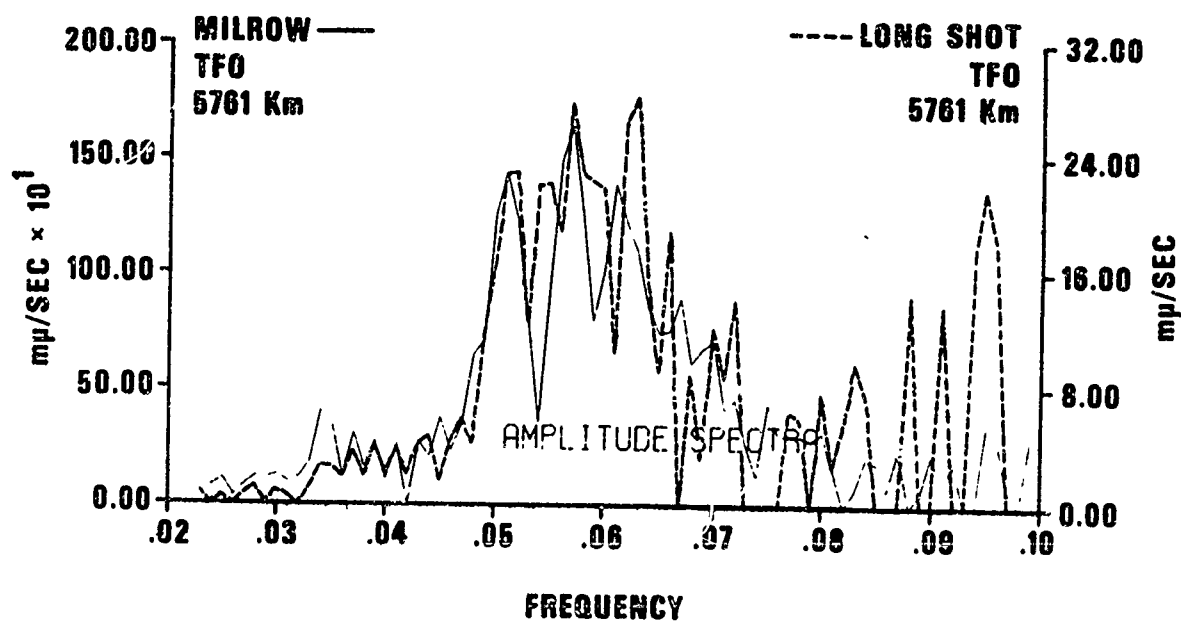
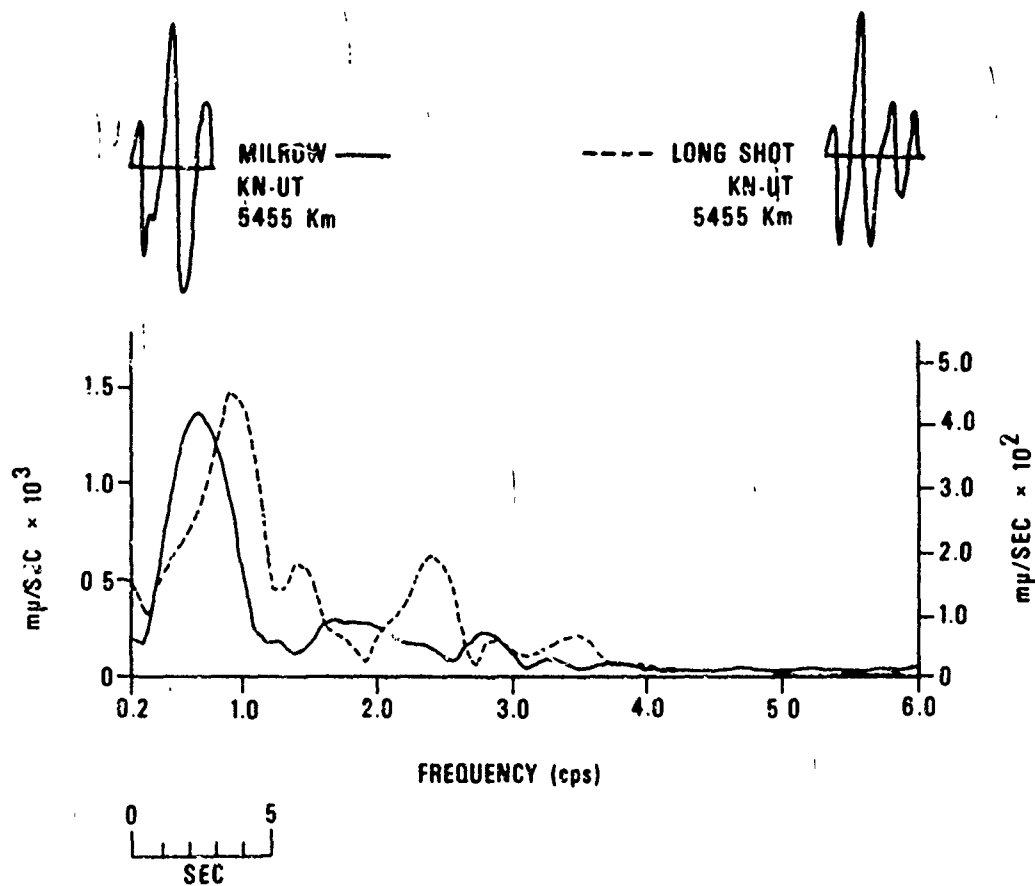Figure 21. (Cont'd.)
Rayleigh-wave spectra for stations common to MILROW and
LONG SHOT.
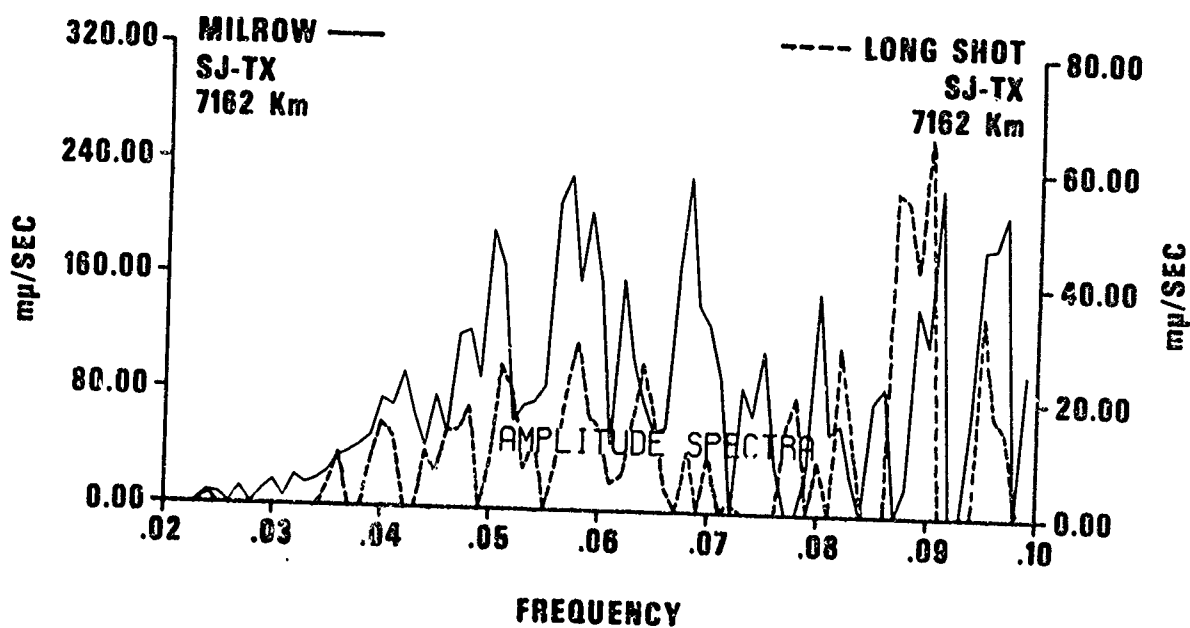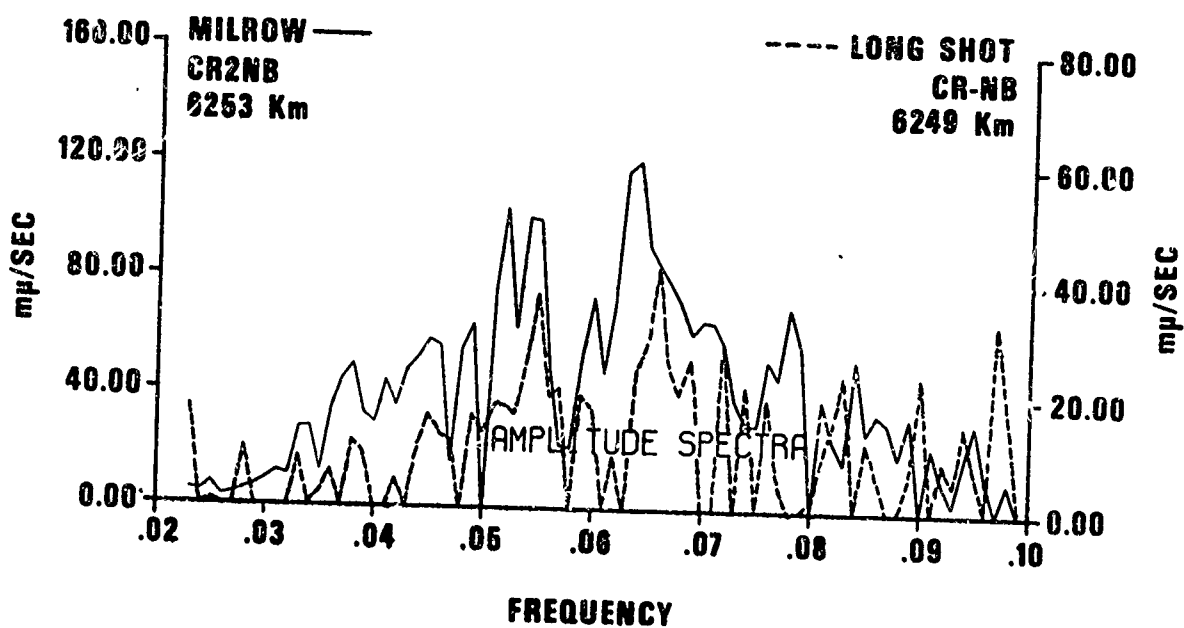
Figure 21. (Cont'd.)
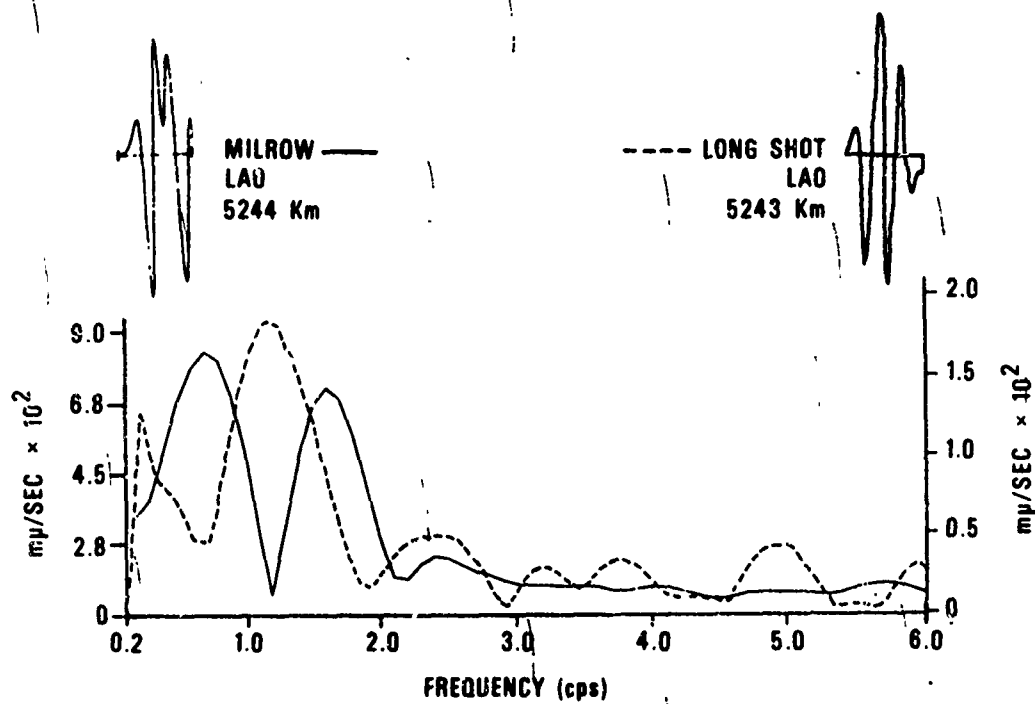Rayleigh-wave spectra for stations common to MILROW and
LONG SHOT.
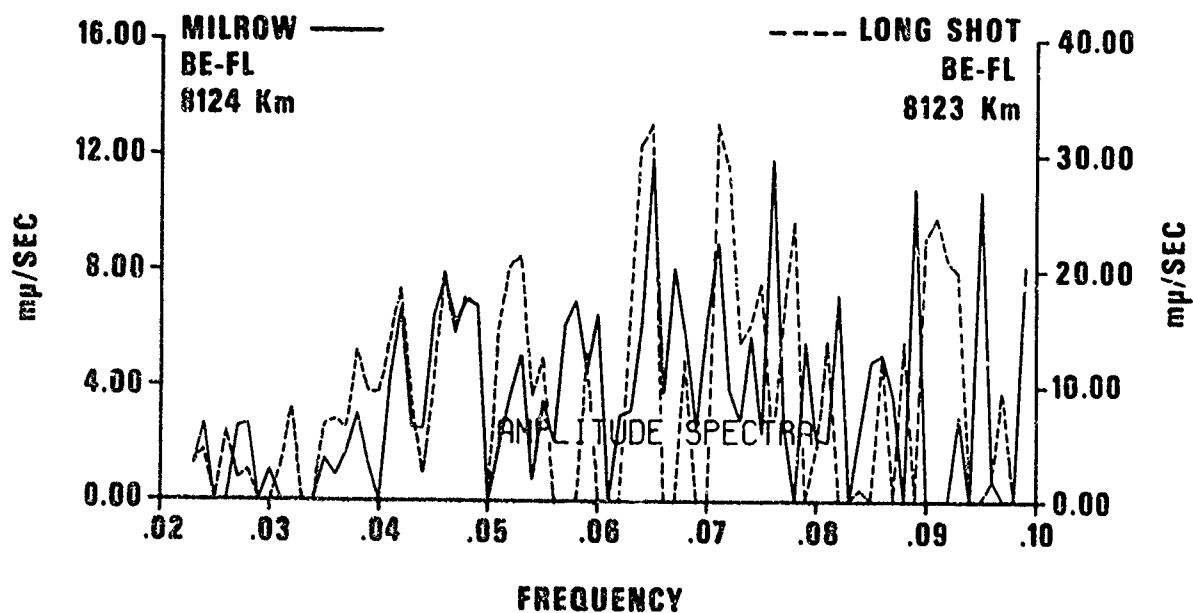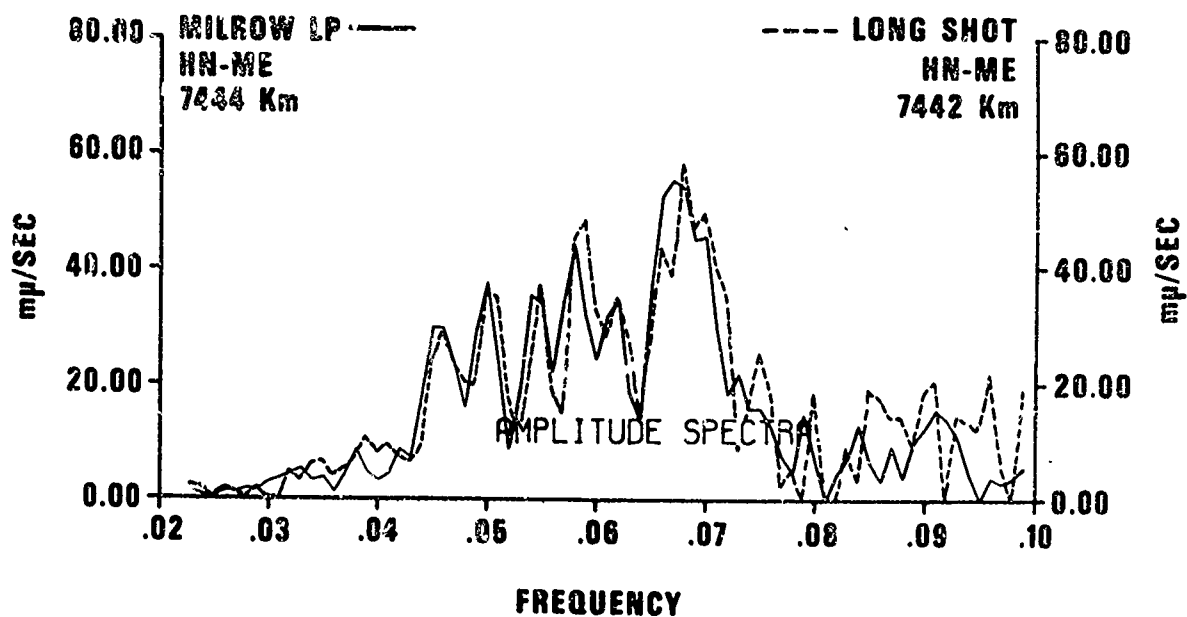
Figure 21. (Cont'd.)
Rayleigh-wave spectra for stations common to MILROW and
LONG SHOT.
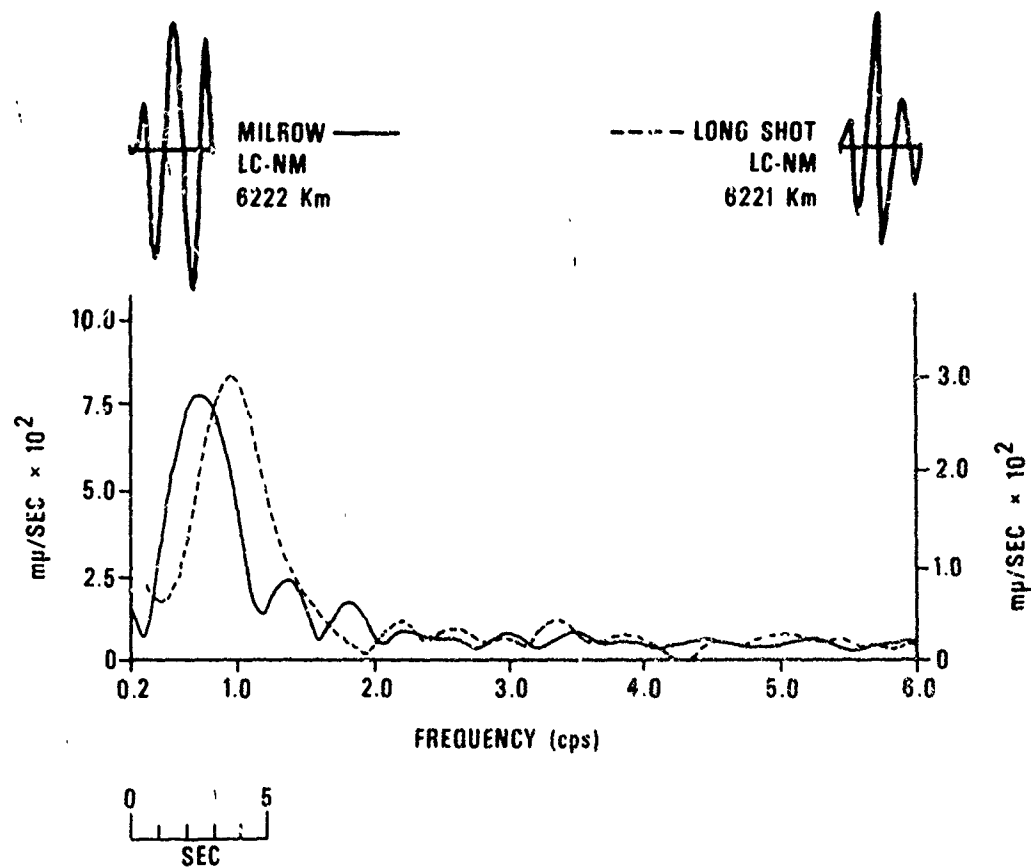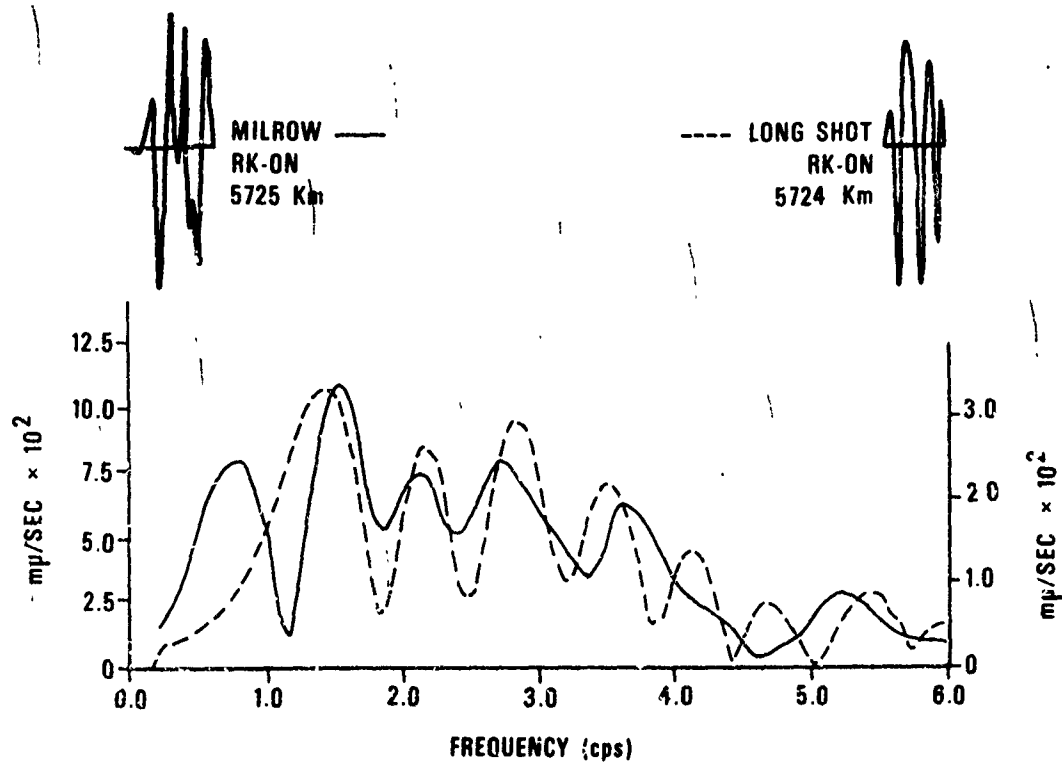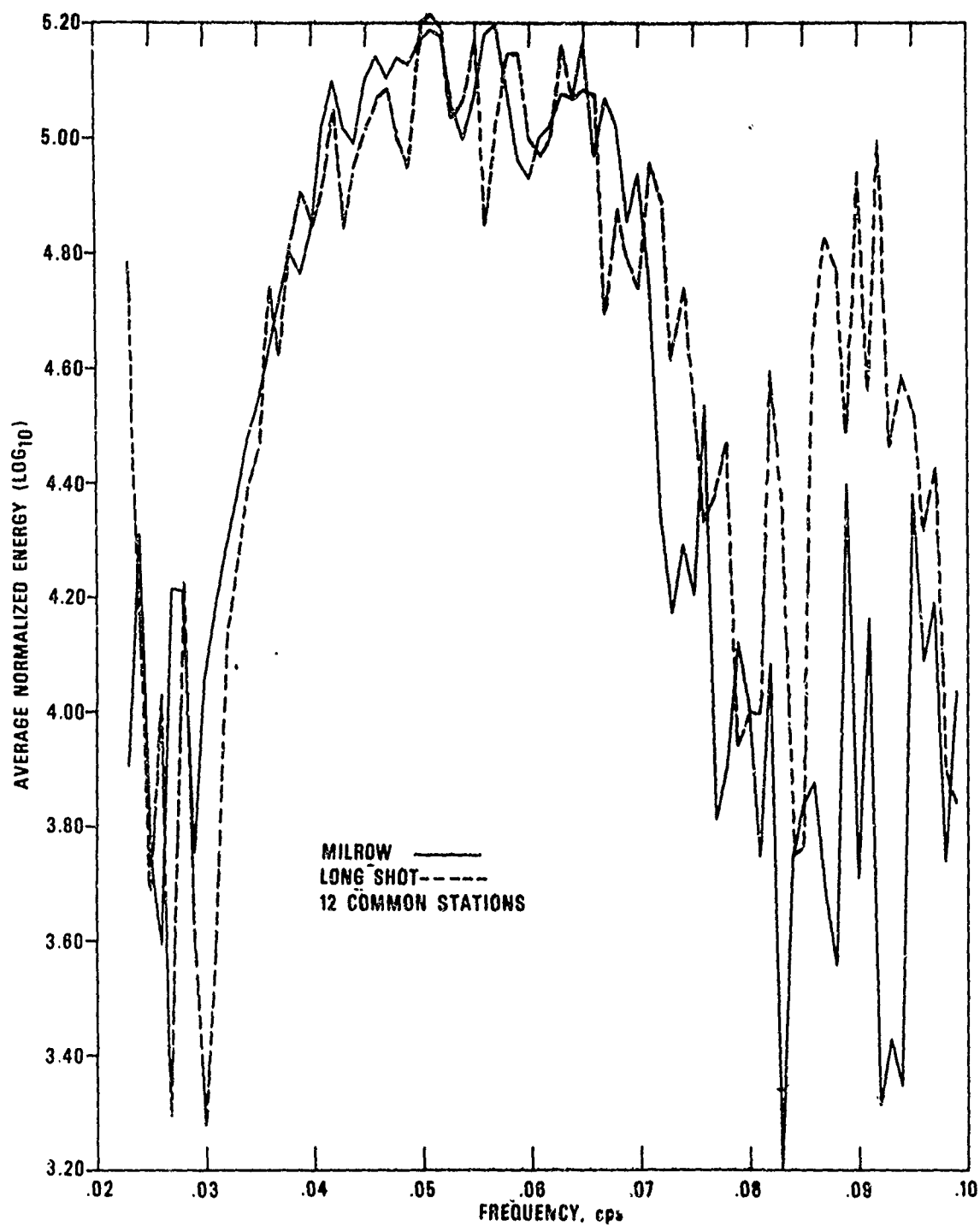
Figure 22. The average Rayleigh-wave normalized energy spectra for MILROW and LONG SHOT using twelve stations common to both events.

88
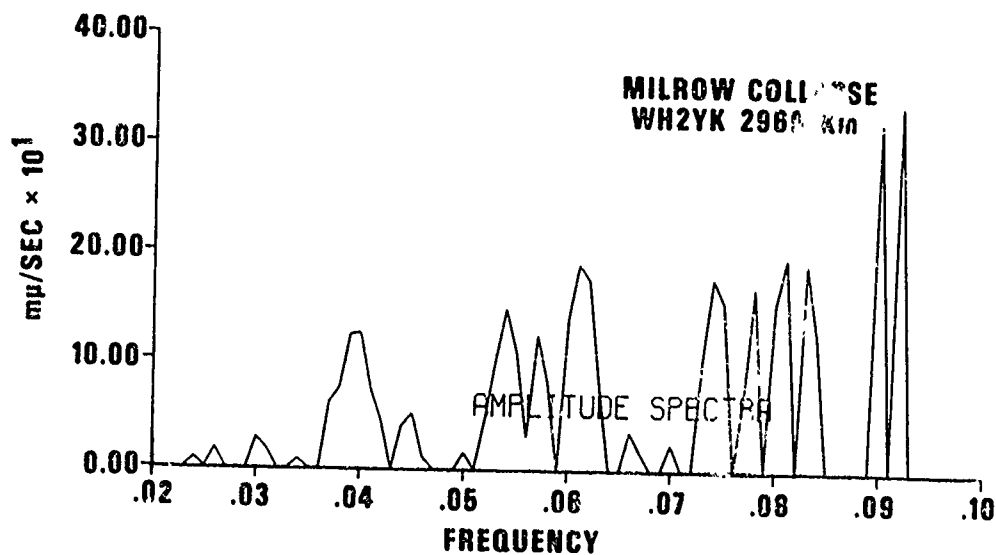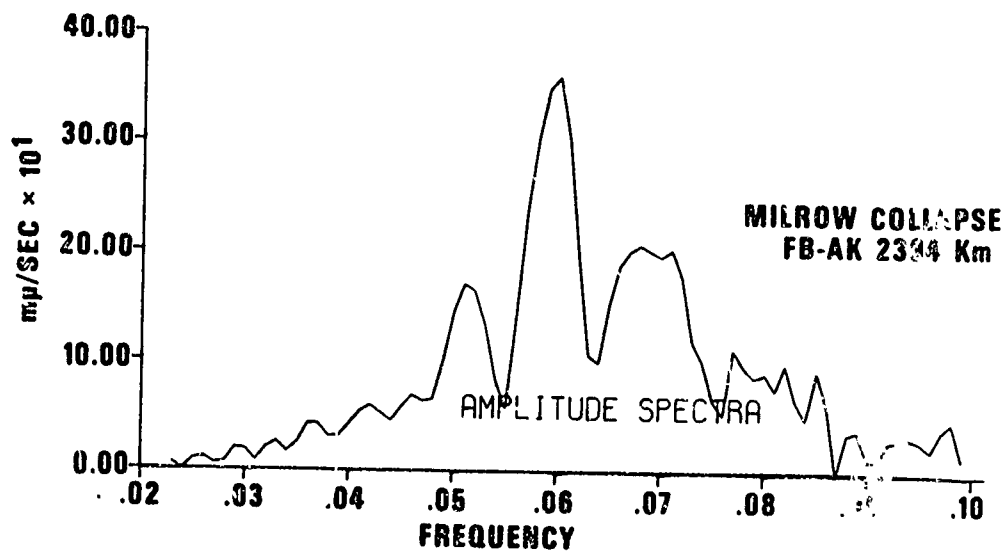
Figure 23. Rayleigh-wave spectra for the MILROW collapse.
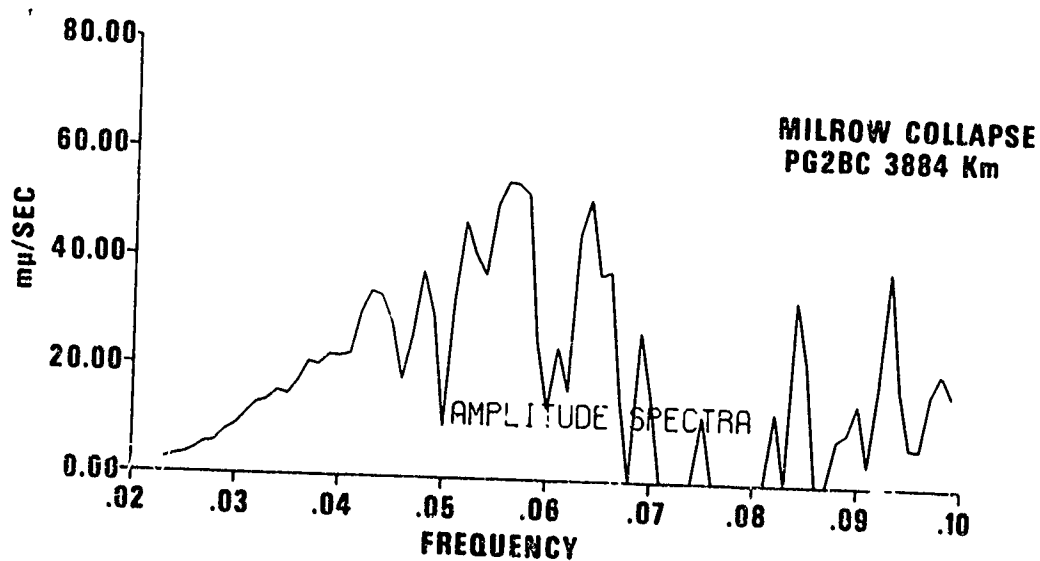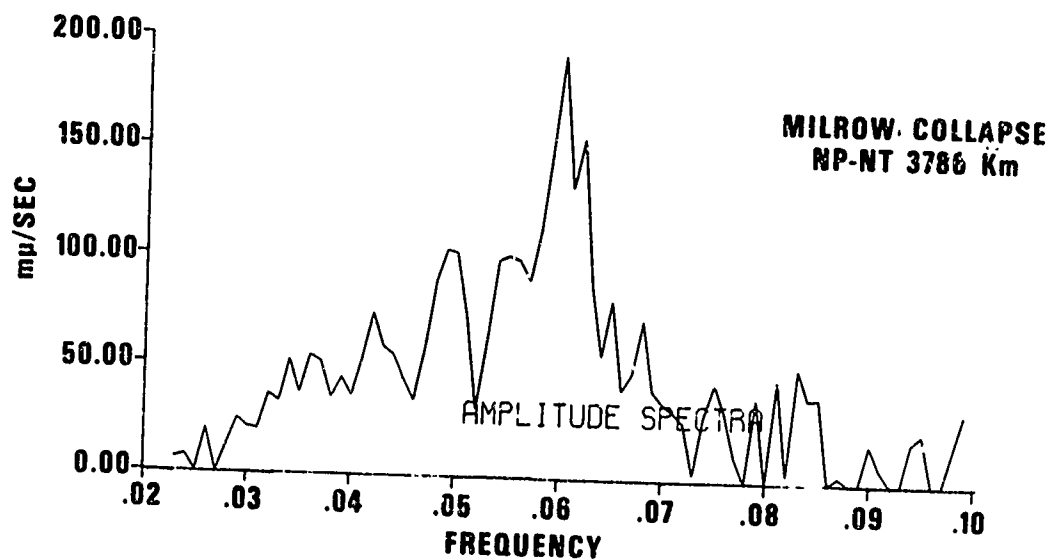
Figure 23. (Cont'd.)
Rayleigh-wave spectra for the MILROW collapse.

Figure 23. (Cont'd.)
Rayleigh-wave spectra for the MILROW collapse.

Figure 23. (Cont'd.)
Rayleigh-wave spectra for the MILROW collapse.

Figure 23. (Cont'd.)
Rayleigh-wave spectra for the MILROW collapse.

Figure 23. (Cont'd.)
Rayleigh-wave spectra for the MILROW collapse.

94
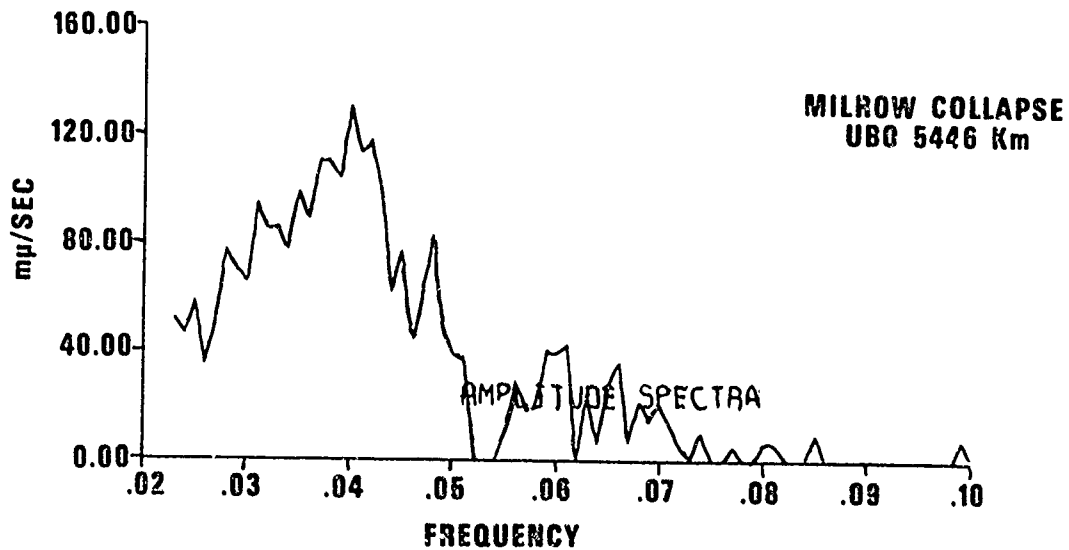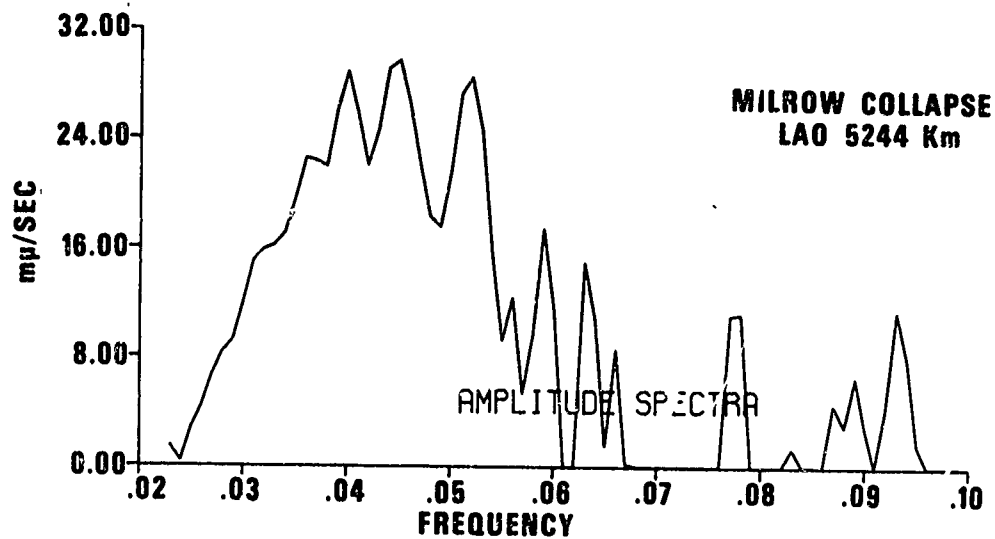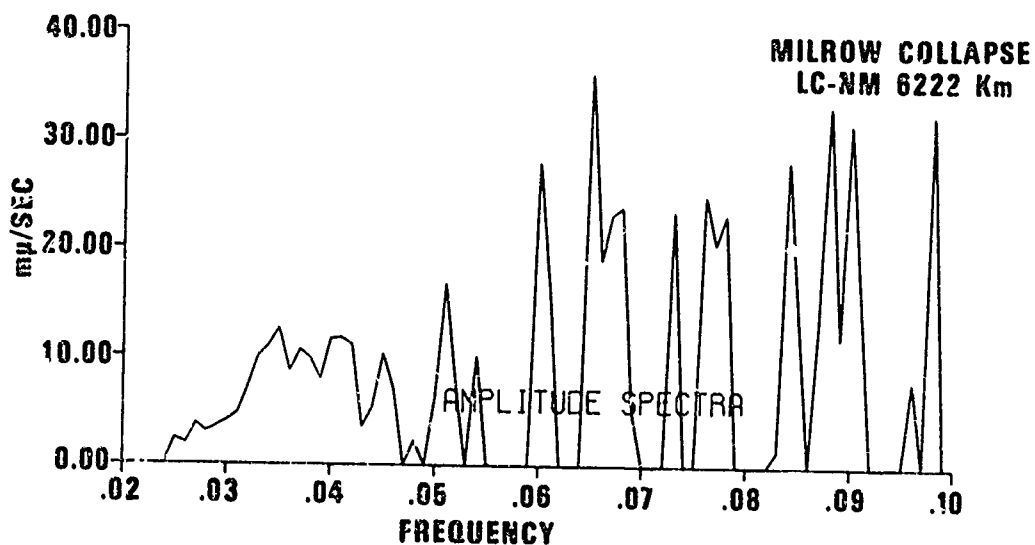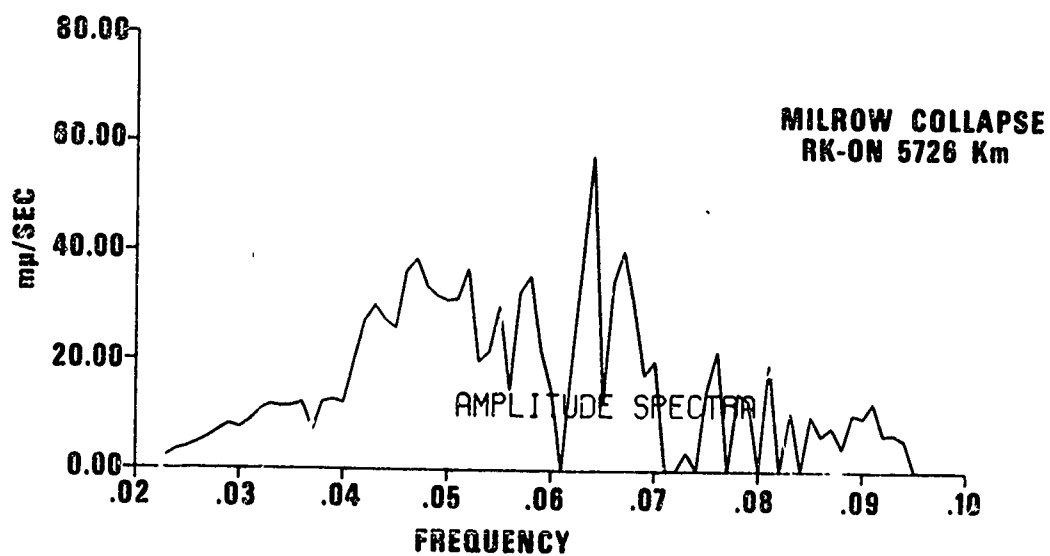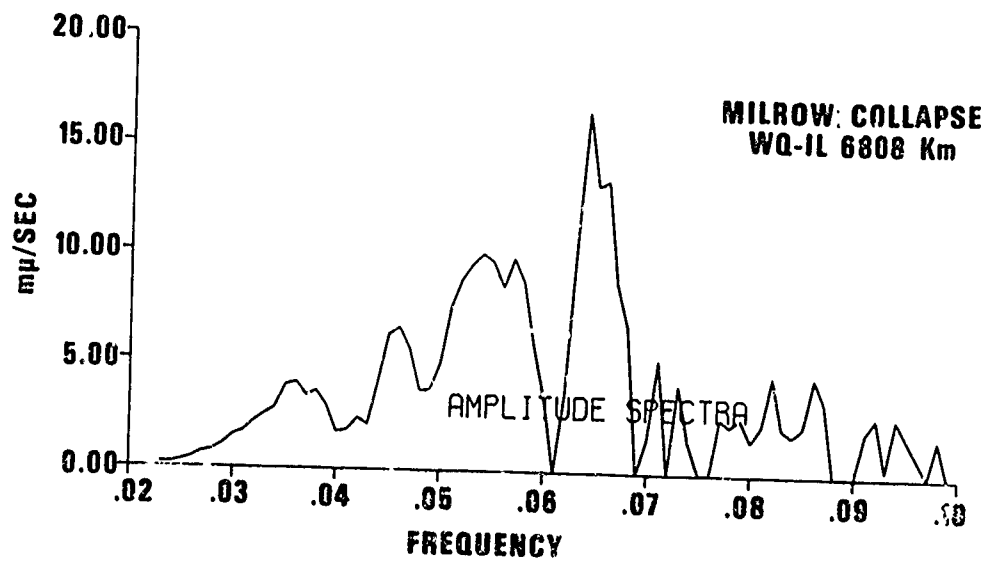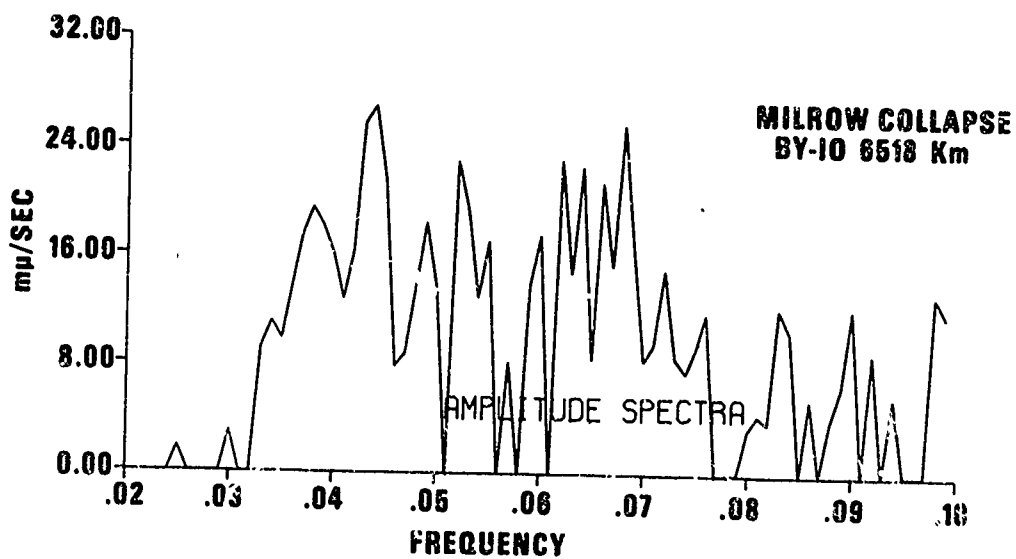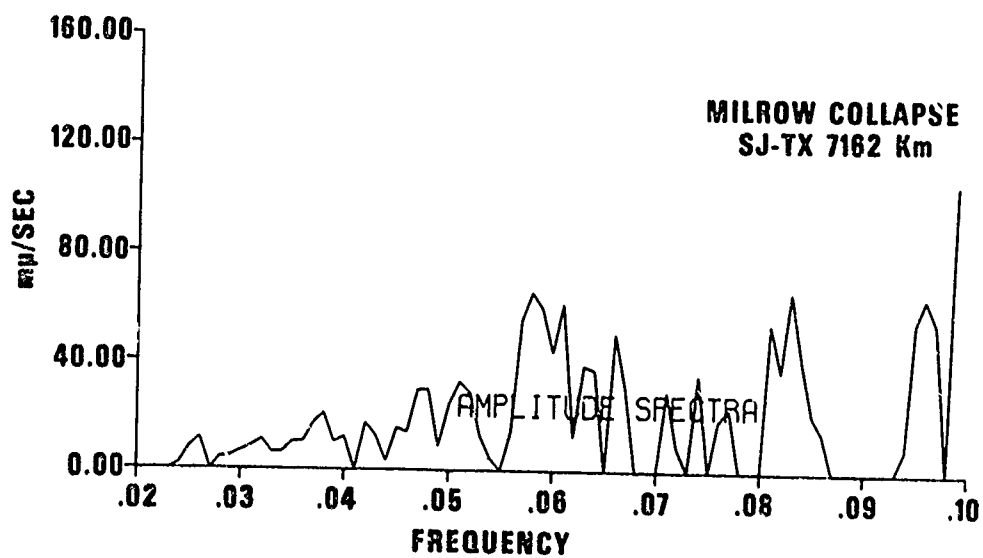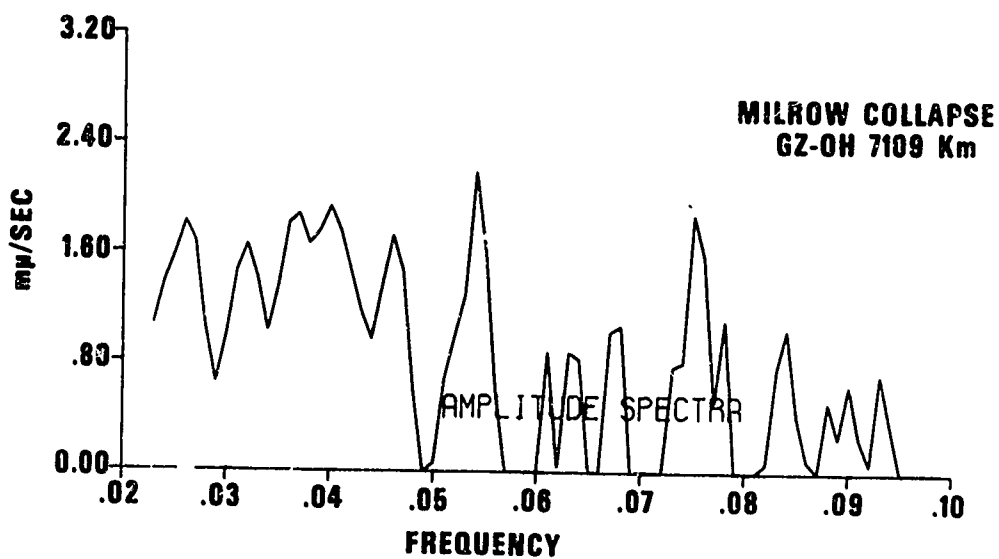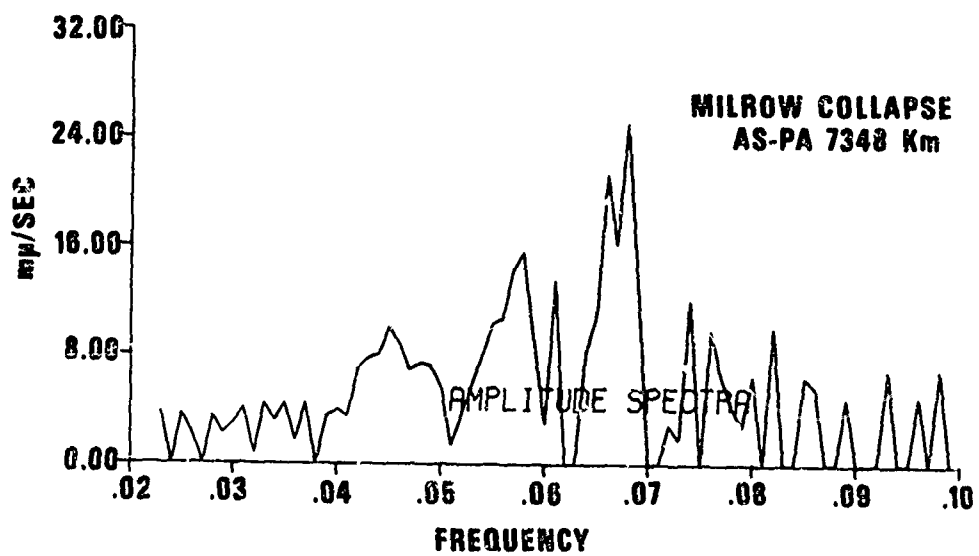
Figure 23. (Cont'd.)
Rayleigh-wave spectra for the MILROW collapse.
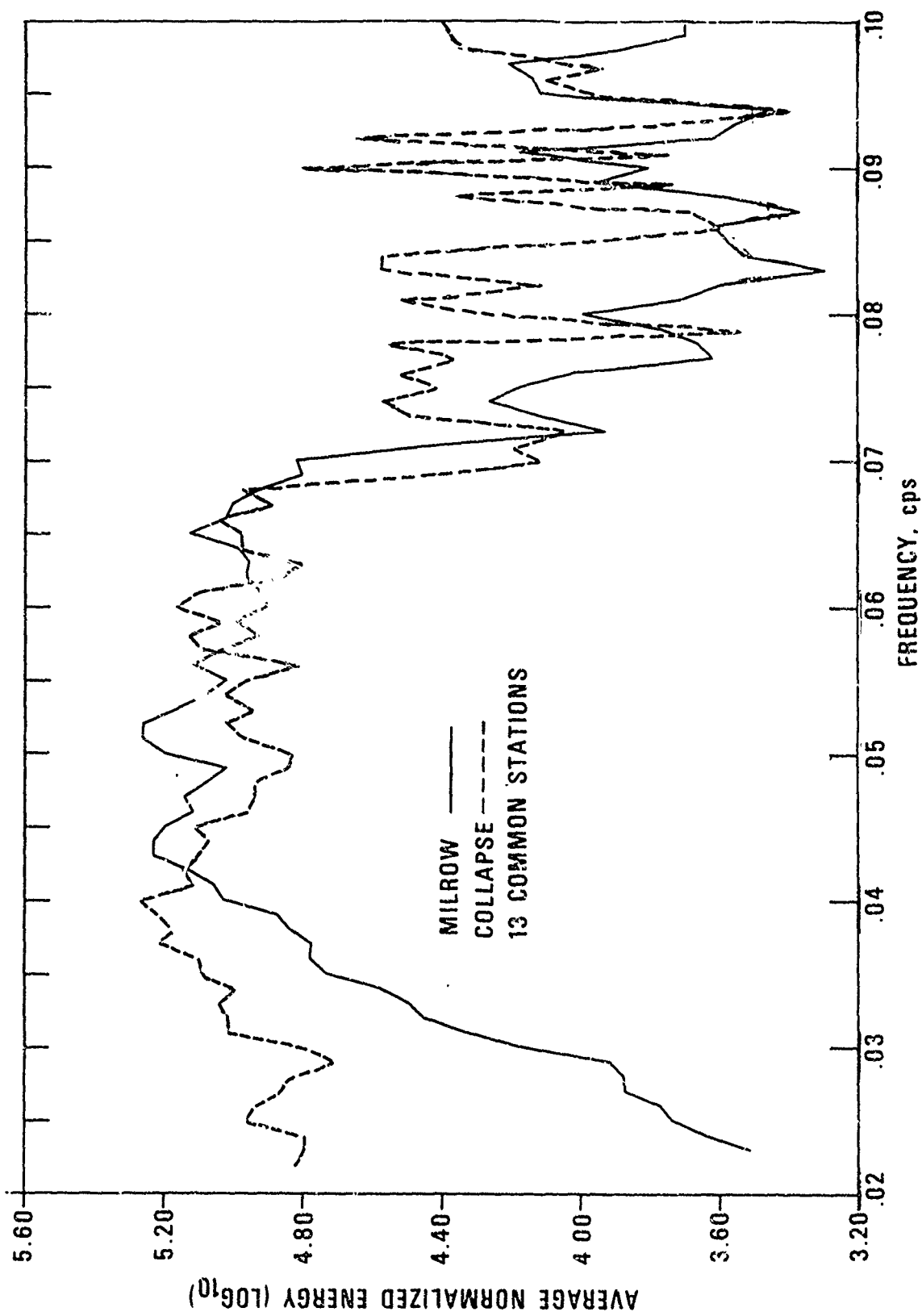
Figure 24. The average Rayleigh-wave normalized energy spectra for MILROW and its collapse using thirteen stations common to both events.
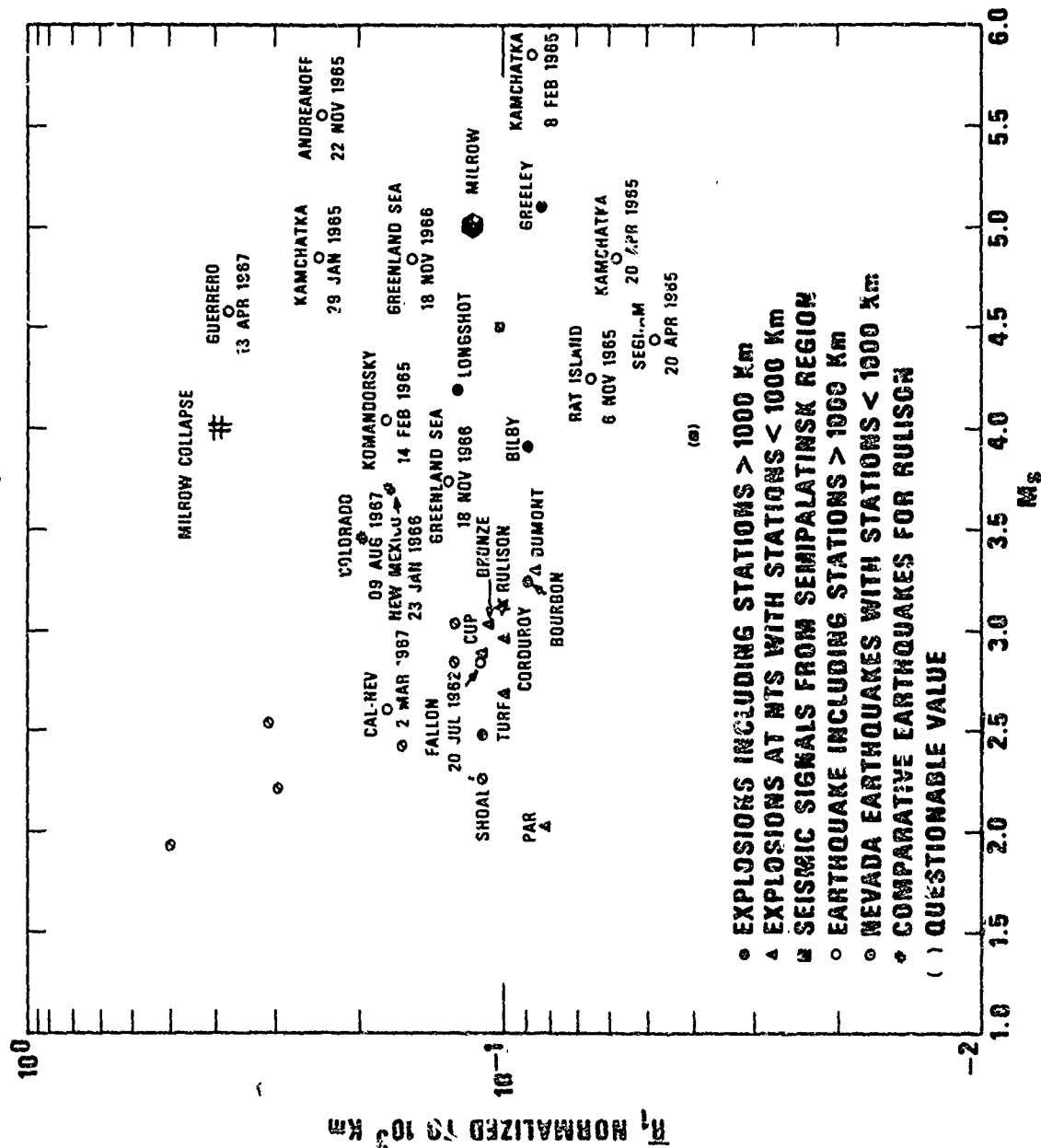
Figure 25. Rayleigh-wave spectral ratio vs Rayleigh-wave magnitude for many events.
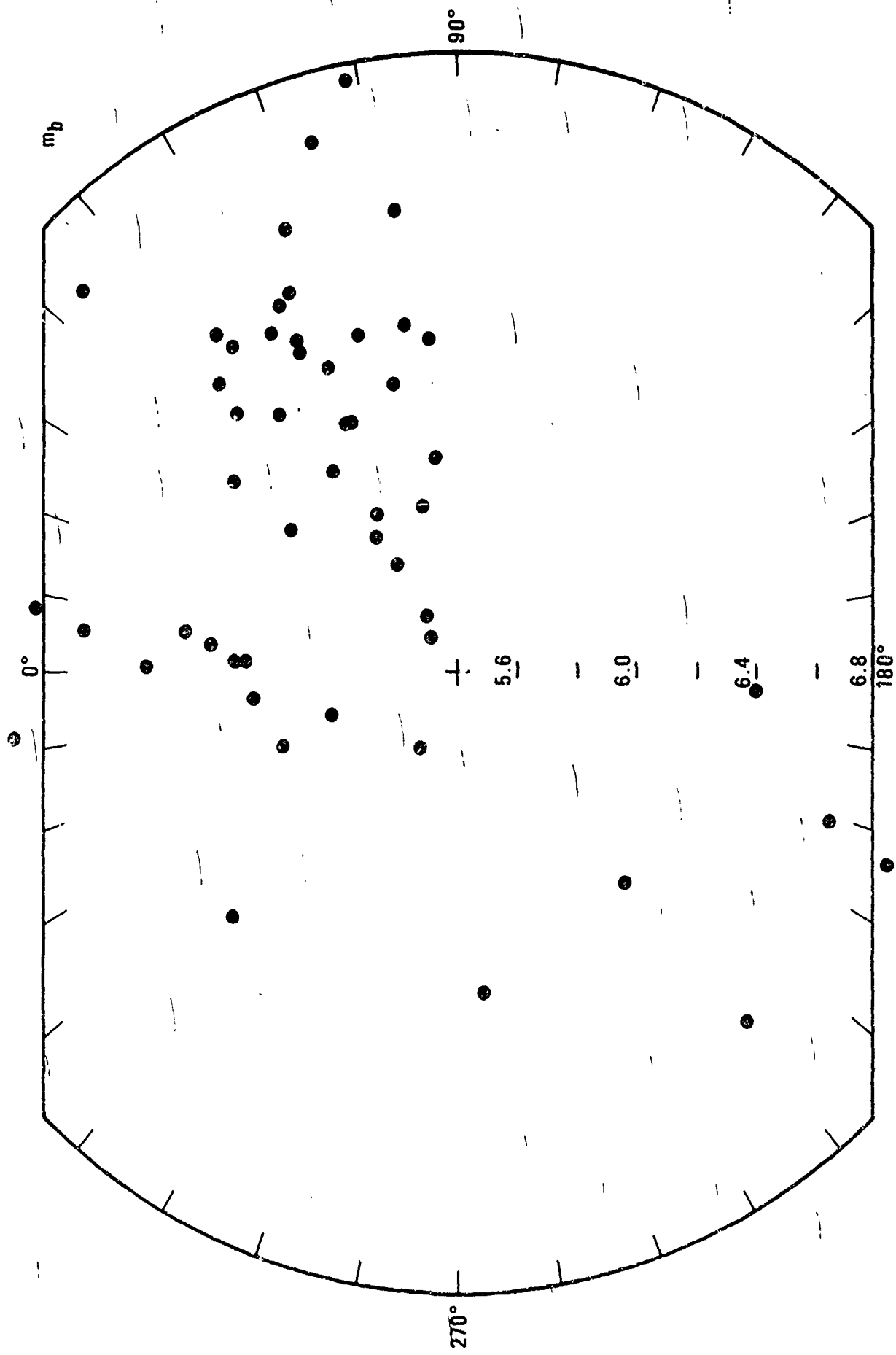
Figure 26. Polar plot of MILROW m_b using epicenter-station azimuth.

98
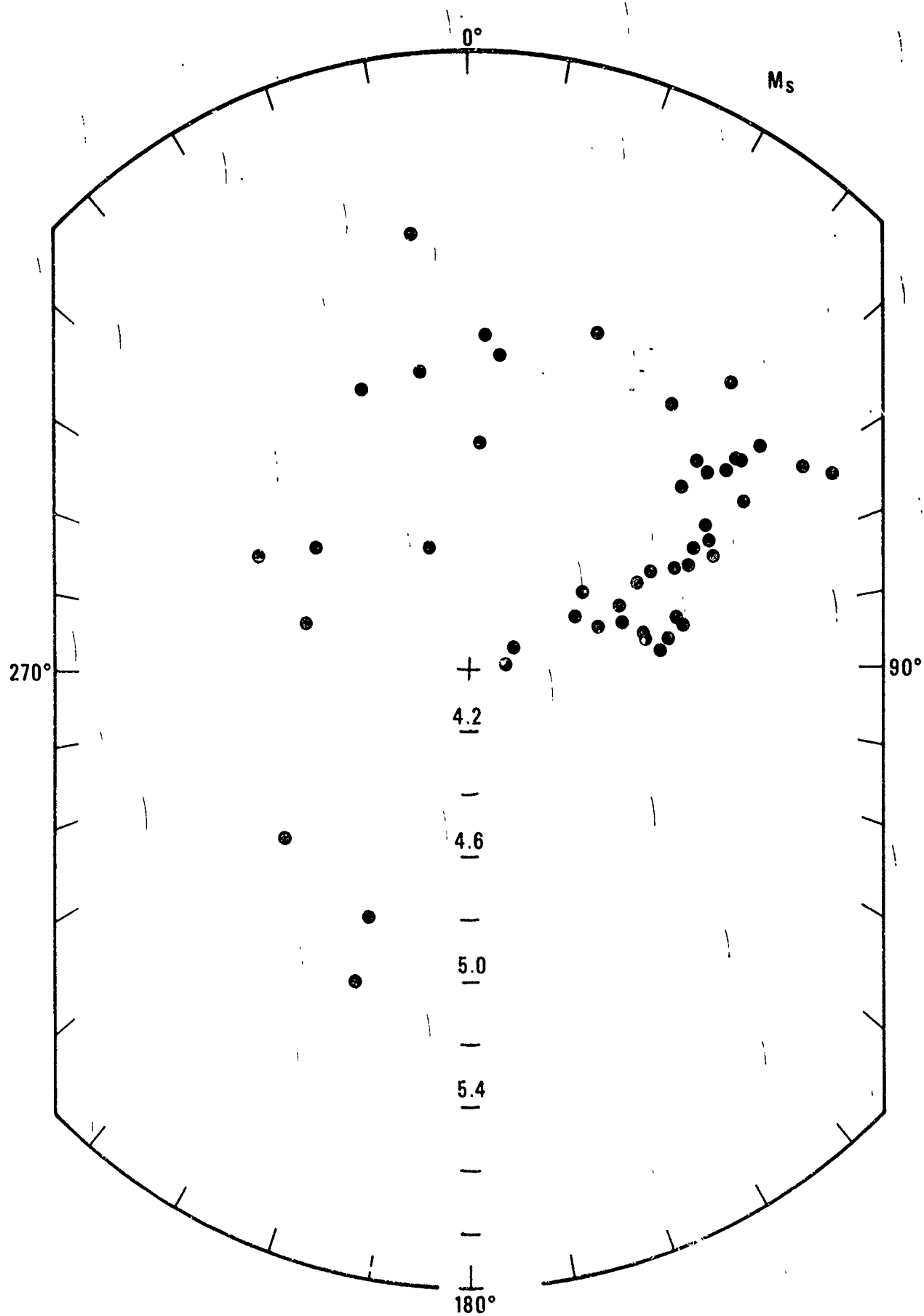
Figure 27. Polar plot of MILROW M_s using epicenter-station azimuth.
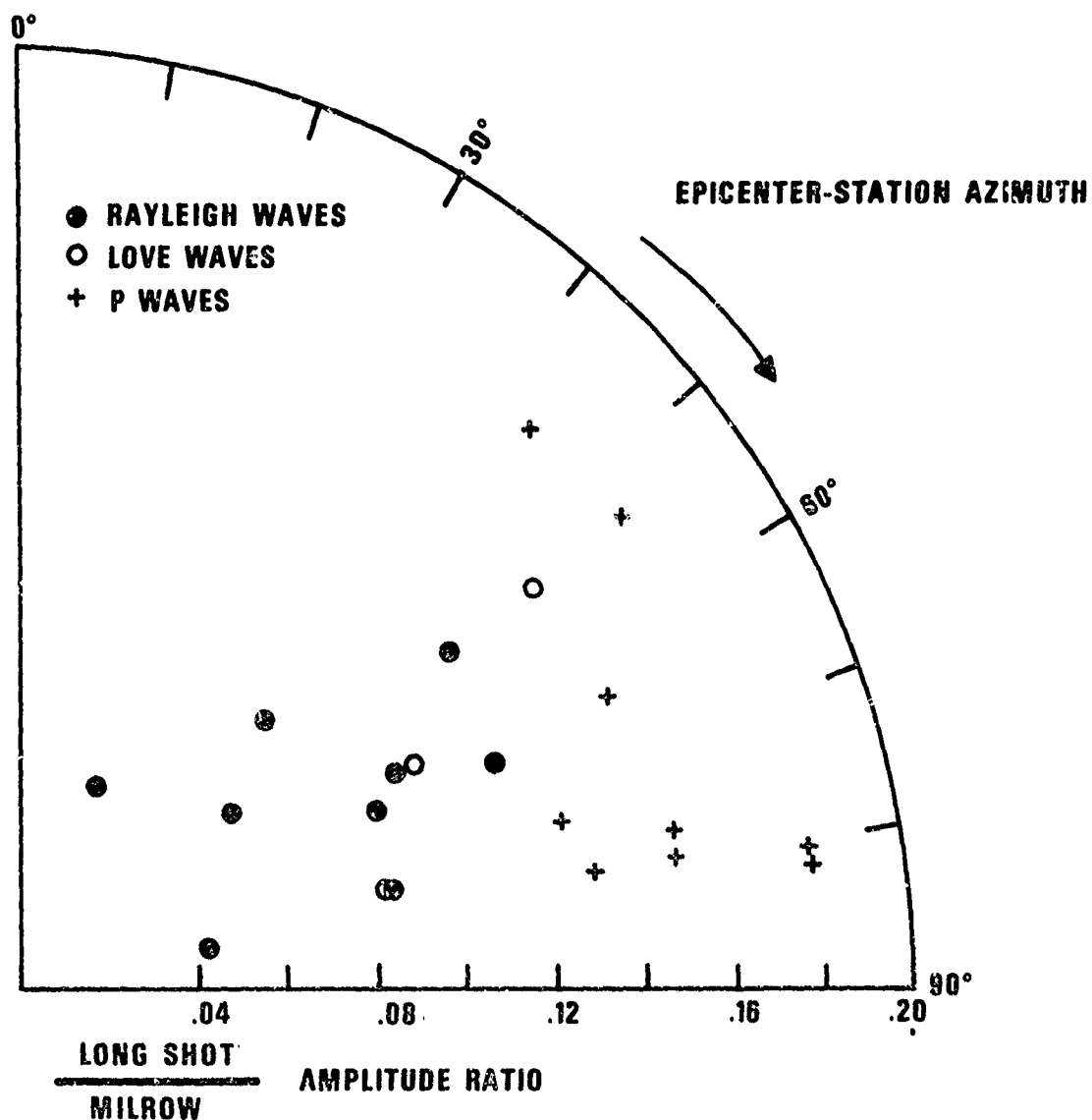
Figure 28. Polar plot of LONG SHOT/MILROW LQ and LR matched-filter amplitude ratios and first quarter-cycle P-wave amplitude ratios vs epicenter-station azimuth.
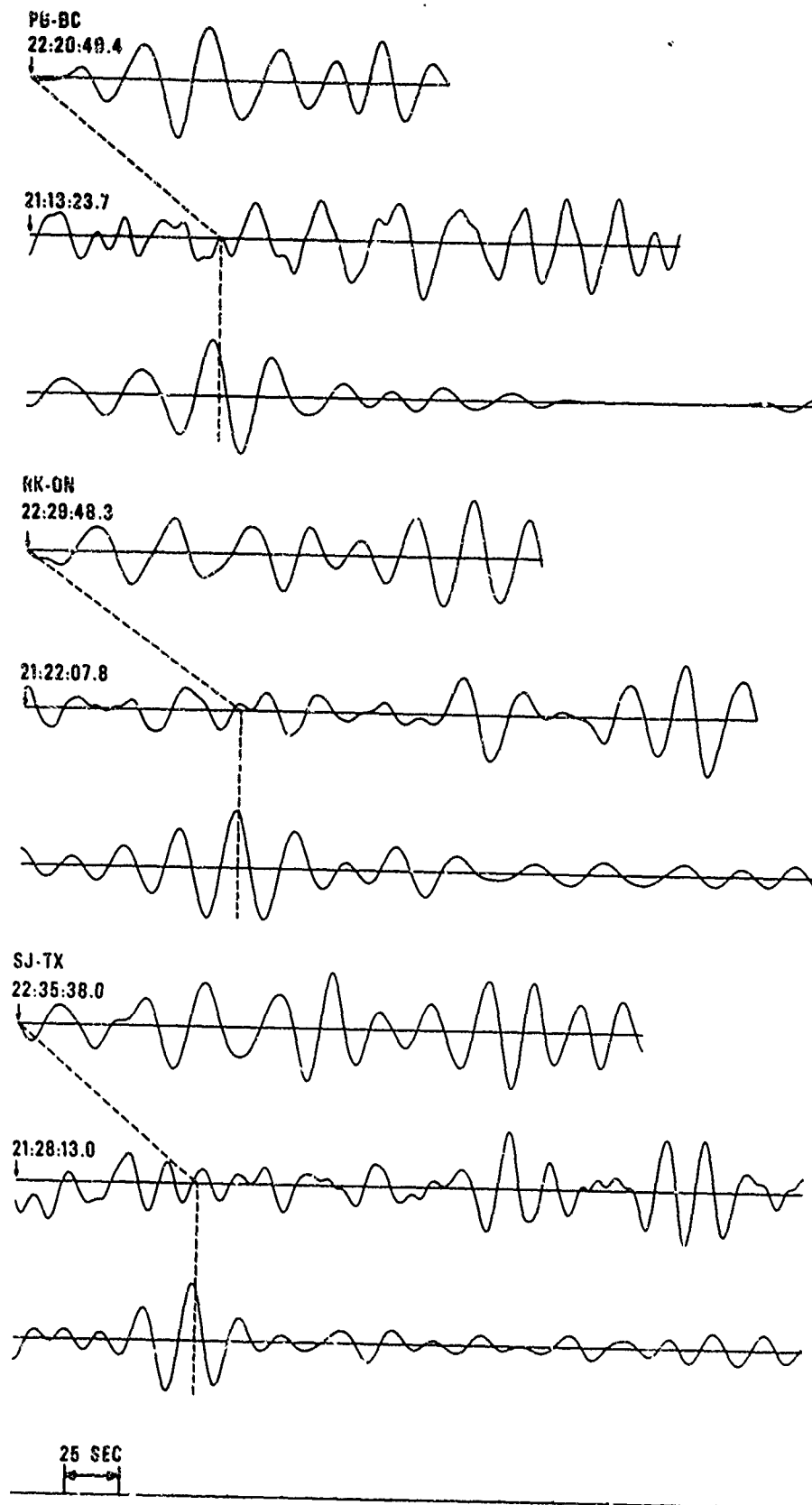
Figure 29. Match filtering of LONG SHOT LQ waves (middle trace) using MILROW recordings (top trace).
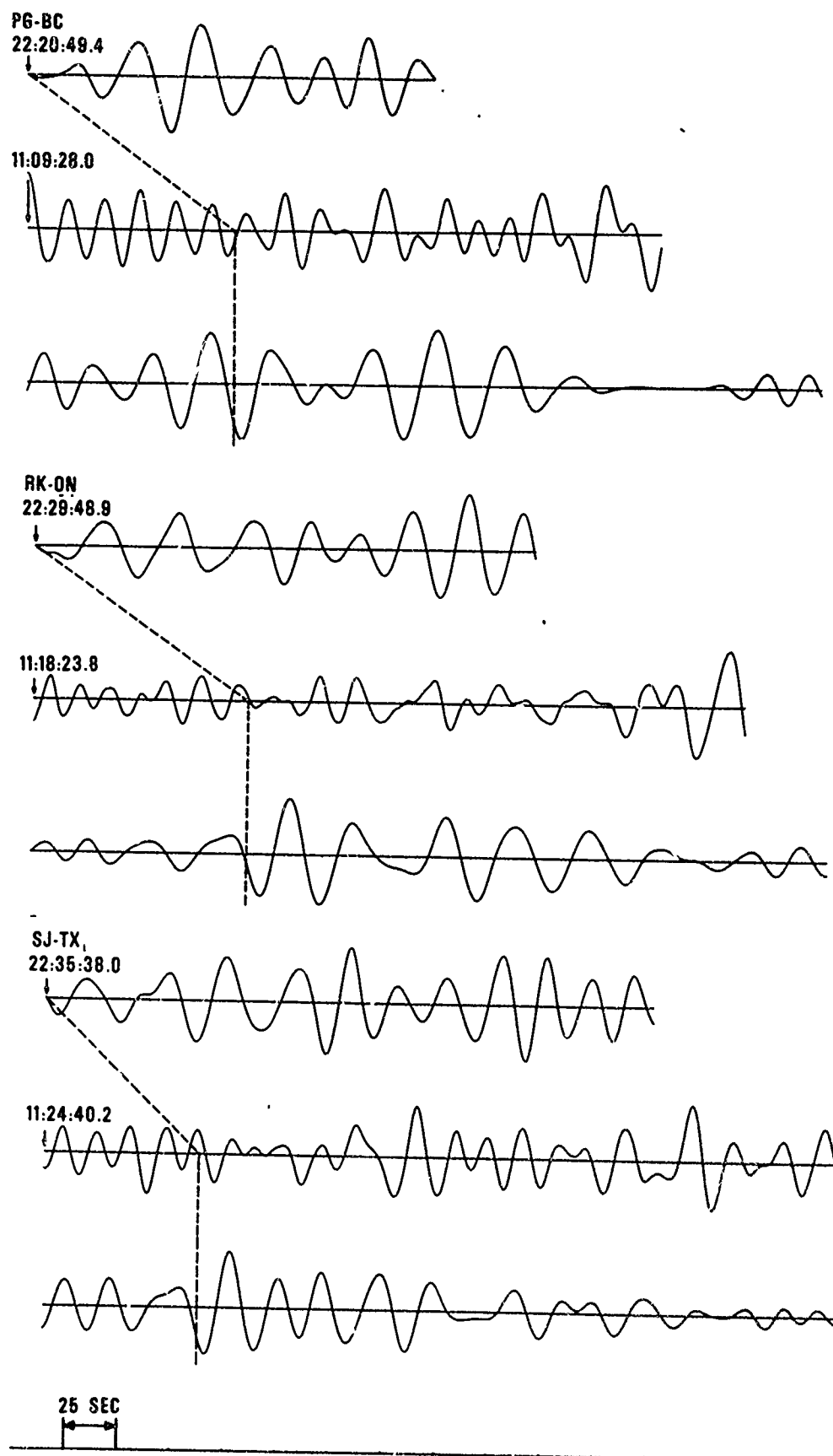
Figure 30. Match filtering of MILROW collapse LQ waves (middle trace) using MILROW recordings (top trace).
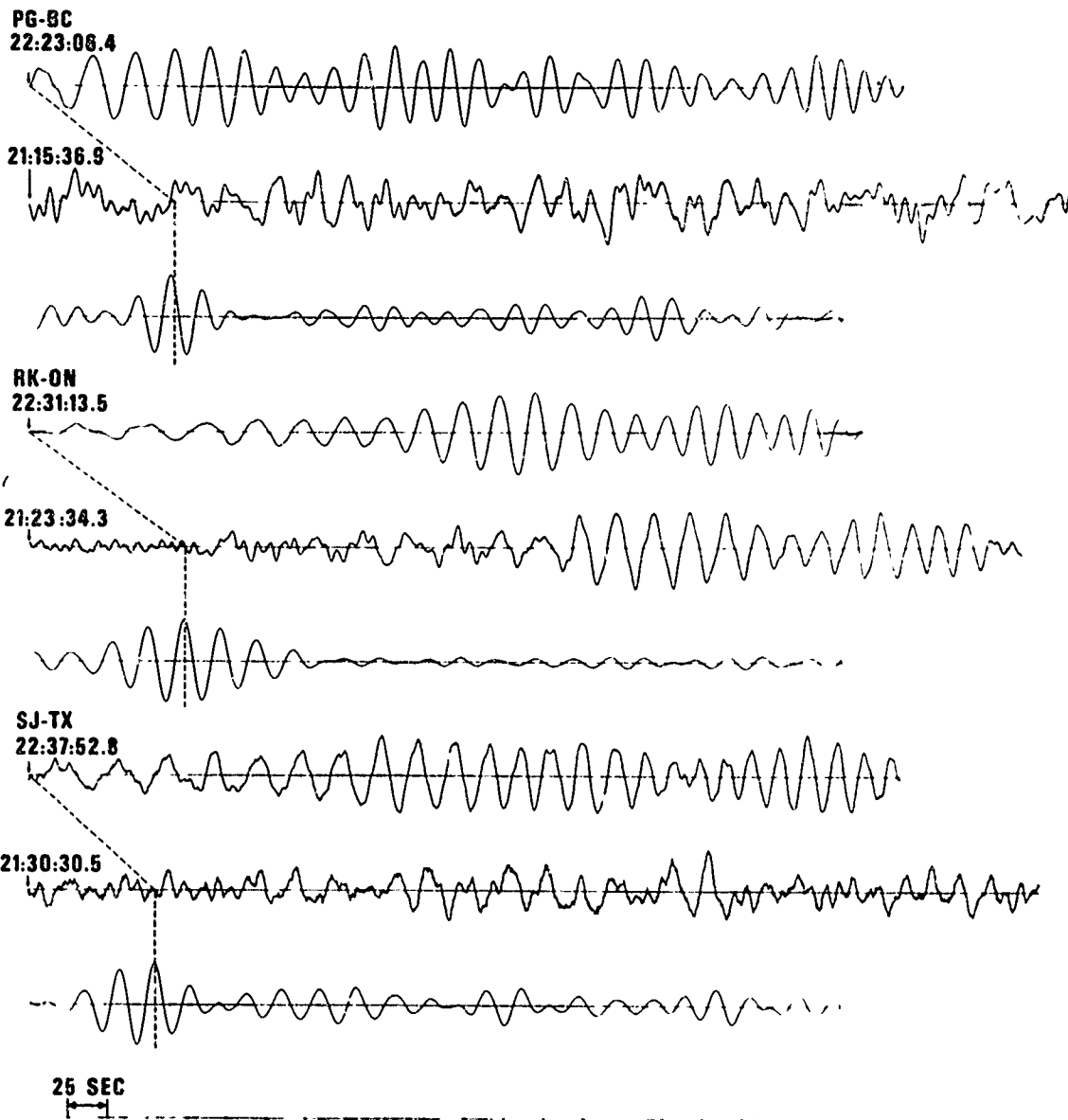
Figure 31. Match filtering of MILROW collapse LR waves (middle trace) using MILROW recordings (top trace).
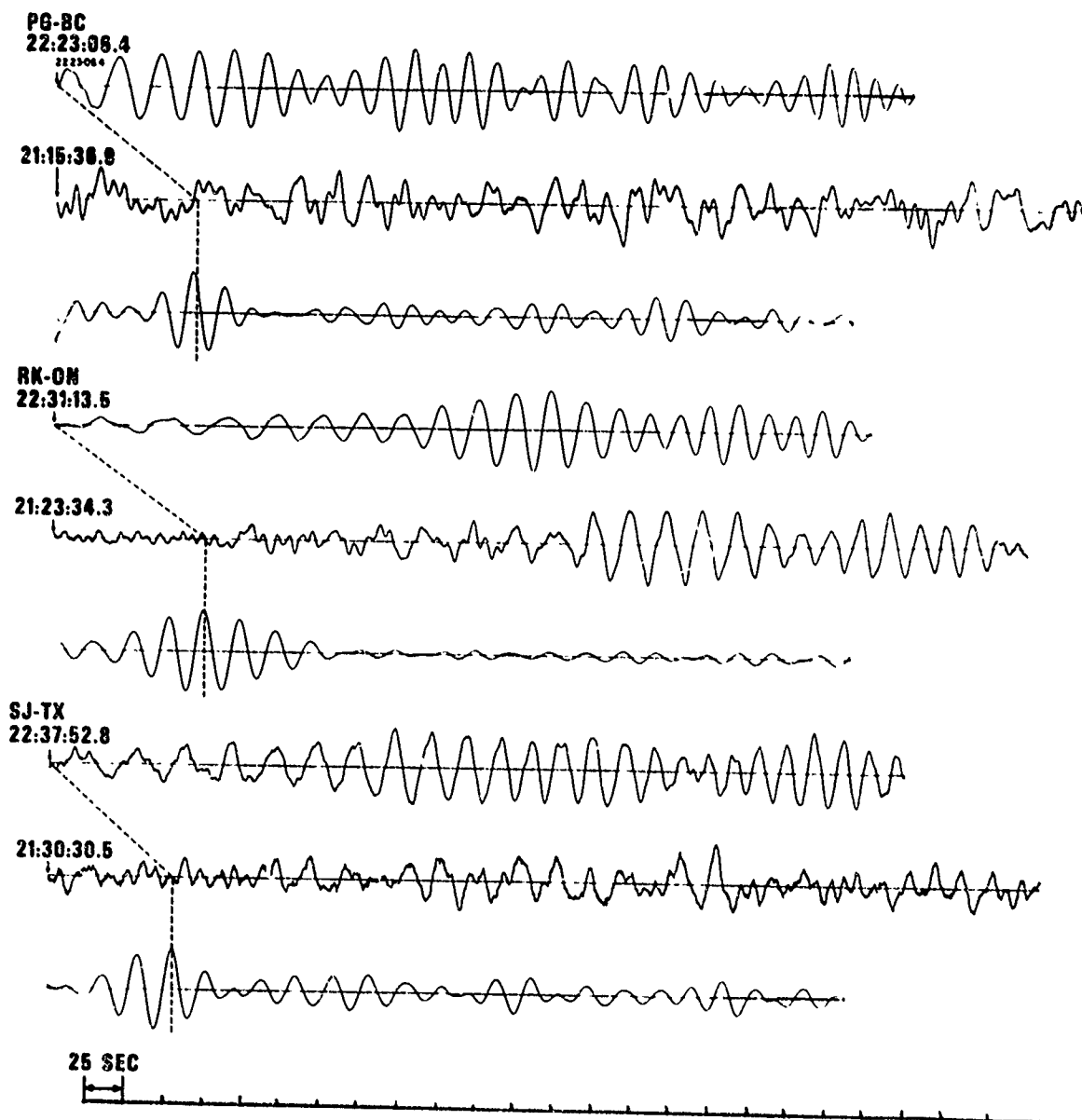
Figure 32. Match filtering of LONG SHOT LR waves (middle trace) using MILROW recordings (top trace).

TABLE I

Basic Epicenter Information for
MILROW and its Collapse

	MILROW	MILROW Collapse
Date	2 October 1969	4 October 1969
Origin Time	22:06:00.04Z	10:56:17.2Z
Location	51°25'02"N, 179°10'56"E	Same
Depth	3992 ft.	Same (?)
Medium	Tuff(?)	Same (?)

TABLE II

196

Arrival-Time Data for MILROW Location

Station	h	m.s	Station	h	m.s	Station	h	m.s	Station	h	m.s	Station	h	m.s
22*														
AAM	16	20.9	DAV	16	22.9	KIR	16	04.5	PJ-PA	16	57.4	UKI	13	47.6
AKU	16	23.1	DBQ	15	54.2	KLG	19	27.5	PMG	16	51.0	UPP	16	57.3
ALE	13	57.1	ODR	12	30.0	KN-UT	14	48.5	PNT	13	17.0	VAL	17	50.2
ALQ	15	26.9	DUG	14	32.5	KRL	18	06.3	PRI	14	14.9	VKA	18	06.0
AS-PA	16	45.7	EDM	13	32.3	KRP	18	55.8	PRU	17	57.7	WEL	19	09.2
ATU	18	49.6	ESX	17	32.4	KTG	15	48.1	PTO	18	46.5	WES	16	59.8
AVE	19	22.8	EUR	14	21.5	LAO	14	31.3	QCP	15	59.0	WH2YK	11	38.4
BAG	15	51.0	EU2AL	16	51.8	LC-NM	15	39.0	QUI	19	36.0	WQ-IL	16	13.8
BAH	12	53.7	FAV	16	10.3	MAL	19	08.0	RAB	16	07.2	YKC	13	01.6
BEC	18	05.0	FBC	15	20.4	MBC	12	44.2	RBA	19	19.0	ZAG	18	19.6
BER	17	0C.2	FB-AK	10	48.9	MDC	10	50.7	RES	13	36.0			
BE-FL	17	29.7	FCC	14	28.5	MEK	13	59.1	RIV	18	53.8			
BGO	16	25.4	FHC	13	35.7	MHC	19	18.5	RK-ON	15	03.6			
BHP	18	59.8	FUR	18	09.0	MIN	14	03.5	SAP	11	40.3			
BKS	13	55.4	GEO	16	58.7	MMA	13	49.0	SCM	10	41.2			
BLC	14	01.1	GH-MS	16	37.8	HNT	15	09.1	SES	13	52.8			
BLR	10	53.8	GIL	1?	50.6	HOK	16	36.7	SFA	16	37.2			
BMO	13	48.8	GNZ	18	58.0	MOX	12	53.6	SIT	11	38.2			
BNS	17	55.8	GRF	18	01.7	MRG	17	55.5	SJG	19	01.0			
BRS	18	50.2	GRK	16	35.5	MSH	16	46.5	SJ-TX	16	38.0			
BRW	10	59.?	GUA	14	28.2	MUN	17	57.8	SLD	14	06.7			
BUD	18	0C.8	GZ-OH	16	31.6	NDI	19	43.0	SOO	16	03.0			
BY-10	15	55.6	NCC	14	05.1	NEH	17	41.4	SRY	12	32.1			
CAR	19	27.0	HHM	13	48.5	NOR	13	34.0	SSS	18	11.1			
CHC	17	07.0	HKC	15	49.4	NP-NT	14	29.9	STC	14	09.3			
CHI	16	08.0	HMR	16	27.2	NTI	12	44.2	STU	18	07.2			
CLE	16	31.8	HM-ME	16	50.4	NUR	13	33.5	TFO	15	09.2			
CLL	17	49.7	HON	12	54.4	OIS	16	48.0	THT	17	36.8			
COL	10	50.0	IFR	19	22.4	OLC	13	02.0	TJC	15	24.0			
COM	17	53.0	IST	18	30.6	OPA	13	53.5	TMH	10	36.9			
COP	17	27.0	JAS	14	05.8	ORT	12	51.5	TOO	19	16.2			
CPO	16	45.7	JCT	16	15.0	OTT	16	48.6	TRI	18	18.2			
CRC	14	01.2	JER	19	04.5	PAS	16	40.6	TRN	19	39.6			
CRZ	18	40.0	KBL	17	40.0	PAX	14	36.0	TSK	12	23.6			
CR2NB	15	38.8	KDB	16	52.0	PG2BC	10	53.8	TJC	15	20.8			
CTA	17	52.3	KHC	18	03.2	PJD	12	47.7	TUL	16	05.5			
DAR	17	48.0	KIP	12	53.1			51.5	UBO	14	47.1			

*22:00:00 hour applies to all recordings

TABLE III

LRSM Van and VELA Array Data for MILROW

STATION	LOCALITY	DISTANCE km	deg	INSTRUMENT	PHASE	OBSERVED TRAVEL TIME		PERIOD (SECONDS)	MAXIMUM AMPLITUDE A/T(mu/sec)	MAGNITUDE m_b	M_s	COMMENTS
FB-AK	Fairbanks, Alaska	2394	21.5	SPZ	P	4	48.9	0.5	1610.0	6.36		PTA Clipping
				SPZ	PcP	8	50.3	0.6	72.3			
				SPZ	PcS	12	26.8	1.3	167.0			
				SPZ	P'P'	38	42.9	1.2	23.8			
				LPZ	P	4	(50)	(20.0)	(29.0)			
				LPZ	Sv	8	(52)	(13.0)	150.0			
				LPT	Sh	8	(55)	(14.0)	(81.0)			
				LPT	LQ			20.0	211.0			
				LPZ	LR			--	--			
WH2YK	Whitehorse, Yukon	2969	26.7	SPZ	P	5	38.4	0.8	--			Magnification unknown on short-period instruments. Used long-period calibration several days prior to 2 Oct.
				SPZ	PP	6	22.3	1.0	--			
				SPZ	PcP	9	02.5	0.9	--			
				LPT	LZ			24.0	(82.0)			
				LPZ	LR			17.0	(354.0)		(5.03)	
NP-NT	Mould Bay Northwest Territories	3785	34.0	SPZ	P	6	44.2	--	--			Clipped on film and tape
				SPZ	PcP	9	(30.0)	1.2	267.0			
				SPZ	P'P'	37	46.4	1.2	58.5			
				SPZ	P2P2	39	09.5	2.0	20.9			
				LPR	P	6	(44)	20.0	24.7			
				LPR	Sv	12	(20)	20.0	34.5			
				LPT	LQ			23.0	19.5			
				LPZ	-R			20.0	193.0		4.95	
PG2BC	Prince George British Columbia	3843	34.6	SPZ	P	6	47.7	1.2	188.0	5.97		
				SPZ	PcP	9	23.4	1.0	1030.0			
				SP2	PcS	13	08.0	1.0	19.5			
				LPT	LQ			31.0	46.3			
				LPZ	LR			22.0	90.5		4.63	

TABLE III (Cont'd.)

STATION	LOCALITY	DISTANCE km	deg	INSTRUMENT	PHASE	OBSERVED TRAVEL TIME		Period (Seconds)	MAXIMUM AMPLITUDE A/T(mμ/sec)	MAGNITUDE m_b	M_s	COMMENTS
BP-CL	Bishop, California	5028	45.2	LPZ	LR			21.5	18.1		4.12	Not operating at time of P arrival
LAO	LASA center, Montana	5243	47.2	SPZ	P	8	32.8	1.5	686.0	6.73		
				LPT	LQ			26.0	54.1		4.77	
				LPZ	LR			23.0	74.7			
USO	Uinta Basin, Utah	5445	49.0	SPZ	P	8	47.1	1.0	2260.0	7.15		
				SPZ	PcP	10	11.0	0.8	173.0			
				SPZ	PiP'	39	10.0	1.4	22.6			
				SPZ	PAP2	40	37.4	1.4	26.3			
				LPT	LQ			26.0	17.6		4.54	
				LPZ	LR			25.0	40.9			
KN-UT	Kanab, Utah	5455	49.1	SPZ	P	8	48.4	1.3	3360.0	7.32		
				SPZ	PcP	10	12.5	0.8	842.0			
				SPT	Sh	15	56.8	2.9	167.0			
				LPZ	Sv			14.0	54.2			
				LPT	Sh			12.0	66.7			
				LPT	LQ			28.0	44.2			
				LPZ	LR			20.0	50.8		4.63	
RK-ON	Red Lake, Ontario	5725	51.5	SPZ	P	9	03.6	0.7	944.0	6.68		
				LPZ	P	9	(04)	(21.0)	(7.8)			
				LPR	Sy	16	(30)	26.0	10.1			
				LPT	LQ			25.0	35.0			
				LPZ	LR			21.5	129.0		5.07	

TABLE III (Cont'd.)

STATION	LOCALITY	DISTANCE km deg	INSTRUMENT	PHASE	OBSERVED TRAVEL TIME	PERIODS (SECONDS)	MAXIMUM AMPLITUDE A/T(mμ/sec)	MAGNITUDE m_b	M_s	COMMENTS
TFG	Tonto Forest, Arizona	5760 51.8	SPZ	P	9 09.2	0.9	661.0	6.52		
			SPZ	PcP	10 22.6	1.3	275.0			
			LPZ	LR		20.0	(42.9)		(4.60)	Magnification uncertain
L,C-NM	Las Cruces, New Mexico	6222 56.0	SPZ	P	9 39.0	1.0	137.0	5.94		
			SPZ	PcP	10 37.2	0.8	161.0			
			SPZ	PKKP	29 57.4	1.0	10.0			
			LPR	Sv	17 (35)	18.0	(8.5)			
			LPT	Sh	17 (35)	19.0	12.6			
			LPT	LQ		30.0	26.5			
			LPZ	LR		15.0	37.7			
CR2NB	Crete, Nebraska	6253 56.2	SPZ	P	9 36.8	0.7	461.0	6.46	4.60	
			SPZ	PcP	10 33.4	0.7	338.0			
			LPZ	P	9 (39)	(14.0)	(30.2)			
			LPZ	LR		18.0	60.6			
BY-IO	Bloomfield, Iowa	6518 58.6	SPZ	P	9 55.6	0.8	803.0	6.71	4.80	
			SPZ	PcP	10 (42.0)	0.8	106.0			
			SPZ	P'P'	39 35.0	(1.0)	(20.0)			
			LPT	LQ		26.0	40.9			
			LPZ	LR		20.0	43.4			
WQ-IL	Watseka, Illinois	6821 61.3	SPZ	P	10 13.8	0.6	79.2	5.80	4.69	
			SPZ	PcP	10 54.8	0.6	77.7			
			LPT	LQ	10 (14)	13.0	5.6			
			LPT			24.0	25.3			
			LPZ	LR		19.0	97.9			
GZ-OH	Galion, Ohio	7109 63.9	SPZ	P	10 31.6	0.5	144.0	6.16	4.45	
			SPZ	PcP	11 06.0	0.8	118.0			
			SPZ	P'P'	39 18.0	1.0	71.5			
			LPZ	P	11 (30)	(20.0)	(4.6)			
			LPZ	LR		25.0	21.8			

TABLE III (Cont'd.)

STATION	LOCALITY	DISTANCE km	deg	INSTRUMENT	PHASE	OBSERVED TRAVEL TIME	PERIOD (SECONDS)	MAXIMUM AMPLITUDE A/T(mμ/sec)	MAGNITUDE m_b	M_s	COMMENTS
SJ-1X	San Jose, Texas	7162	64.4	SPZ	P	10 38.0	0.7	346.0	6.54		
				SPZ	PcP	10 09.0	1.0	73.8			
				SPZ	P'P'	39 22.8	1.5	28.2			
				LPT	P	10 (38)	(17.0)	(25.0)			
				LPZ	LQ		22.0	48.8			
				LPZ	LR		22.0	42.7		4.75	
GH-MS	Greenville, Mississippi	7188	64.6	SPZ	P	10 37.8	1.0	835.0	6.92		
				LPZ	LR		20.0	26.6		4.55	
AS-PA	Altoona, Pennsylvania	7348	66.1	SPZ	P	10 45.7	0.5	269.0	6.41		
				SPZ	PcP	11 20.0	0.8	69.9			
				SPZ	P'P'	39 18.4	1.2	29.6			
				LPZ	P		23.0	25.8			
				LPZ	LR		23.0	107.0			
EU2AL	Eutaw, Alabama	7432	66.8	SPZ	P	10 51.8	(0.8)	(184.0)	(6.27)		
				SPZ	PcP	11 19.0	1.0	56.1			
				SPZ	P'P'	39 (20.0)	1.1	10.2			
				LPZ	LR		18.0	10.5		5.17	
HN-ME	Houlton, Maine	7444	66.9	SPZ	P	10 50.4	1.2	1370.0	7.14		
				SPZ	PcP	11 25.4	1.0	141.0			
				SPZ	P'P'	39 (13.0)	1.3	26.2			
				LPZ	LR		20.0	132.0		4.17	
PJ-PA	Pottstown, Pennsylvania	7550	67.9	SPZ	P	10 57.4	1.0	560.0	6.74		
				SPZ	PcP	11 35.8	0.6	59.9			
				SPZ	P'P'	39 21.0	1.1	34.6			
				LPZ	LR		22.0	91.5		5.12	

TABLE III (Cont'd.)

STATION	LOCALITY	DISTANCE km deg	INSTRUMENT	PHASE	OBSERVED TRAVEL TIME	PERIOD (SECONDS)	MAXIMUM AMPLITUDE A/T(mµ/sec)	MAGNITUDE m_b	M_s	COMMENTS
BE-FL	Bellevieu, Florida	8124 73.1	SPZ SPZ LPZ	P PcP LR	11 29.7 11 47.4	0.7 0.8 23.0	236.0 138.0 31.4	6.27	4.71	

111

TABLE IV

Data for MILROW from NOS Reporting Stations

STATION	LOCALITY	DISTANCE km	deg	INSTRUMENT	PHASE	OBSERVED TRAVEL TIME		PERIOD (SECONDS)	MAXIMUM AMPLITUDE A/T(mu/sec)	MAGNITUDE m_b	M_s	COMMENTS
KDC	Kodiak, Alaska	1946	17.5	SPZ	P	4	00.0	0.8	1020.0	5.9T		
AMU	Anchorage Methodist U., Alaska	2100	19.0	SPZ	P	4	31.0	1.3	3190.0	6.50		
COL	College Outpost, Alaska	2413	21.7	SPZ	?	4	49.9	1.1	837.0	6.12		
				SPZ	Pc?	8	51.0	0.8	183.0			
				SPE	S	9	07.0	1.6	223.0			
				SPN	PcS	?2	28.0	1.4	129.0			
				SPZ	P'P'	38	44.0	1.6	89.3			
				LPZ	LR		18.0		544.0		5.07	
SIT	Sitka, Alaska	2900	26.4	SPZ	P	5	38.0	1.1	147.0	5.61		
				SPZ	PcP	9	03.0	1.4	383.0			
				SPZ	PcS	12	46.0	1.1	55.0			
KIP	Kipapa, Hawaii	3871	34.8	SPZ	P	6	53.3	--	--			Unreadable
				SPZ	PcP	9	25.0	0.6	29.5			
BMO	Blue Mountains, Oregon	4637	41.7	SPZ	P	7	48.6	1.1	1045.0	6.52		
				SPZ	PcP	9	45.2	1.2	208.0			
				LPZ	LR			20.0	91.6		4.77	
BKS	Byerly, California	4747	42.7	SPZ		7	55.4	1.0	919.0	6.46		
				SPZ		9	48.5	1.1	271.0			
				LPZ				20.0	68.4		4.66	

TABLE IV (Cont'd.)

STATION	LOCALITY	DISTANCE km	deg	INSTRUMENT	PHASE	OBSERVED TRAVEL TIME	PERIOD (SECONDS)	MAXIMUM AMPLITUDE A/T(mu/sec)	MAGNITUDE m_b	M_s	COMMENTS
SLD	San Luis Dam, California	4950	43.5	SP7	P	8 06.0	1.0	388.0	6.09		
GUA	Guam, Mariana Islands	5203	46.8	SPZ	P	8 28.5	0.8	930.0	6.87		
				SPZ	PcP	10 02.0	0.8	801.0			
				SPZ	PP	10 10.0	1.7	227.0			
				SPN	S	15 25.0		235.0			
				LPZ	LR		18.0	85.5		4.82	
NOR	Nord, Greenland	5220	46.9	SPZ	P	8 29.5	1.0	161.0	6.11		
				SPZ	PP	10 25.0	1.0	68.9			
				LPZ	LR		18.0	134.0		5.02	
TUC	Tucson, Arizona	5941	53.4	SPZ	P	9 20.7	1.1	762.0	6.88		
				SPZ	PcP	10 29.0	1.1	125.0			
				SPZ	PP	11 17.0	1.6	73.1			
				SPN	S	16 54.0	(3.4)	(42.0)			
				SPN	PS	17 18.0	(3.2)	(34.7)			
				SPZ			1.6	36.2			
				LPZ	LR	39 07.0	18.0	42.7		4.62	
ALQ	Albuquerque, New Mexico	6040	54.3	SPZ	P	9 26.9	0.6	350.0	6.34		
				SPZ	PcP	10 29.0	1.1	110.0			
				SPZ	PP	11 19.0	1.3	24.5			
				SPZ	P'P'		1.1	4.6			
				LPE	LQ		28.0	20.4			
				LPZ	LR	39 23.0	22.0	54.5		4.73	
HKC	Hong Kong, China	6380	57.4	SPZ	P	9 49.4	1.2	417.0	6.42		
KTG	Kap Tobin, Greenland	6395	57.5	SPZ.	P	9 48.4	1.3	332.0	6.32		
FLO	Florissant, Missouri	6798	61.1	LPZ	LR		24.0	67.0		4.91	

113

174

TABLE IV (Cont'd.)

STATION	LOCALITY	DISTANCE km	deg	INSTRUMENT	PHASE	OBSERVED TRAVEL TIME		PERIOD (SECONDS)	MAXIMUM AMPLITUDE A/T (mμ/sec)	MAGNITUDE m$_b$	M$_s$	COMMENTS
AKU	Akureyri, Iceland	6947	62.5	SPZ	P	10	23.1	1.6	763.0	6.83		
HNR	Honiara, Solomon Islands	6988	62.8	SPZ LPZ	P LR	10	27.2	1.2 22.0	558.0 92.0	6.73	5.07	
OXF	Oxford, Mississippi	7197	64.7	LPZ	LR			16.0	59.5		4.90	
CPO	Cumberland Plateau, Tennessee	7350	66.1	SPZ SPZ SPZ LPZ	P PcP P'P' LR	10 11 39	45.7 15.0 22.0	0.7 0.6 1.3 24.0	384.0 288.0 25.2 168.0	6.58		
SCP	State College, Penna.	7380	66.4	LPZ	LR			22.0	62.5		5.36	
WES	Weston, Mass.	7601	68.4	SPZ LPZ	P LR	10	59.9	0.8 20.0	413.0 71.5	6.61	4.94	
SHL	Shillong, India	7651	68.5	SPZ SPH LPZ	P S LR	11 20	01.2 (03.5)	-- 1.3 18.0	-- 53.0 26.5		5.02	
COP	Copenhagen, Denmark	8084	72.7	SPZ LPZ	P LR	11	26.5	1.1	909.0 155.0	6.90	4.59	Clipped
ESK	Eskdalamuir, Scotland	8185	73.6	SPZ	P	11	32.2	1.0	380.0	6.44	5.40	

TABLE IV (Cont'd.)

STATION	LOCALITY	DISTANCE km	deg	INSTRUMENT	PHASE	OBSERVED TRAVEL TIME		PERIOD (SECONDS)	MAXIMUM AMPLITUDE A/T(mu/sec)	MAGNITUDE m_b	M_s	COMMENTS
KBL	Kabul, Afghanistan	8312	74.8	SPZ LPZ	P LR	11 	40.0 22.0	-- 22.0	-- 27.5		 4.67	Clipped
NDI	New Delhi, India	8343	75.0	SPZ LPZ	P LR	11 	41.5 19.0	1.3 19.0	75.0 37.0	5.67	 4.80	
VAL	Valencia, Ireland	8529	76.7	SPZ	P	11	50.2	1.0	580.0	6.66		
MSH	Meshed, Iran	8661	77.9	SPZ SJZ	P PP	11 14	57.8 (51.0)	1.0 1.0	387.0 225.0	6.49		
BEC	Bermuda-Columbia, Bermuda	8841	79.5	SPZ LPZ	P LR	12 	05.5 20.0	1.0 20.0	60.0 43.1	5.54	 4.91	
STU	Stuttgart, Germany	8876	79.8	SPZ SPZ SPZ SPZ	P PcP PP P'P'	13 13 15 38	07.0 19.0 21.0 55.0	0.6 0.8 1.1 0.8	248.0 126.0 50.5 15.7	6.09		
TRI	Trieste, Italy	9167	82.4	SPZ LPZ	P LR	12 	18.2 20.0	-- 20.0	-- 45.5		 4.96	Clipped
IST	Istanbul, Turkey	9376	84.3	SPZ LPZ	P LR	12 	30.6 20.0	1.4 20.0	107.0 45.0	6.03	 4.97	

TABLE IV (Cont'd.)

STATION	LOCALITY	DISTANCE km deg	INSTRUMENT	PHASE	OBSERVED TRAVEL TIME	PERIOD (SECONDS)	MAXIMUM AMPLITUDE A/T(mu/sec)	MAGNITUDE m_b	MAGNITUDE M_s	COMMENTS
PTO	Porto, Portugal	9738 87.6	SPZ LPZ	P LR	12 46.5	1.2 20.0	129.0 47.0	6.23	5.01	
RIV	Riverview, Australia	9828 88.4	SPZ LPZ	P LR	11 53.5	1.1 21.0	811.0 27.5	6.96	4.79	
ATU	Athens, Greece	9833 88.4	SPZ SPZ LPZ	P PP LR	12 49.6 16 22.0	1.0 1.1 22.0	48.0 48.0 12.6	5.84	4.45	
MAL	Malaga, Spain	10,200 90.0	SPZ LPE LPZ	P LQ LR	12 08.0	1.5 24.0 18.0	141.0 18.0 51.0	6.15	5.07	
SJG	San Juan, Puerto Rico	10,056 90.4	SPZ SPZ SPZ LPZ	P PP PKKP LR	13 00.1 16 30.0 30 13.0	-- 1.1 1.1 25.0	-- 63.6 27.3 33.3		4.89	Clipped
WEL	Wellington, New Zealand	10,275 92.4	SPZ	P	13 09.2	0.8	200.0	6.40		
TRN	Trinidad, West Indies	11,026 99.2	SPZ LPZ	P LR	13 40.4	1.1	140.0 74.0	6.64	5.30	
MUN	Mundaring, Australia	11,090 99.7	SPZ	P	13 43.3	1.4	69.0	6.27		

TABLE IV (Cont'd.)

STATION	LOCALITY	DISTANCE km deg	INSTRUMENT	PHASE	OBSERVED TRAVEL TIME	PERIOD (SECONDS)	MAXIMUM AMPLITUDE A/T(mμ/sec)	MAGNITUDE m_b M_s	COMMENTS
LZ-BV	La Paz, Bolivia	12,949 116.5	SPZ	PKP	18 44.6	1.0	46.0		
			SPZ	PP	20 01.2	2.0	4.2		
			LRR	LQ		23.0	11.4		
			LPZ	LR		20.0	31.0		
SDB	Sa da Bandeira, Angola	15,768 141.8	SPZ	PKP	19 24.4	1.0	168.0		
			SPZ	PP	22 32.0	1.5	30.0		
PRE	Pretoria, South Africa	16,255 146.2	SPZ	PKP	19 39.2	1.5	1273.0		
			LPZ	LR					
WIN	Windhoek, Southwest Africa	16,460 148.0	SPZ	PKP	19 42.5	1.0	415.0		
			LPZ	LR		20.0	28.8		
GRM	Grahamstown, South Africa	17,028 153.1	SPZ	PKP	19 49.3	1.6	270.0		

TABLE V

LONG SHOT - MILROW P Amplitude
Ratio From First Quarter-Cycles of Motion

STATION	LONG SHOT MILROW
TUC	.179
ALQ	.149
KN-UT	.132
HN-ME	.164
LC-NM	.149
RK-ON	.167
TFO	.179
UBO	.126
LAO	.145

Average ratio = .154
Standard deviation = .019

TABLE VI
LONG SHOT - MILROW LR Amplitude
Ratio From Match-Filter Output

STATION	LONG SHOT / MILROW
WH-YK*	.060
NP-NT	.090
PG-BC*	.096
KN-UT	.086
RK-ON	.118
CR-NB*	.116
SJ-TX	.085
HN-ME	.078
BE-FL	.088

Average ratio = .091
Standard deviation = .014

*Moved to WH2YK, PG2BC, and CR2NB for MILROW

119

TABLE VII

LRSM Van and VELA Array Data for MILROW Collapse

STATION	LOCALITY	DISTANCE km	deg	P-WAVE SPZ INSTRUMENT PERIOD (Seconds)	MAXIMUM AMPLITUDE A/T(mμ/sec)	m_b	LR WAVE LPZ INSTRUMENT PERIOD (Seconds)	MAXIMUM AMPLITUDE A/T(mμ/sec)	M_s	P-WAVE ARRIVAL TIME
FB-AK	Fairbanks, Alaska	2394	21.5	(0.7)	9.08	4.11	18.0	57.1	4.09	11:01:06.7
WH2YK	Whitehorse, Yukon	2969	26.7				18.0	85.3	4.42	
PG2BC	Prince George, British Columbia	3843	34.6				24.0	18.9	3.95	
LAO	LASA beam, Montana	5243	47.2	1.0	1.18	3.97	24.0	21.2	4.22	11:04:49.5
UBO	Uinta Basin, Utah	5445	49.0	1.1	6.96	4.64	27.0	18.9	4.20	11:05:04.7
KN-UT	Kanab, Utah	5455	49.1	0.9	2.38	4.13	24.0	16.2	4.13	11:05:06.0
RK-ON	Red Lake, Ontario	5725	51.5				24.0	15.2	4.14	
TFO	Tonto Forest, Arizona	5760	51.8	0.8	1.39	3.94				11:05:27.0
LC-NM	Las Cruces, New Mexico	6224	56.0	1.3	4.00	4.40	15.0	13.0	4.13	11:05:56.9
BY-IO	Bloomfield, Iowa	6518	58.6				18.0	13.5	4.18	
WQ-IL	Watseka, Illinois	6821	61.3				18.0	2.62	3.50	
GZ-OH	Galion, Ohio	7109	63.9				19.0	5.00	3.81	
SJ-TX	San Jose, Texas	7162	64.4				16.0	2.86	3.58	
AS-PA	Altoona, Penna.	7348	66.1				20.0	5.88	3.91	
HM-ME	Houlton, Maine	7444	66.9				18.0	28.7	4.61	

TABLE VIII

Summary of Shear-to-Compressional
Ratios for MILROW, BENHAM, and BOXCAR

MILROW Short-Period	Phase	Shear A/T (mμ/sec)	S/P Ratio
Station	Phase	(mμ/sec)	S/P Ratio
SHL	S_h	53.	P unreadable
COL	S_h	223.	.27
GUA	S_h	235.	.25
TUC	S_h	42.	.06
KN-UT	S_h	167.	.05
			.16 Average

MILROW Long-Period

LC-NM	S_h	12.6	No P
LC-NM	S_v	8.5	No P
KN-UT	S_h	66.7	No P
KN-UT	S_v	54.2	No P
FB-AK	S_h	81.0	2.79
FB-AK	S_v	150.0	5.17
RK-ON	S_v	10.1	1.30
NP-NT	S_v	34.5	1.40

BENHAM Short-Period

NP-NT	S_h	38.0	.10

BENHAM Long-Period

PG2BC	S_h	114.	1.48
RK-ON	S_h	175.	2.92
FB-AK	S_h	114.	1.43

BOXCAR Short-Period

RK-ON	S_h	274.	.12

BOXCAR Long-Period

RK-ON	S_h	81.	1.42
WMO	S_h	125.	1.25

TABLE IX
Summary of Love-to-Rayleigh Ratios
for MILROW, BENHAM, and BOXCAR

MILROW Station	LQ A/T (mµ/sec)	LQ/LR	
WH2YK	82.0	.23	
NP-NT	19.5	.10	
PG2BC	46.3	.51	
LAO	54.1	.72	
UBO	17.6	.43	
KN-UT	44.2	.87	
RK-ON	35.0	.27	
LC-NM	26.5	.70	
BY-IO	40.9	.94	
WQ-IL	25.3	.26	
SJ-TX	48.8	1.14	
		.56	Average-MILROW
BENHAM			
KN-UT	19,100	1.30	
UBO	4,740	1.07	
PG2BC	1,950	.40	
BOXCAR			
AT-NV	14,000	.66	
EY-NV	11,300	.29	
BF-CL	3,850	.59	
WW-UT	9,860	.86	
KG-AZ	5,240	.41	
ND-CL	25,800	.49	
CP-CL	13,700	.36	
TFO	3,520	.20	
UBO	3,300	.92	
PG-BC	2,390	.24	
SV3QB	713	.46	
		.59	Average-BENHAM and BOXCAR

TABLE X

Complexities for MILROW, LONG SHOT
and the MILROW Collapse

Station	Distance (Deg.)	F_c MILROW	LONG SHOT	MILROW Collapse
FB-AK	21.5	4.19		6.78
WH2YK	26.7	9.63	9.92	
PG2BC	34.6	6.79	7.93	
LAO	47.2	2.18	2.14	3.64
UBO	49.0	1.68		5.01
KN-UT	49.1	2.87	2.63	6.00
RK-ON	51.5	1.20	1.22	
TFO	51.8	2.76	2.28	8.92
LC-NM	56.0	1.61	1.41	7.13
CR2NB	56.2	2.31	1.66	
BY-IC	58.6	1.63		
WQ-IL	61.3	1.08		
SJ-TX	64.4	1.70	1.32	
AS-PA	66.1	2.11		
EU2AL	66.8	2.56		
PJ-PA	67.9	2.13		
BE-FL	73.1	2.32	1.10	

TABLE XI
Short-Period P-wave Spectral Ratios for
MILROW, LONG SHOT and the MILROW Collapse

SPECTRAL RATIO (S_1)

Station	MILROW	LONG SHOT	MILROW Collapse
FB-AK	1.39	----	1.83
WH2YK*	2.04	0.84	----
PG2BC*	6.77	11.52	----
LAO	2.16	1.64	2.66
UBO	11.37	----	10.44
KN-UT	0.86	2.99	10.01
RK-ON	1.30	0.52	----
TFO	2.67	----	1.61
LC-NM	5.40	2.67	5.09
CR2NB*	1.62	0.36	----
BY-IO	2.28	----	----
WQ-IL	1.19	----	----
SJ-TX	6.12	1.71	----
GH-MS	5.17	----	----
AS-PA	1.81	----	----
EU2AL	2.14	----	----
PJ-PA	3.32	----	----
BE-FL	4.18	1.84	----

*Were at WH-YK, PG-BC, ٮ ٮ CR-NB for LONG SHOT

TABLE XII

Synopsis of Diagnostics for MILROW and the MILROW Collapse

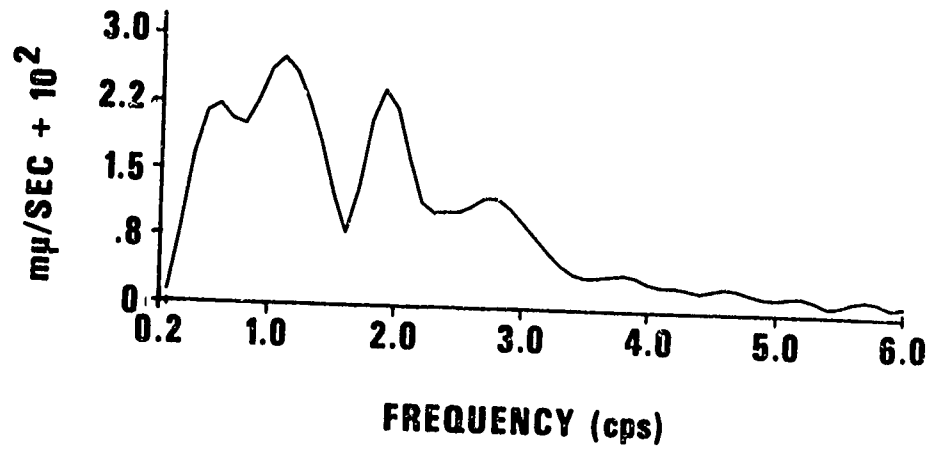| Diagnostic | Does it Identify Event as an Explosion | | Comments |
	MILROW	Collapse	
Location and Depth of Focus	No	No	Cepstral pP depth analysis gives good results for both. With LONG SHOT travel-time anomalies, MILROW would appear as a near-surface event. Even with anomalies, collapse locates off Amchitka Island.
M_s vs m_b	Yes	No	MILROW is clearly in explosion population, and collapse is clearly in earthquake population.
Shear Waves	Yes	Yes?	MILROW short-period SH/P ratio is less than any Aleutian earthquakes analyzed, and long-period shear waves (direct S and LQ) are both low relative to m_b. No visible direct shear phases from the collapse were found.
Complexity	Yes?	No?	Complexities for only one earthquake in the Aleutians have been reported (Lambert et al., 1969).
Short-Period Spectra	Yes?	No?	Only Asian presumed-explosion and earthquake ratios were available as the two background populations (Lacoss, 1969). MILROW spectra differed considerably from those of LONG SHOT and individual spectral ratios were generally higher than for LONG SHOT
Long-Period Spectra	Yes?	No?	MILROW follows trend of explosions from three test areas, but is amidst six Aleutian Islands earthquakes. MILROW spectra were very much like LONG SHOT. Collapse had more longer-period energy.
Radiation Patterns, Including First Motion	Yes?	?	No rarefactional first motion for MILROW. Analysis of more Aleutian earthquakes is necessary. MILROW patterns do not appear to differ from those of LONG SHOT.

TABLE XIII

Relative Values of LONG SHOT and MILROW
Collapse LQ Amplitudes to Those of MILROW

Station	$\dfrac{\text{LONG SHOT LQ}}{\text{MILROW LQ}}$	$\dfrac{\text{MILROW Collapse LQ}}{\text{MILROW LQ}}$
PG2BC	.099	-.029
RK-ON	.143	-.039
SJ-TX	.084	-.038
AVERAGE	.109	-.035

APPENDIX I

ADDITIONAL MILROW P-WAVE SPECTRA

MILROW
FB-AK
2394 Km
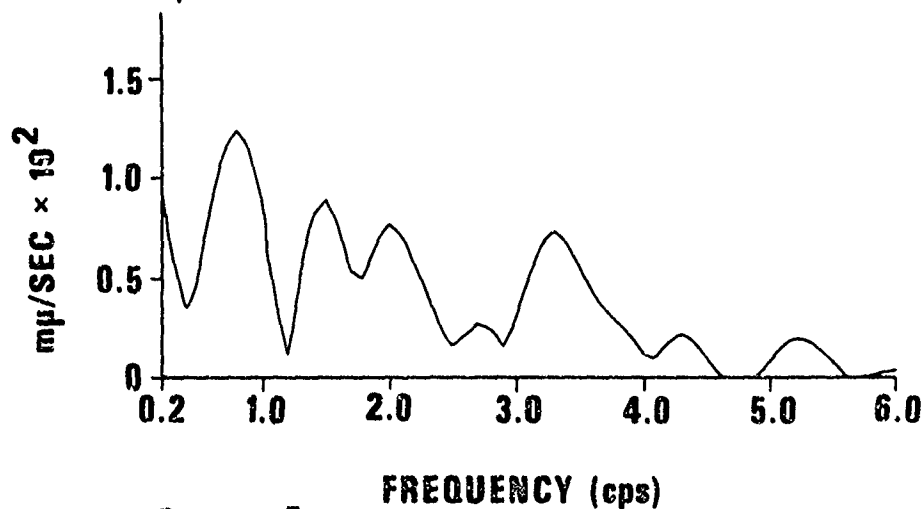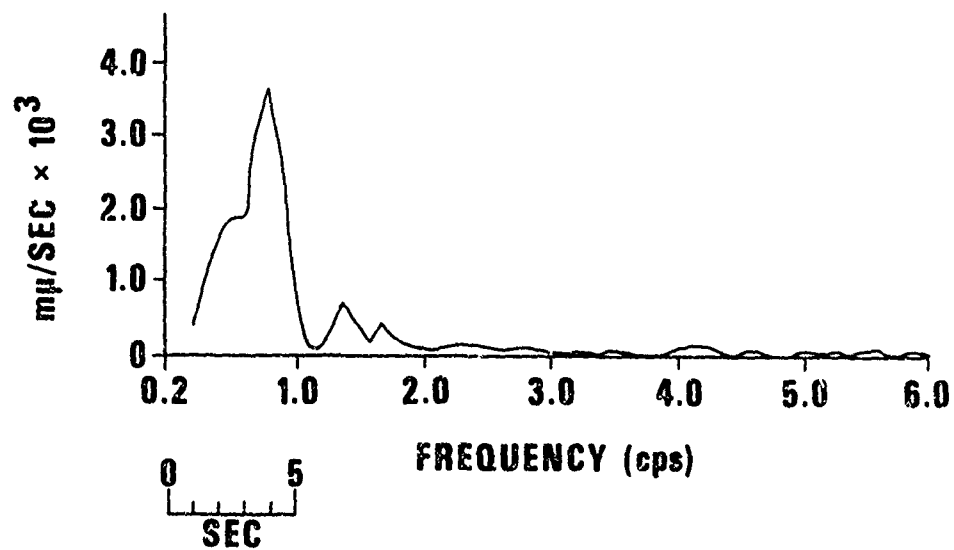
MILROW
WQ-IL
6821 Km

MILROW
BY-IO
6518 Km

FREQUENCY (cps)

FREQUENCY (cps)

SEC

139
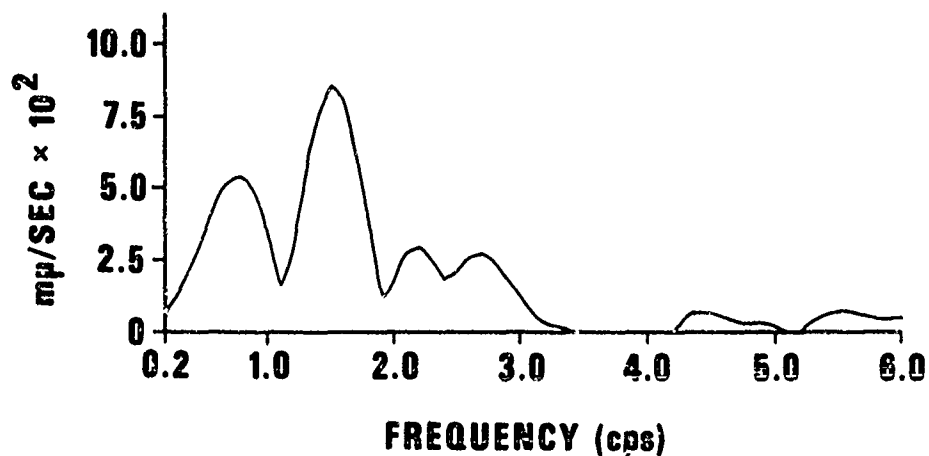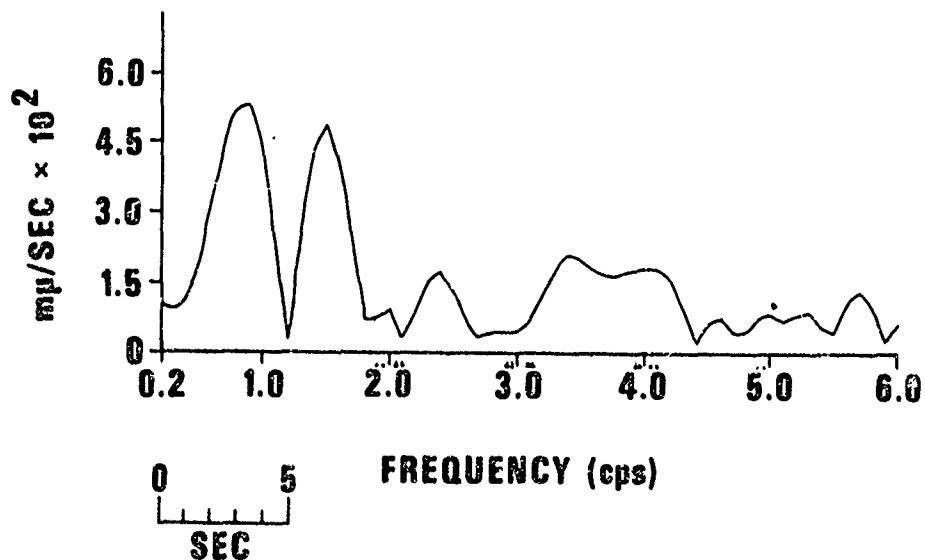
MILROW
AS-PA
7348 Km

MILROW
EU2AL
7432 Km

FREQUENCY (cps)

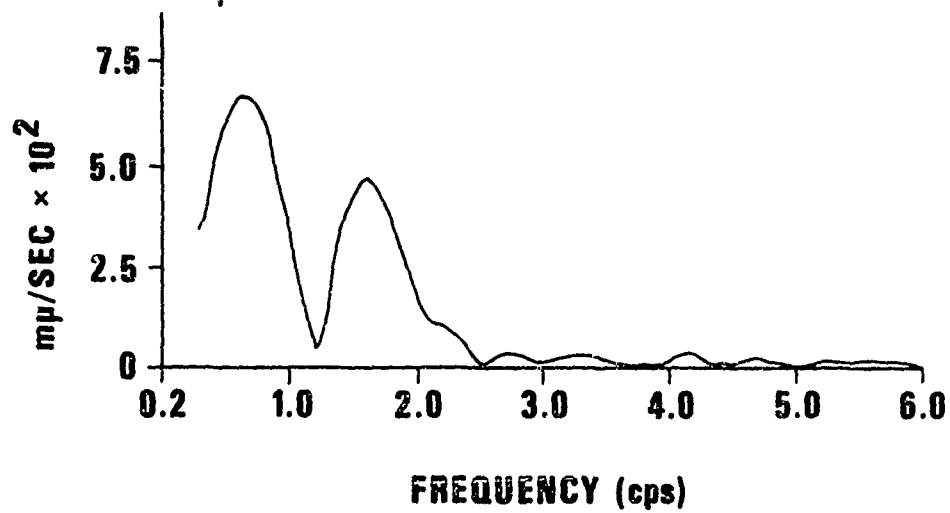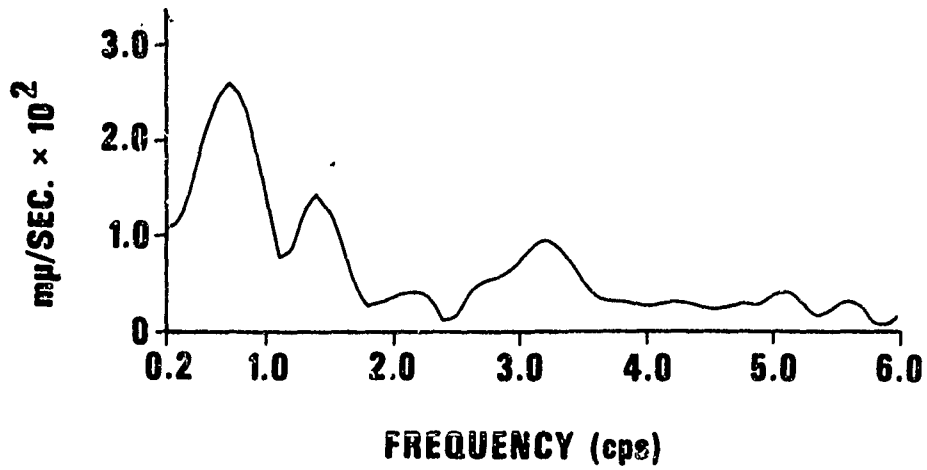FREQUENCY (cps)
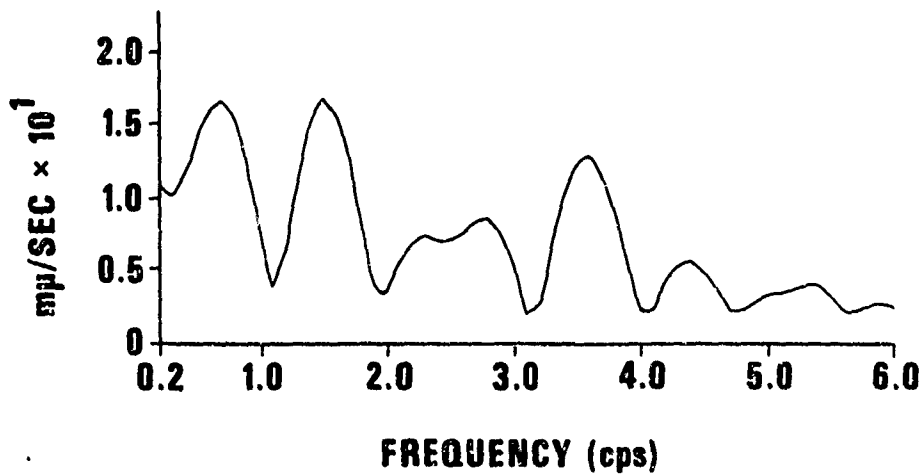
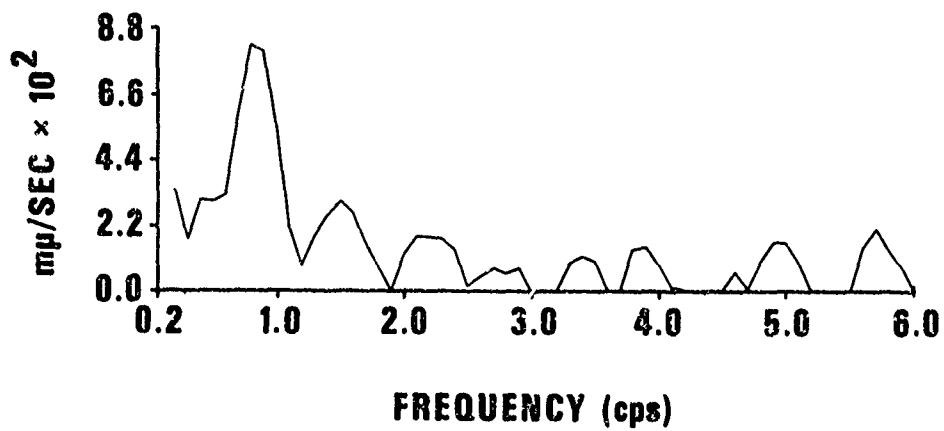MILROW
TFO
5760 Km
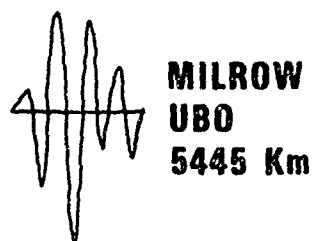
MILROW
UBO
5445 Km

MILROW
PJ-PA
7550 Km

MILROW
GH-MS
7188 Km

0 ——— 5
SEC

132

APPENDIX II
ADDITIONAL MILROW RAYLEIGH-WAVE SPECTRA

MILROW
LAO
5244 Km

AMPLITUDE SPECTRA

MILROW
BY-IO
6518 Km

AMPLITUDE SPECTRA

MILROW
WQ-IL
6808 Km

AMPLITUDE SPECTRA

MILROW
GZ-OH
7109 Km

AMPLITUDE SPECTRA

MILROW
GH-MS
7188 Km

AMPLITUDE SPECTRA

MILROW
AS-PA
7348 Km

AMPLITUDE SPECTRA

136

MILROW
EU2AL
7432 Km

AMPLITUDE SPECTRA